
Physics of Traffic on Ant Trails and Related Systems

In a u g u r a l - D i s s e r t a t i o n
zur
Erlangung des Doktorgrades
der Mathematisch-Naturwissenschaftlichen Fakultät
der Universität zu Köln



vorgelegt von
Alexander John
aus Leverkusen

Köln 2006

Berichterstatter:

Prof. Dr. A. Schadschneider
Prof. Dr. D. Stauffer

Tag der mündlichen Prüfung:

8. Dezember 2006

Contents

1	Introduction	1
1.1	Motivation	1
1.2	Outline	3
2	The ASEP and its Variants	5
2.1	Definition	5
2.1.1	Boundary Conditions	6
2.1.2	Update Schemes	7
2.2	The TASEP	8
2.2.1	Models based on the TASEP	13
2.3	The TASEP with Static Disorder	18
2.3.1	Particlewise Disorder	19
2.3.2	Lattice-wise Disorder	22
3	The Unidirectional Model	27
3.1	Definition	27
3.1.1	Some Aspects Concerning Reality	28
3.1.2	Exact Mapping to Other Models	29
3.2	Properties of the Unidirectional ATM	31
3.2.1	Observed Patterns	31
3.2.2	Coarsening Behaviour	32
3.2.3	The Stationary State	35
3.3	Discussion	38
4	The Bidirectional Models	41
4.1	Definitions and Properties	41
4.1.1	Bidirectional Trail with Separated Pheromone Lattices ..	43
4.1.2	Bidirectional Trail with Common Pheromone Lattice ...	45
4.1.3	Single-lane Bidirectional Ant Trail Model	47
4.2	Common Features	51
4.2.1	Moving Clusters	52

4.2.2	Localised Clusters	52
4.3	Extending the Parameter Regime	59
4.3.1	Different Hopping Rates	59
4.3.2	Different Particle Numbers	59
4.4	Discussion	60
5	Empirical Results	63
5.1	Experimental Scenario	63
5.1.1	Observed Species	64
5.1.2	Environment and Ecological Context	64
5.1.3	Mapping the Model to Real Trails	65
5.2	Methodology of Observations	67
5.2.1	Qualitative Observations and Preliminary Results	67
5.2.2	Quantitative Observations	69
5.3	Results of Quantitative Observations	74
5.3.1	The Simple Unidirectional Trail (Video 13)	74
5.3.2	The Complex Unidirectional Trail (Video 19)	79
5.3.3	The Bidirectional Trail (Videos 6a, b, c)	84
5.4	Discussion	90
5.4.1	The Simple Unidirectional Trail (Video 13)	92
5.4.2	The Complex Unidirectional Trail (Video 19)	92
5.4.3	The Bidirectional Trail (Videos 6a, b, c)	93
5.4.4	Mechanisms of Platoon Formation	94
6	Conclusions	97
6.1	Summary and Discussion of Results	97
6.1.1	Theoretical Results	97
6.1.2	Empirical Results	99
6.1.3	A Comparison between Theory and Empiricism	100
6.2	Outlook	102
6.2.1	Theoretical Studies	102
6.2.2	Experiments	103
A	Appendix	107
A.1	Error Correction	107
A.1.1	Detectable Errors	107
A.1.2	Correction of Detectable Errors	108
A.1.3	Hidden Errors	108
A.2	Statistical Errors	109
A.2.1	Average Velocity	109
A.2.2	Time- and Distance Headway	109
A.3	Distance Headway Cut-Off	110
A.4	Supplementary Data	111
A.4.1	Video 13	111
A.4.2	Video 19	111
A.4.3	Video 6 (Parts A, B, C)	113

1 Introduction

1.1 Motivation

Traffic or traffic related transport systems are ubiquitous in nearly any part of nature and everyday life. First systematic investigations of vehicular traffic were carried out at about the middle of the 20th century (following [60]). In recent years studies are extended from the classical field of vehicular traffic [19, 34, 60] to pedestrians dynamics [48, 75], routing of different kinds of load like data, passengers, packages, [8] or even to transport within a living cell [20, 37, 59]. Like in vehicular traffic concepts known from statistical physics are applied to those systems. Especially microscopic models implemented as computer simulations (e.g. [3, 14, 18, 19]) have attracted a lot of interest. They allow to incorporate directly the microscopic rules of interaction between the agents of the modelled system [5, 65, 87]. If different choices for particular sets of parameters like the number of lanes on a highway or a speed limit are available these models can be simulated faster than realtime. With respect to practical application this is probably the most striking feature as it allows to adapt to a dynamically changing situation. Examples are emergency situations like evacuation in pedestrian dynamics or the routing of vehicular- or data-traffic in a network. Nevertheless for gaining deeper insights the physics of the systems has to be explored. Unlike in pure physical systems a description based on first principles is hardly possible. For example the so-called social force between car drivers or pedestrians does not obey Newton's third axiom (e.g. [48, 75]). So the microscopic rules of interaction have to be included directly into the underlying description. Additionally modelling often has to incorporate some degree of stochasticity (e.g. [65]). This is done mainly for two reasons. First, the rules for interacting are only valid on average as not all microscopic details are known. Therefore fluctuations have to be expected. But also systems might exhibit an intrinsic stochasticity [5, 6, 36]. In vehicular traffic for example different drivers might react differently in the same situation. Resulting collective phenomena due to these fluctuations like *phantom jams* are a widely known [19, 65]. Fluctuations have a different impact in different situations [22]. For high densities

of cars, e.g. caused by a bottleneck like construction works or an accident, the system is more susceptible to *phantom jams* as the average distance headway is decreased. From that point of view even *phantom jams* exhibit some deterministic components. Nevertheless they might also emerge without any directly visible cause [19].

Besides the wish to understand the physics or to improve the description the main aim still is the optimisation of the traffic systems. In recent years different kinds of biologically inspired approaches have been applied to various systems [6,7,7,21]. Especially the *social insect metaphor* is used quite frequently (e.g. [8,55]). One takes the aspects of the biological system resembling to those of the artificial system one seeks to optimise. Then one tries to adapt properties or strategies from the biological system. Basically one makes use of solutions to problems which have already been solved by nature.

From evolutionary and behavioural biology different kinds of optimisation are known. Prominent examples are found among the group of the so-called *eusocial insects*¹. Due to evolutionary pressure properties crucial for the survival of a species can be assumed to be optimised. For example ant colonies are competing for limited food sources. Ineffective foraging strategies of one colony in comparison to the other competitors, namely other colonies, would very likely result in the death of that colony. As a solution all ants belonging to one colony cooperate to a very high degree. The employed behavioural patterns depend to a large extent [36] on the particular species. So the same mechanism from this example is also found in the competition between different species. Optimisation in that context means to be better adapted to the problem than the other competitors.

Due to the cooperative nature of social insects (see Fig. 1.1, left) a system optimum can be expected. Especially in systems without living agents like package routing in networks this is reasonable. For a system composed out of self-conscious individuals also the user optimum plays a role. Here the more egoistic interests of the agents have to be taken into account. In traffic engineering this is known as the level of service provided to the driver (e.g. minimisation of travel time) whereas the system optimum corresponds to an optimisation of capacity (maximisation of flow) [60].

The present work applies the formalism from traffic engineering and statistical physics to a traffic system of social insects namely to those of ants. Belonging to the group of eusocial insects traffic flow at least for some particular species can be expected to exhibit some kind of optimisation [11,12,25,26,36]. From behavioural biology different degrees of intrinsic stochasticity are known [36,84]. This stochasticity is a crucial part e.g. of raiding or routing strategies [6,7,13]. Therefore microscopic stochastic cellular automaton models are well suited for simulating traffic flow on preexisting trails. Like in most traffic systems flow has only one direction. This is also reflected in the corresponding transition rates from one configuration of the system to another. The rates are such that for example all cars or ants move into the same direction. With respect to the

¹ truly social in a narrow sense

underlying master-equation, stationarity can not be realised by detailed balance. Overall ant traffic as well as the corresponding models are generically stochastic and far from equilibrium systems.



Fig. 1.1. The left photography shows cooperative transport of prey on a trail of *Oecophylla smaragdina*, a weaver ant species. On the right an ant belonging to the species *Leptogenys processionalis* is shown. Antennas touch the ground in search for pheromones. As this species is monomorphic the bodysize can be used as a natural scale.

1.2 Outline

Originally the present work was intended mainly to discuss the physics of stochastic cellular automaton models inspired by the traffic flow of real ants on their trails. Therefore the models incorporate only the most essential interactions [16,41,76]. So in contrast to high-fidelity models, e.g. in traffic engineering or behavioural biology, tractability of the mathematical description was given priority. For first investigations this approach has the advantage that the main features of the models emerge quite clearly. Once those have been understood the next step towards more realistic and thus more complex models is still possible. But this is not always necessary. It is known from experience that not all the details of interaction contribute to the emergence of a particular collective pattern (e.g. [13]).

The employed models basically show some analogy to those of vehicular traffic [65] as well as to pedestrians dynamics [48]. Overall the main focus lies on the organisation of traffic flow rather than on the patterns exhibited by the trail system itself which have already been investigated extensively (e.g. [13]). All models are based on the TASEP (*Totally Asymmetric Simple Exclusion Process*). Due to its paradigmatic status for non-equilibrium systems a huge amount of analytical and numerical results is available [23,38,70,72,73,78]. An overview of some results for a later comparison to the ant trail models will be given in *chapter 2*.

In *chapters 3 and 4* models for traffic flow on preexisting uni- and bidirectional ant trails are discussed. The unidirectional ant trail model is basically a direct extension of the *TASEP* [16, 66]. The incorporated means of interaction between the ants induce dynamical particlewise disorder. Analogies to the *TASEP* with static particlewise disorder are drawn. In *chapter 4* the unidirectional model is extended to the next step of complexity namely the multilane case [45, 76]. Unlike for example in models of vehicular traffic [3] an additional lane in counterdirection is added. Different variants are discussed and common and particular features are being identified [41, 43, 56]. Generally the models show some kind of dynamically induced latticewise disorder. Again the physical properties in analogy to the *TASEP* are emphasised. In comparison to reality the models appear quite simple. One advantage of this simplicity is also flexibility. Like demonstrated for the *TASEP* also the ant trail models might be used in a different context like pedestrians dynamics or a network of bus stops [68, 69]. For application to non-biological systems it is also necessary to add some kind of artificial flavour up to a certain degree [46]. In this context modelling is not given priority. Instead the aim is to solve a problem in an artificial system. Therefore some aspects of the biological system which are assumed not to be important are neglected.

Complementary to the theoretical investigations empirical field studies have been carried out. In *chapter 5* an experimental setup for collecting ant-traffic data is discussed. Employing tools from traffic engineering [60, 83] velocity- and distance headway distributions as well as fundamental diagrams are extracted for the uni- and the bidirectional case. Till now only few investigations of that kind have been carried out [10, 12, 47]. Besides data-collection a comparison between the properties of the ants on a real trail and the models is drawn. By preparing a strict experimental setup even the simple models can be applied to certain trail-scenarios. Concluding the discussion the empirical results are compared to the theoretical predictions of the models in *chapter 6*. The observed patterns will also be discussed from a more biological point of view. Finally the question concerning the assumed optimisation of flow in ant-traffic will be addressed for a particular group of species.

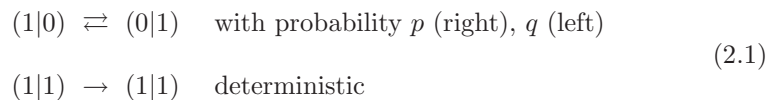
2 The ASEP and its Variants

The ASEP (*Asymmetric Simple Exclusion Process*) is a one-dimensional stochastic process of particle hopping. Originally it was intended as a simple model for the dynamics of biopolymerization [59] in 1968. Later in 1970, a more general version for mathematical studies of Markov processes [79] was introduced. Although quite simple the ASEP in its different variants exhibits a wide range of interesting physics. Like the Ising-chain in equilibrium physics the ASEP has reached a paradigmatic status for non-equilibrium physics [27, 78].

This chapter starts with a brief introduction to the ASEP. Different variants regarding dynamics and boundary conditions have been developed. Due to its simplicity the ASEP is quite flexible and has become the basis for many cellular automaton models. Some of them, like the Nagel-Schreckenberg model [65] for vehicular traffic and a model for surface growth [27, 78], are discussed in this chapter. Finally for practical application the more general case of disordered ASEP turns out to be very useful.

2.1 Definition

The name ASEP itself originates from the description of the underlying process. Particles move along a one-dimensional lattice by hopping to one of the two next-neighboring sites (see Fig. 2.1) under time evolution (*process*). Each site can only be occupied by one particle. So hopping takes place to a site not already being occupied (*simple exclusion*). Hopping can be described just by incorporating the occupation of two lattice sites i and $i + 1$:



Hereby "1" denotes an occupied site whereas "0" means that the site is empty. Depending on direction two different hopping rates are used. Generally this induces an asymmetry (*asymmetric*) leading to an effective current in the

direction of the higher rate. In case of equal hopping rates for both directions the effective current vanishes and an equilibrium state is reached. Nevertheless also the general case can be described by an appropriate mapping of the master equation to a stochastic Hamiltonian defining a time-evolution operator. For analytical calculations this technique has turned out to be very useful [23, 78]. The state of the system at a particular instance of time is thereby given by the occupation of the lattice. This is in analogy to a spin chain with $s_i = \frac{1}{2}$ where each of the two possible states is associated with the spin direction at a particular lattice site i . For implementing the ASEP different variants exist. They basically differ in the choice of boundary conditions and update scheme. Depending on the particular purpose of modelling boundary conditions and dynamics are chosen.

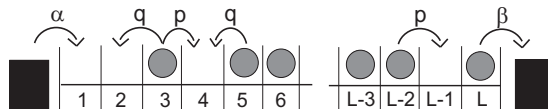


Fig. 2.1. Definition of the ASEP: In case of open boundary conditions particles are injected e.g. at the left and ejected at the right boundary. On the non-boundary sites of the lattice, particles move to the left with rate q and to the right with rate p . This can lead to ambiguities especially in case of time-parallel dynamics. The particles at sites 3 and 5 would attempt to hop to site 4 at the same time. Obviously additional rules are needed in order to preserve the simple exclusion principle.

2.1.1 Boundary Conditions

Particles occupying the non-boundary sites (sites $i \in [2, L - 1]$) are treated according to the rules already described. The two ends (sites $i = 1$ and $i = L$) have to be treated with an additional set of rules. Mainly two frequently used variants exist. The first is the use of so called periodic boundary conditions where both ends of the lattice are connected to a ring. So the two next nearest neighbouring sites of a particle at site 1 are sites 2 and L . Analogous a particle at site L has the nearest neighbouring sites $L - 1$ and 1. The local rules for hopping are applied to the corresponding sites, leading to an translational invariant lattice. Although similar with respect to translational invariance, a lattice with such a geometry is still different from an infinitely large one. For implementing the ASEP or an ASEP-based model finite-size effects have to be taken into account [38]. Due to the ring-like geometry particles in principle might effectively interact with themselves. Also in case of non-ring-like geometries effects arising from a finite system size are known. But if the lattice-size is large enough such effects can be neglected.

Nevertheless also the natural systems one seeks to describe are of finite size so those effects might be a generic part of the system. Quite frequently only the

bulk of the system is incorporated for which effects arising from the boundaries can often be neglected.

For practical application, especially for modelling traffic systems, so-called open boundary conditions are frequently used [71]. On one end of the lattice, e.g. the left one, a particle reservoir is placed, injecting particles to site 1 with rate α if this site is not already occupied. On the other end, e.g. the right one, a particle drain is placed. A particle at site L will hop into this drain with rate β (see Fig. 2.1). Commonly one also finds an alternative formulation of these rules. The hopping rules for the lattice (sites $i \in [1, L]$) are also applied to the source (site 0) and the drain (site $L+1$). For incorporating the injection or ejection rate one defines fixed densities for these sites. At the source $\rho_+ := \alpha$ and $\rho_- := 1 - \beta$ at the drain will realise the corresponding rates α and β . Generally translational invariance is broken. As discussed later one still recovers the occupation known from periodic boundary conditions for an appropriate choice of parameters. But overall boundary conditions are well known to have a strong influence on the system. So a rich phase diagram with boundary-induced phase transitions is known [1, 23, 27, 52, 78].

2.1.2 Update Schemes

Besides boundary conditions also the choice of the update scheme is known to influence the physics [74] by inducing additional correlations. The rules defining the ASEP only describe a process in time by setting some local rules for hopping. But the way e.g. the order of applying these rules to the sites of the lattice is not defined by that. Two quite extreme variants for implementing the update of the actual lattice-occupation are frequently used.

The first one is the so-called *random-sequential* dynamics. At each update, one lattice site is chosen at random. The local rules for particle hopping (e.g. (2.1)) are applied to that site and its neighbours. This happens sequentially for succeeding updates in random order. Nevertheless the same site might be selected at two immediately succeeding updates. With respect to the efficiency of implementation this appears to be quite ineffective as random numbers have to be generated just for choosing a site. On average it takes $T = L$ procedures to ensure that all sites have been updated. Random-sequential dynamics describe a process in continuous time. Two updates are separated by $\Delta T = \frac{T+1}{L} - \frac{T}{L}$. For a system of infinite length time becomes continuous as $\Delta T \rightarrow 0$ for $L \rightarrow \infty$. One additional property of random-sequential dynamics is the missing of dynamically induced correlations in the ASEP (with periodic boundary conditions). As discussed later on this is also part of the modelling of particular systems.

Unlike for random-sequential dynamics it is also possible to apply the local rules for hopping to all lattice sites at one update step. So all sites are updated in parallel giving rise to the name (*time-*) *parallel* or synchronous update. With respect to practical implementation only $T_p = 1$ instead of $T = L$ updates are needed on average for incorporating all lattice sites. Obviously the

stochastic element of choosing one site at random for updating is missing. As a result time-parallel updates in the $(T)ASEP$ are known to induce particle-hole attraction [74]. Generally an analytical treatment becomes more difficult. Nevertheless these correlations are part of the Nagel-Schreckenberg model for vehicular traffic [19,65]. Here one makes use of the existence of a shortest possible time-scale originating from the parallel update procedure. In comparison to the random-sequential update the parallel update is discrete in time with time scale T_p .

Between both update schemes a huge variety of combinations such as sublattice forward- or backward-sequential exists [74]. One recently proposed update does not fit into that scheme namely the so-called *shuffled* update [88]. For each update the order of sites being updated is set at random for one update of all sites. In contrast to the random-sequential update, the same site can not be updated at two succeeding updates of a single site. That new kind of update has been introduced in the context of simulating pedestrians dynamics [88]. For example the situation that two particles try to hop to the same site would not occurred due to the shuffled update (see Fig. 2.1). Nevertheless this ambiguity might also be part of the model. Models with time-parallel update are widely used. In order to resolve the ambiguity additional rules for deciding which particle namely which pedestrian is allowed to occupy the vacant site [48,75] are used. This is not only done for resolving the ambiguity but also for incorporating certain aspects of the observed behaviour of pedestrians.

2.2 The TASEP

One of the most commonly encountered variants of the ASEP is the special case $q = 0$. Now hopping takes place only in one direction giving rise to the *Totally Asymmetric Simple Exclusion Process* (see Fig. 2.2). The special case of equal hopping rates $p = q$ is no longer possible (except for the uninteresting case $p = 0$). So the TASEP can be expected to be far from equilibrium as a non-vanishing particle flow only exists for one particular direction. Although this is a restriction of the general case it is an quite important one, for example for describing traffic flow.

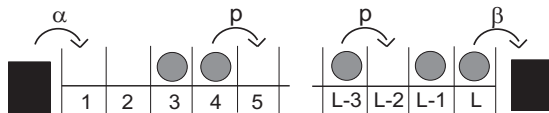


Fig. 2.2. Definition of the TASEP: Particles are still injected at the left and ejected at the right boundary. But on the non-boundary sites of the lattice, particles are only allowed to move in one direction with rate p . In contrast to the ASEP case, time-parallel updating causes no ambiguity.

For characterising the actual state of the lattice a binary variable $c_i \in \{0, 1\}$ with $i \in \{1, \dots, N\}$ describes the occupation of each site. An occupied site corresponds to $c_i = 1$ whereas $c_i = 0$ denotes an empty site which is also called "hole". Averaging over time-evolution with different histories leads to the occupation probability $\langle c_i(t) \rangle$ for one particular site i . Incorporating the local rules for hopping the ASEP in continuous time (random-sequential dynamics) is described by:

$$c_i(t + dt) = \begin{cases} c_i(t) & \text{with prob. } (1 - 2p) \cdot dt \\ c_i(t) + [1 - c_i(t)]c_{i-1}(t) & \text{with prob. } p \cdot dt \\ c_i(t)c_{i+1}(t) & \text{with prob. } p \cdot dt \end{cases} \quad (2.2)$$

Hereby the time for updating one site is of infinitesimal length dt . Due to the structure of the equations the hopping probability p can be absorbed into dt . Obviously the description of the process is not affected by rescaling time which turns out to be equivalent to changing the bulk hopping rate p . The first line of (2.2) describes the case in which the occupation of site i is not changed by any of the other two possible cases. In the second line the coupling to site $i - 1$ is incorporated. If site i is not occupied a particle can hop from site $i - 1$ to site i thereby changing the occupation of site i . The same might also happen from site i as described by the third line. If site $i + 1$ is not occupied a particle can hop from site i to site $i + 1$. As a result the occupation of site i becomes zero. If site $i + 1$ is occupied blocking takes place therefore the occupation of site i stays unchanged. Generally only the actual occupation of the two next neighboring sites $i - 1$ and $i + 1$ needs to be incorporated.

Making use of the formal definition of the TASEP (2.2) one derives equations of motion for the occupation of each lattice site:

$$\begin{aligned} \frac{d\langle c_i \rangle}{dt} &= \langle c_{i-1}(1 - c_i) \rangle - \langle c_i(1 - c_{i+1}) \rangle \quad \text{Bulk } i \in \{1, \dots, L\} \\ \frac{d\langle c_1 \rangle}{dt} &= \langle \alpha(1 - c_1) \rangle - \langle c_1(1 - c_2) \rangle \quad \text{Injection at } i = 1 \\ \frac{d\langle c_L \rangle}{dt} &= \langle c_{L-1}(1 - c_L) \rangle - \langle c_L\beta \rangle \quad \text{Ejection } i = L \end{aligned} \quad (2.3)$$

The first equation describes the time evolution of occupation for each bulk site. For incorporating particle injection and ejection, occupation probability is set to $\langle c_0 \rangle := \alpha$ and $\langle c_{L+1} \rangle := 1 - \beta$. So the second and third equation are just a special case of the first one. In the same way one defines $\langle c_0 \rangle := \langle c_{L+1} \rangle$ for periodic boundary conditions. One observes that only correlations between nearest neighboring sites $i - 1$, i and $i + 1$ are important for the time-evolution of $\langle c_i \rangle$. So flow in the stationary state is of the following structure:

$$F_{in} = \langle \alpha(1 - c_1) \rangle = \dots = \langle c_i(1 - c_{i+1}) \rangle = \dots = F_{out} = \langle c_i\beta \rangle \quad (2.4)$$

For other update procedures flow is roughly of the same structure. But correlations like e.g. the particle-hole attraction for a time-parallel update have to be incorporated [19]. By definition density is constant in the stationary state forcing the flow to be the same at each sites.

If long-ranged correlations can be neglected mean-field descriptions are frequently used. Generally these descriptions are not exact but show a good agreement with simulations. They are especially used because usually an exact analytical treatment is quite difficult. As discussed later on the mean-field approximation becomes exact for an appropriate choices of boundary conditions. More sophisticated calculations [23] also justify this approach:

$$F = \langle c_i(1 - c_{i+1}) \rangle \approx \langle c_i \rangle \langle 1 - c_{i+1} \rangle \quad (2.5)$$

Making use of the factorisation of expectation values one obtains a recursion relation for the occupation probabilities namely the density profile ($\langle c_i \rangle$ vs. i):

$$\langle c_{i+1} \rangle = 1 - \frac{F}{\langle c_i \rangle} \quad (2.6)$$

As already mentioned flow F is independent from the particular site i due to the continuity equation. In general $\langle c_i \rangle$ and $\langle c_{i+1} \rangle$ can be expected to have different values depending on the choice of the boundaries $\langle c_0 \rangle$ and $\langle c_{L+1} \rangle$. Nevertheless for $\alpha = 1 - \beta$ a flat density profile $\langle c_i \rangle = \langle c_{i+1} \rangle \quad \forall i \in [0, L+1]$ as for periodic boundary conditions is found. It can be shown that the mean-field treatment becomes exact for that particular choice of parameters [23].

From (2.6) one derives the density profile for each choice of boundary rates once flow is known. One way of determining flow is the so-called extremal principle [52, 72]. According to that principle the flow in the open system can be determined from the flow ($F(\rho) = \rho(1 - \rho)$) of the system with periodic boundary conditions:

$$F = \max_{\rho \in [\rho_-, \rho_+]} F(\rho) \quad \text{for } \rho_+ > \rho_- \quad (2.7)$$

$$F = \min_{\rho \in [\rho_+, \rho_-]} F(\rho) \quad \text{for } \rho_+ < \rho_- \quad (2.8)$$

One obtains the current inside a system with open boundaries as the maximum or minimum (depending on the choice of boundary rates $\rho_+ = \alpha$ and $\rho_- = 1 - \beta$) of flow in the system with periodic boundary conditions. The principle is quite stable and has been proven to be valid for more complicated lattice-gas models [72]. Even if flow is known only numerically for periodic boundary conditions the flow for the open system can be obtained. Obviously the extrema of the periodic system (see (2.7) and (2.8)) determine the topology of the phase-diagram for the open system.

Overall the whole mean-field phase diagram of the TASEP has been derived. With respect to flow three phases can be distinguished. Generally one finds a

flat density profile $\langle c_i \rangle = \rho_{bulk}$ within the bulk of the system for the high- and low density phase. In the maximal current phase even in the bulk no flat density-profile is found [23] due to the algebraic decay of $\langle c_i \rangle$.

A. Low-density phase: ($\alpha < \beta$, $\alpha < \frac{1}{2}$):

The input rate α controls the bulk density and also flow: Particles are ejected at a higher rate than they are injected.

$$F(\rho) = \alpha(1 - \alpha) \quad \text{with} \quad \rho_{bulk} = \alpha$$

B. High-density phase: ($\alpha > \beta$, $\beta < \frac{1}{2}$):

The ejection rate β controls the bulk density and also flow: Particles are injected at a higher rate than they are ejected.

$$F(\rho) = (1 - \beta)\beta \quad \text{with} \quad \rho_{bulk} = 1 - \beta$$

C. Maximal current phase: ($\alpha \geq \frac{1}{2}$, $\beta \geq \frac{1}{2}$):

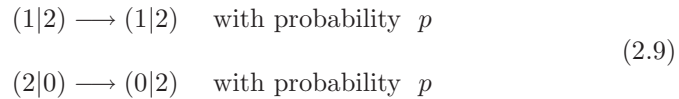
The flow reaches its maximal bulk value (see (2.5)) and becomes independent from the injection and ejection rate [78].

$$F(\rho) = \frac{1}{2}(1 - \frac{1}{2}) = \frac{1}{4} \quad \text{with} \quad \rho_{\frac{1}{2}} = \frac{1}{2}$$

More sophisticated techniques reveal the division of phases A and B into two subphase AI/AII and BI/BII (see Fig. 2.3). Those phases can be distinguished by the asymptotic behaviour of the density profile.

It has been shown that the actual shape of the phase-diagram can be understood by the underlying shock dynamics [51, 72]. A jump in the density profile say from ρ_- to ρ_+ is called as a shock. It can be shown that for $\alpha = \beta < \frac{1}{2}$ the shock performs a random walk along the lattice with a vanishing effective velocity (see (2.12)). Any position of the density jump has the same probability finally leading to a linearly increasing density profile say from ρ_- at site $i = 1$ to ρ_+ at site $i = L$. For other values of ρ_+ and ρ_- the effective shock velocity is non-zero and the shocks move to one of the boundaries and vanish.

One way of tracing the actual position of the shock are so-called second-class particles (e.g. [38, 39]). They move passively on the lattice and do not affect the original "first-class" particles ("1"). By definition they ("2") behave like holes (unoccupied sites) in exchange with particles and like particles in exchange with holes ("0"):



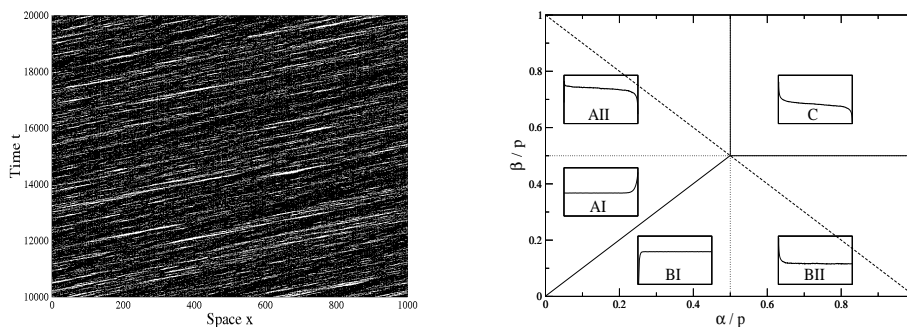


Fig. 2.3. The left figure shows the time-evolution of the particle distribution for $p = 1$ and $\rho = 0.2$. On average particles are distributed homogeneously on the lattice. On the right the phase-diagram is shown. The dashed line $\alpha + \beta = 1$ corresponds to the flat density-profile where the mean-field treatment becomes exact. On the coexistence line $\alpha = \beta < \frac{1}{2}$ the density profile shows a linear increase. Generally the transition point is found at $\frac{p}{2}$ and a flat density profile emerges for $\alpha + \beta = p$. Rescaling time is obviously equivalent to choosing $p = 1$.

In a high density region the second-class particle will predominantly move to the left as first-class particles exchange their position with the position of holes. When no first-class particles are around in a low-density area second-class particles are not blocked and move to the right. Generally they will move with a domain-wall separating the low- from the high-density area. The velocity of movement is just given by:

$$V_{coll} = \frac{\partial F(\rho)}{\partial \rho} = \rho p - (1 - \rho)p = (1 - 2\rho)p. \quad (2.10)$$

Hereby V_{coll} describes the velocity at which the centre of mass [51] of the first-class particles moves. Again the results can be understood in terms of a mean-field picture. Consider a second-class particle sitting at site i . In the TASEP case it will find a first-class particle to its right with probability ρ . Both particle will exchange positions with probability p leading to one step to the left for the second-class particle. On the other hand an empty site is found with probability $1 - \rho$ on the right of the second-class particle. By definition it will hop to that site with probability p .

For further investigations it is useful to describe the movement of the second-class particle or equivalently that of the domain-wall in a more coarse-grained picture. It can be shown that some kind of homogeneous density regime exists near the boundaries. So one finds a flat density profile with $\rho_+ = \alpha$ and $\rho_- = 1 - \beta$ at the corresponding ends of the lattice. Making use of the fact that the continuity equation

$$\frac{\partial \rho}{\partial t} + \frac{\partial F}{\partial x} = 0 \quad \text{with} \quad \rho = \rho(x - vt) \quad (2.11)$$

has a travelling wave solution one obtains by integrating over the whole lattice:

$$v_d = \frac{F_- - F_+}{\rho_- - \rho_+} \quad (2.12)$$

Hereby $F_{\pm} = \rho_{\pm}(1 - \rho_{\pm})$ denotes the flow within each region. As (2.12) is quite general the same picture also applies for example in traffic engineering. A slow car induces a domain-wall. Cars are accumulating behind it (ρ_+) and only few (ρ_-) are found ahead of it. The velocity of the domain-wall is positive as the position of the slow car is identical with the position of the domain wall. If the slow car is removed the traffic jam dissolves leading to a domain-wall travelling upstream¹. As a result the effective velocity of the domain-wall becomes negative (changes sign).

Due to the stochasticity of the process v_d is the effective velocity of a biased random walk performed by the domain-wall. Generally fluctuations are found leading to diffusion. For incorporating fluctuations (2.12) is decomposed into direction dependent diffusion constants:

$$D_{\pm} = \frac{F_{\pm}}{\rho_- - \rho_+} \quad \text{and} \quad D = \frac{1}{2}(D_- + D_+) \quad (2.13)$$

2.2.1 Models based on the TASEP

Two examples for models based on the TASEP show its huge versatility. The first one is a mapping of the TASEP to a model for surface growth [61]. In the second part a model for vehicular traffic is discussed [65]. Although some extensions are necessary the TASEP-case is still recovered for an appropriate choice of parameters.

Surface Growth

Instead of modelling a stream of particles also an exact mapping to a model of surface growth exists. Although not discussed here the (T)ASEP has also been studied extensively in this context in connection with the KPZ-equation [27, 64, 78]. The configuration of particles on the one-dimensional lattice used for the (T)ASEP is mapped onto the slope of stacks of particles on a two-dimensional lattice (see Fig. 2.4). The presence of a particle at site i leads to a decrease of slope from one particle stack to another:

$$m_i(t) = h_{i+1}(t) - h_i(t) = 1 - 2c_i(t). \quad (2.14)$$

As $c_i(t) \in \{1, 0\}$ slope $m_i(t)$ might only change from $+1$ to -1 or vice versa. Although height might locally increase by 2 the height difference between two neighboring sites only changes by one. In that sense the mapping leads to a

¹ opposite to driving direction

single-step growth model [61,78]. The boundary conditions from the (T)ASEP can be chosen accordingly to those of the surface.

As the mapping is exact some relations between quantities characterising the particle movement and the surface growth exist. A particle leaving an empty site always increases height h_i by two as it has to decrease m_i by one. This leads to

$$h_i(t + 1) = h_i(t) + 2. \tag{2.15}$$

As the number of particles passing site i in a time-interval ΔT is given by $\Delta T \cdot F$, this relates the velocity of surface growth to the flow F in the TASEP:

$$\Delta h = v_{sf} \cdot \Delta T = 2N = 2 \cdot \Delta T \cdot F \Rightarrow v_{sf} = 2F. \tag{2.16}$$

The particle number N and the corresponding number of holes $L - N$ (unoccupied sites) can be used to calculate the average slope of the surface:

$$M = \frac{(L - N)(+1) + (N)(-1)}{L} = 1 - 2\frac{N}{L} = 1 - 2\rho. \tag{2.17}$$

Obviously the average slope is identical to the average velocity found for the second-class particles. By definition these particles sit at a domain-wall from a low- to a high-density region which corresponds to a local maximum of the surface. The domain-wall corresponding to a change in the density-profile from a high- to a low-density area is obviously equivalent to a local minimum. Making use of another kind of passive particle invented in the context of surface-growth models one is able to trace both kinds of domain-walls in the TASEP [64].

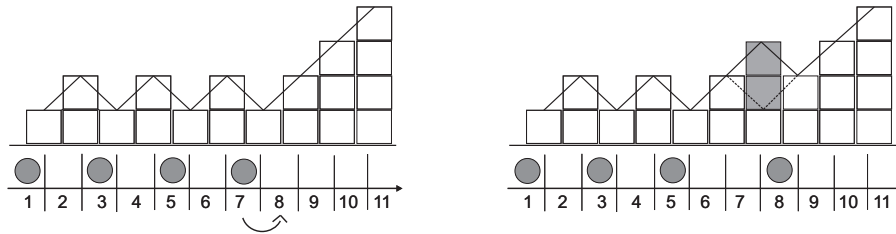


Fig. 2.4. The TASEP mapped to surface growth: The left part of this figure shows the surface corresponding to a homogeneous distribution of particles on the (T)ASEP-lattice. As only local slopes of ± 1 are possible, the surface is slightly rough. The hopping of two particles at succeeding updates results in the surface shown on the right.

The Nagel-Schreckenberg Model

One of the prominent examples for modelling based on an extended TASEP is the Nagel-Schreckenberg model of highway traffic [65]. Basically the model

consists of a one-dimensional TASEP with time-parallel update. In fact full equivalence is recovered for an appropriate choice of parameters.

The model of Nagel and Schreckenberg belongs to the class of probabilistic cellular automaton models. N cars move along a one-dimensional lattice of length L (see Fig. 2.5). The state of each car is characterised by its position $x_n \in \{1, \dots, L\}$ and velocity $v_n \in \{0, \dots, v_{max}\}$. So obviously the state variables as well as the derived quantities like density $\rho = \frac{N}{L}$ or the distance $d_n = x_{n+1} - x_n - 1$ between two succeeding cars are discrete. Nearly all interactions are incorporated into determining the number of cells $v_n(t+1)$ by which the n th car is moved, during the next update step. Different rules are applied leading to a structure of substeps. As a parallel update is used, the rules are applied synchronously to all cars.

Step 1: Acceleration

If $v_n < v_{max}$, increase velocity by one:

$$v_n(t + \frac{1}{4}) = \min \{v_n + 1, v_{max}\}$$

Step 2: Braking

If $d_n \leq v_n$, reduce velocity to $d_n - 1$:

$$v_n(t + \frac{2}{4}) = \min \{v_n, d_n - 1\}$$

Step 3: Noise

If $v_n > 0$, reduce velocity to $v_n - 1$ with probability p :

$$v_n(t + \frac{3}{4}) = \max \{v_n - 1, 0\} \text{ with probability } p$$

Step 4: Driving

Move car with velocity $v_n(t+1)$:

$$x_n(t+1) = x_n + v_n(t+1)$$

The first step just increases velocity by one unit as long as the maximum velocity v_{max} is not reached which is one of the models parameters. As this is the same for all cars, it corresponds to a speed limit rather than to the maximum of attainable speed which might be different for different vehicles. Overall this step reflects the wish of the drivers to move as fast as possible. The wish is of course restricted by the desire to avoid collisions. So in the second step, velocity is decreased such that collisions are avoided. For incorporating time latencies, only distance d_n at time t is incorporated. It turns out, that this is already sufficient

for reproducing basic properties of real traffic flow [19]. The third step describes some randomness in the drivers' behaviour by introducing a stochastic element namely the braking noise p . One reason is just that even on an uncrowded road where in principle driving is possible at an exactly constant speed v_{max} , small fluctuations are observed. But as density is low, the resulting effect will be small. The main effect of this step is the introduction of an asymmetry between acceleration and deceleration. Acceleration (if possible) takes place with probability $1 - p$ whereas deceleration occurs with probability p . This kind of asymmetry is also observed empirically (e.g. [34]). It originates just from the fact that braking leads to a stronger change in velocity than accelerating. So in the worst case a car brakes due to step 2 and slows down further due to step 3. The result might be the reduction of velocity by two units at one update whereas velocity can just increase by one unit per update. After applying the first three steps, velocity at time $t + 1$ results in the movement of cars in step 4 by $v_n(t + 1)$ sites.

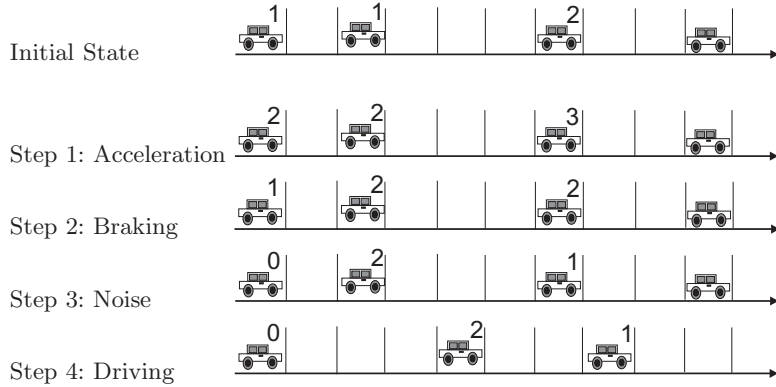


Fig. 2.5. Nagel-Schreckenberg model: The figures show the update procedure which basically consists of the application of the hopping rules to all cars at the same time. For this particular example the maximum velocity was set to $v_{max} = 3$. In case of $v_{max} = 1$ the model turns out to be equivalent to the TASEP with time-parallel dynamics.

In comparison to the *TASEP* hopping now is allowed by more than one cell in a particular direction at one update. The number of cells for hopping is set according to the rules incorporating the drivers' behaviour. As the cars ability to accelerate (and decelerate) is limited by inertia velocity can only increase by one unit per update. This induces some kind of memory to the process as the actual velocity depends on the velocity before the last update at $t - 1$. Also velocity itself is limited by v_{max} . With respect to reality a time-parallel update appears most realistic. It has been shown that some of the main features like

the occurrence of phantom jams [19, 65] depend on the use of that particular update procedure and also on the choice of $v_{max} > 1$.

For simulating real traffic flow parameters have to be chosen in accordance with the traffic system. A size of 7.5 meters for each cell is widely used. Although this is not the actual length of a normal car also larger vehicles like trucks are incorporated. Using that cell size leads to a density of one for (non-moving) vehicles forming a traffic jam. Typically vehicles are not waiting "bumper to bumper" so the cell size also incorporates some kind of minimal distance.

As already mentioned velocity is limited to v_{max} for example by a speed limit. Also here a finer discretisation of velocity steps would be possible. For a German freeway the maximal velocity is frequently assumed to be $120 \frac{km}{h}$. So one identifies $v_{max} = 5$ with $120 \frac{km}{h}$. The randomisation parameter p is frequently set to $p = 0.5$. Overall the length of one timestep using the latter set of parameters is given by:

$$\frac{7.5m}{cell} \times \frac{[5 - (0.5 \times 1)] cell}{time - step} \times \frac{3.6sec}{120m} \approx 1 \frac{sec}{time - step} \quad (2.18)$$

For calculating the time-scale the maximum velocity reduced by one unit through randomisation has been used. In comparison to reality the duration of one time-step is of the same order of magnitude as the typical reaction time of a driver. So this is in good agreement with the interpretation of the time-parallel update for incorporating time-latencies.

Simulation results from the Nagel-Schreckenberg model show some resemblance to real traffic data [19]. The fundamental diagram for $v_{max} = 5$ exhibits features like the freeflow and the jammed state (see Fig. 2.7). At low densities flow shows a linear increase. Cars in principle can move at their desired velocity v_{max} . In the deterministic case of vanishing braking noise $p = 0$ no fluctuations in the drivers behaviour occur². Due to the model's rules cars will distribute homogeneously on the road (lattice). As long as the distance to the preceding car is large enough ($d_n \geq v_{max}$) cars are able to move constantly at v_{max} . The density at which cars begin to block each other therefore depends on v_{max} :

$$\rho_{max} = \frac{N}{L} = \frac{N}{N(v_{max} + 1)} = \frac{1}{v_{max} + 1}. \quad (2.19)$$

For $\rho > \rho_{max}$ the average distance per car is given by $\bar{d} = \frac{1}{\rho} - 1 = \bar{v}$ and is equal to the average velocity \bar{v} . Overall flow in both regimes is given by:

$$F(\rho) = \begin{cases} v_{max}\rho & \text{for } \rho < \rho_{max} \\ 1 - \rho & \text{else} \end{cases} \quad (2.20)$$

For $0 < p < 1$ roughly the same behaviour is observed. One finds that due to fluctuations the transition to the jammed state occurs for $\rho < \rho_{max}$. The corresponding spatial pattern of the jammed state is shown at (see Fig. 2.7).

² In case of $p = 1$ a car is not able to increase velocity once $v_n = 0$ has been reached.

High density areas namely jams caused by fluctuations emerge and start travelling against the driving direction. But also due to fluctuations they dissolve again.

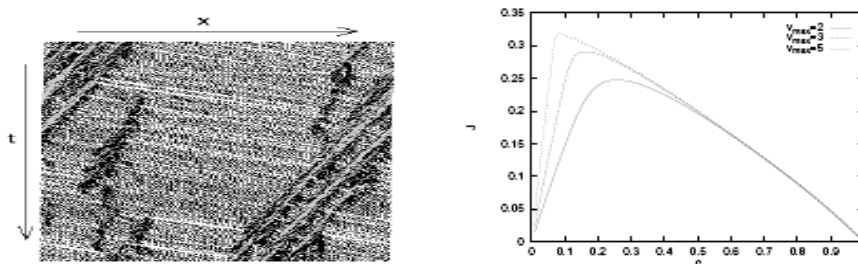


Fig. 2.6. Space-time plot and fundamental diagram: The space-time plot shows the lattice configuration for $\rho = 0.2$, $p = 0.25$ and $v_{max} = 5$. The fundamental diagram shows flow for different values of v_{max} and $p = 0.25$. For $v_{max} = 1$ the TASEP with time-parallel update is recovered (taken from [18]).

As shown above the distance between cars is a crucial quantity for characterising traffic states. So additionally distance headway distributions are of interest. In case of $v_{max} = 1$ basically the *TASEP* is recovered (see Fig. 2.6). At low densities distances show a quite broad distribution. With increasing density or equivalently decreasing available space the distribution gets less broad. The probability for $d_n = 0$ obviously corresponds to mutual blocking leading to $v_n = 0$. So the probability for $d_n = 0$ increases with increasing density. Using analytical results originating from investigations of the TASEP with time-parallel update the probability for d_n is exactly known (e.g. [19]). For $d_n > 0$ one observes a monotonic decrease. For large velocities in case of $v_{max} = 5$ roughly the same behaviour is found. A local maximum of probability at $v_{max} = 5$ reflects the fact that cars try to attain $d_n \leq 5$.

Besides distance headways also time headways and single-car velocity distributions are used for a microscopic characterisation of traffic flow [34, 50]. Each of the latter quantities has a corresponding macroscopic one [60]. Distance headways correspond to density, time headways to flow and single-car velocities contribute to the average velocity. Some of them will be used for the investigations of ant-traffic in chapter 5.

2.3 The TASEP with Static Disorder

Another way of extending the TASEP for describing real systems is to incorporate different kinds of quenched disorder. Two choices appear to be natural.

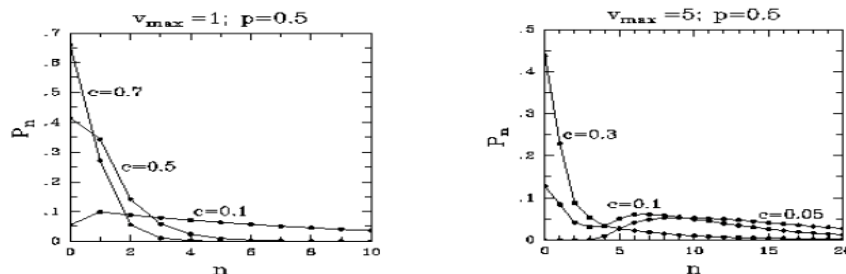


Fig. 2.7. Distance headway distribution: For different values of ρ and $v_{max} = 1$ (left), 5(right) at $p = 0.5$ the distribution of distance headways has been measured. On the left basically the distribution for the TASEP case is shown. For a larger range of attainable velocities maximums are shifted to higher densities (taken from [18]).

First one can introduce hopping rates depending on the particle i itself (particlewise disorder). So one sets hopping rates according to $p = p_i$ which are independent of the particles' position or time evolution. Complementary the second kind of disorder assigns hopping rates depending on the particles' position x_i (latticewise disorder). So hopping rates are set according to $p = p(x_i)$. In this case the modified hopping rate of each particle is time independent in the sense that p only depends on the position x_i itself. Generally all particles are affected in the same way. As a common feature of both types of disorder phase separation depending on the global particle density is observed. The emerging high- and low-density areas are in analogy to the shocks already known from plain TASEP with open boundaries. Basically the time evolution towards stationarity as well as the stationary state itself are of interest. The formation of these high-density regions the so-called coarsening, during time evolution from a random initial distribution, has been studied in great detail [15, 38, 39, 53]. In the stationary state one is interested in the spatial distribution of particles depending on the global density.

Both kinds of disorder are encountered quite frequently. For example in vehicular traffic vehicles are generally not identical (e.g. different drivers, cars, trucks), leading to different driving characteristics. The resulting distribution of velocities can be used to assign different hopping rates. But also latticewise disorder is found quite frequently. Accidents or construction works, different local slopes of the road but also other inhomogeneities like different speed limits or on- and off-ramps might change the behaviour of the vehicles depending on the environment (e.g. [49]).

2.3.1 Particlewise Disorder

The TASEP with particlewise disorder has been studied in great detail. This was done for a random distribution of hopping rates [53, 54]. Also a mapping to

the *zero-range process* [54, 78] and models of coalescence [27] has been shown. Basically the formation of phase-separation as well as the dependence on the global density have been investigated. For a later comparison to the ant trail models a brief summary of the properties of the stationary state will be given.

Generally the particles tend to move with an average velocity $v_i = p_i$ if they are not blocked by another one. Due to the simple exclusion principle the "faster" particles accumulate behind the slower ones which determine the average velocity of all other particles:

$$v = \min_{i \in [1, N]} \{p_i\} \quad \text{for } \rho < \rho_c. \quad (2.21)$$

In the stationary state a platoon moving with velocity v is formed (see Fig. 2.8). Like in the *TASEP* a characterisation using the density profile is possible. But the system is still translational invariant so phase-separations will not be localised. Therefore densities have to be measured relative to the moving system. Otherwise one just obtains a flat density profile as the platoon moves along the lattice with constant average velocity. By definition a second-class particle will follow the left end of the moving high-density area namely the platoon as this is just a domain-wall from $\rho_- = 0$ to $\rho_+ > 0$. Measuring densities seen from that position will be used for characterising the structure of the particle distribution.

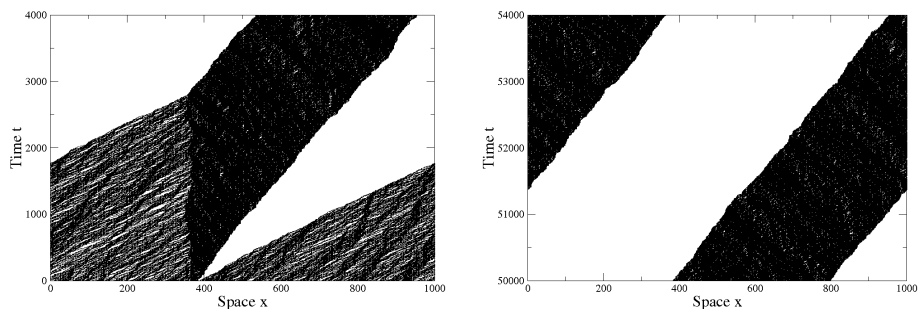


Fig. 2.8. Space-time plot: On the left the coarsening process out of a homogeneous distribution of particles in the initial state is shown. In the stationary state particles have accumulated behind the slowest one, forming a platoon. For that particular example only one "slow" particle with $p_1 = 0.1$ and "fast" particles with $p_i = 1 \forall i \in \{2, \dots, N\}$ have been used.

The density $\langle c_i \rangle := \rho_i$ at the site in front of the i th particle now defines the density profile. So densities are measured with respect to the moving particles.

Under the assumption that a mean-field description is still reasonable one finds

$$(1 - \rho_i)p_i = v = \text{const.} \quad \forall i \in [1, N] \quad (2.22)$$

as all particles within the platoon have to move with the same average velocity v . As long as the global density ρ is low enough this regime exists. For a later comparison to the ant trail models it is sufficient to restrict to $p_i =: p > I \quad \forall i \in \{2, \dots, N\}$ and $p_1 := I = v$. In case of $\rho = 1 - \frac{I}{p} = \rho_c$ obviously no difference between the high- and low-density area can be made. The first particle leading the platoon is also blocked with probability ρ like all the other particles. The two different regimes can be distinguished using second-class particles (see Fig. 2.9, right). In the jammed phase the second-class particle moves with the velocity of the platoon. As $\rho_- = 0$ there is only drift and no diffusion. At high densities particles are distributed homogeneously. The velocity of the second-class particle now depends on the global density according to (2.10).

The density profile seen from the moving system can also be used for measuring the cluster length. By definition the cluster is the number of consecutive sites (particles) with $\rho_i > \rho$ thus belonging to the high-density area:

$$l := \max_{i \in [1, N]} \# \left\{ \text{sites } i \mid (\rho_i, \rho_{i+1}) > \rho = \frac{N}{L} \right\} \quad (2.23)$$

In the stationary state only one cluster exists comprising all particles of the system. Depending on the impurity hopping rate I a linear increase is observed (see Fig. 2.9, left). From (2.22) one also would have expected that kind of behaviour as the mean-field platoon length is given by:

$$\rho_i = 1 - \frac{I}{p_i} = \frac{N}{l} \quad \text{leading to} \quad l = L \left(\frac{\rho}{1 - \frac{I}{p}} \right) \quad \text{for } p_i =: p \quad (2.24)$$

From (2.24) one observes that the density ρ_i is independent of the particle number N . So an increase of the global density is compensated by an increase of the cluster length and thus does not lead to an increase of ρ_i . The platoon length increases until the global density ρ reaches the density within the moving platoon ρ_i . As a result no difference between the densities ρ_i and $\rho = \frac{N}{L}$ can be made anymore as $\rho_i = 1 - \frac{I}{p} = \rho$. The cluster length reaches the system size. Now also the leading particle becomes blocked and flow recovers the TASEP case. Nevertheless also the limitations of the mean-field picture become visible. From (2.24) the cluster dissolves for $l = L$. But one observes that depending on I the cluster dissolves even for $\rho < \rho_c$ (see Fig. 2.9, left) before $l = L$ is reached. With increasing defect hopping rate obviously fluctuations also increase which are not incorporated by the mean-field approximation.

It has been pointed out that the transition from particles distributed homogeneously on the lattice $\rho > \rho_c$ to the platoon $\rho < \rho_c$ exhibits some analogy to the *Bose-Einstein condensation* [54]. The unoccupied sites, namely the holes, are considered as bosons and the particles as states. For $\rho > \rho_c$ most holes are distributed homogeneously. Each state is occupied with probability $(1 - \rho)$

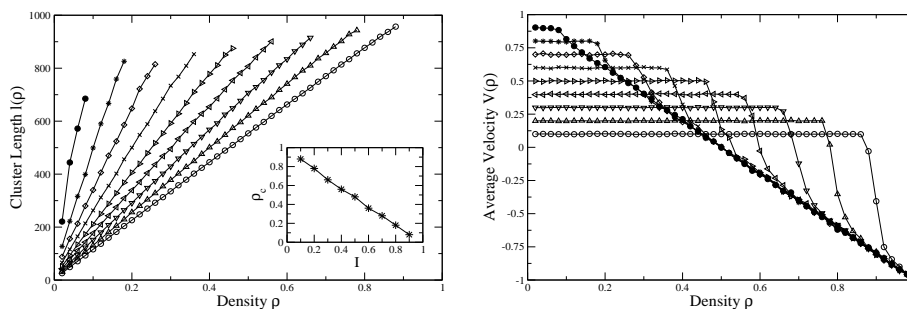


Fig. 2.9. Cluster length and velocity of the second-class particle: ($Q = 1, I = 0.1$ (\circ), 0.2 (Δ), 0.3 (∇), 0.4 (\triangleleft), 0.5 (\triangleright), 0.6 (\times), 0.7 (\diamond), 0.8 ($*$), 0.9 (\bullet)). On the left the increase of the platoon length with increasing global density ρ is shown. At a sufficiently high density $\rho_c = 1 - I$ (inset) the platoon vanishes. On the right the velocity of the second-class particle is shown. For $\rho < \rho_c$ the particle performs drift following the platoon. At $\rho > \rho_c$ the TASEP is recovered.

at least for the *TASEP* with random-sequential dynamics. By reducing global density below ρ_c platoon formation takes place. Holes are distributed within the platoon with probability $(1 - \rho_i) = \frac{I}{p_i}$. Depending on the platoon length the leading particle or equivalently the ground state has an occupation number of $N_1 = L - l$. In comparison to the others the leading particle has the largest number of holes in front of it. Bosons obviously are condensed in the corresponding state. This has also been found in case of time-parallel update [27]. Nevertheless this analogy is of a formal nature as bosons within an ideal Bose gas are non-interacting. They also condensate in real-space instead of momentum-space. But as particles in the *TASEP* are interacting this is also true for holes. Even the choice of the update-procedure can induce interaction. A time-parallel update induces particle-hole attraction or equivalently hole-hole repulsion.

The stationary state is characterised using fundamental diagrams. According to the already observed behaviour the average velocity stays constant for $\rho \in [0, \rho_c(I)]$. Flow shows a linear increase. For $\rho \in [\rho_c(I), 1]$ all particles have the same probability of being blocked. Obviously the TASEP case is recovered as mutual blocking dominates over different hopping rates.

2.3.2 Latticewise Disorder

Also the TASEP with quenched latticewise disorder has been studied in great detail [38, 39, 81, 82]. In comparison to particlewise disorder a larger number of variations has been introduced. With respect to a comparison to the features of the ant trail model we will focus here only on two of them. The most simple case is just one defect site i_0 . Particles hopping from i_0 to $i_0 + 1$ have a reduced hopping rate $I < p$. At all other sites hopping takes place with rate p . With respect to reality also the case of extended defects $p(x_i) = I \quad \forall i \in \{i_1, \dots, i_2\}$

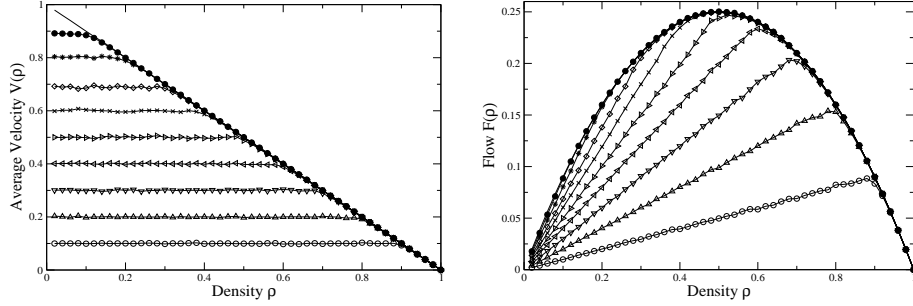


Fig. 2.10. Fundamental diagrams: ($Q = 1$, $I = 0.1$ (\circ), 0.2 (Δ), 0.3 (∇), 0.4 (\triangleleft), 0.5 (\triangleright), 0.6 (\times), 0.7 (\diamond), 0.8 ($*$), 0.9 (\bullet)). For $\rho < \rho_c$ the average velocity stays constant and flow increases linearly. At sufficiently high densities finally the TASEP case is recovered.

will be of interest. Other variants not being discussed here are for example a random distribution of defect sites [81, 82].

Starting from the spatial pattern exhibited by a system with one defect site one again observes a separation into a high- and low-density phase. Unlike in the case of particlewise disorder the areas are localised (see Fig. 2.11).

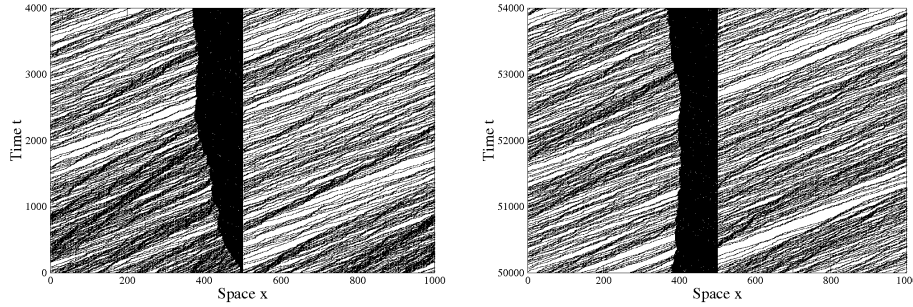


Fig. 2.11. Space-time plot: The left figure shows the formation of high- and low-density areas. On the right the stationary state has been reached. On the left of the defect site $x_{i_0} = 500$ a high density area has formed.

As the density areas are static besides fluctuations at the boundaries [38, 39] this should also be visible in the second-class particles velocity (see Fig. 2.13, left). Depending on the global density one observes three regimes. Fluctuations obviously increase with increasing defect rate I (see Fig. 2.13, left, inset). Like in the case of particlewise disorder phase separation takes place starting at a density ρ_- and ending at ρ_+ (see Fig. 2.13, right, lower inset). One observes a particle-hole symmetry $\rho_- = 1 - \rho_+$. This can also be seen in measuring

the length of the localised particle cluster namely the high-density regime. The cluster length obviously increases linearly with the global density (see Fig. 2.13, right). Investigating the density profile directly shows that this linear increase compensates additional particles originating from increasing the global density in such a way that the density in the high-density area stays constant (see Fig. 2.13, right, upper inset). This is possible until the cluster length reaches a critical value. Then an increase of the particle number can no longer be compensated. As a result the global density exceeds the density inside the high-density area ρ_+ which obviously ceases to exist. In a similar way the existence of a lower bound ρ_- for the regime can be explained. As long as the global density is below ρ_- the system obviously is not able to segregate into a high- and a low-density area.

The fundamental diagrams also exhibit the three regimes already identified. The average velocity shows a strict monotonic decrease. But flow exhibits a characteristic feature (see Fig. 2.12 left). Depending on the defect rate I flow becomes independent from density. The so-called plateau regime extends from ρ_- to ρ_+ . For densities smaller than ρ_- and larger than ρ_+ the behaviour known from TASEP is recovered.

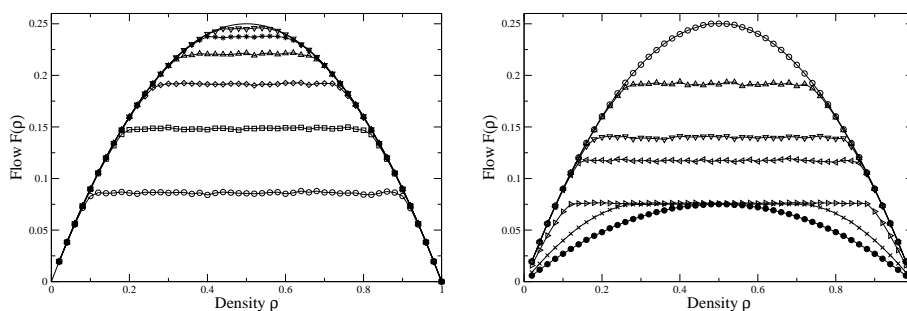


Fig. 2.12. Fundamental diagrams: On the left for one defect site with $Q = 1$, $I = 0.1$ (\circ), $0.2(\square)$, $0.3(\diamond)$, $0.4(\triangle)$, $0.5(*)$, $0.6(\nabla)$, 1 (solid line). The right figure shows flow for sitewise defects ($Q = 1$, $I = 0.3$) extending over $\frac{L}{I} = 1(\bullet)$, $0.5(\times)$, $0.1(\triangleright)$, $0.0003(\triangleleft)$, 0 (\circ). As a common features plateaus in flow exist.

Incorporating the described mechanisms a phenomenological approach has been developed for the case of random-sequential dynamics. Assuming a flat density profile within the macroscopic high- and low-density area flow is given by:

$$F_-(\rho_-) = \rho_-(1 - \rho_-)p \quad \text{and} \quad F_+(\rho_+) = \rho_+(1 - \rho_+)p \quad (2.25)$$

In accordance to the previous observations (see Fig. 2.13 right, upper inset) the particles can be assumed to be distributed homogeneously within the high-

and low-density region. As the global density stays constant in time by definition flow must be conserved due to the continuity equation: $F_- = F_+$. This leads to the already observed property of the density profile: $\rho_+ = 1 - \rho_-$.

Assuming that the region of decrease from ρ_+ to ρ_- at the defect site is negligible, the flow through the defect is given by:

$$F_d(\rho_-, \rho_+) = \rho_+(1 - \rho_-)I = \rho_+^2 I = (1 - \rho_-)^2 I \quad (2.26)$$

As discussed the homogeneous distribution of particles namely the TASEP case is recovered for $\rho < \rho_-$ and $\rho > \rho_+$. The corresponding flow is then given by (2.25). For densities $\rho_- < \rho < \rho_+$ flow stays constant. Incorporating the flow through the defect site, the conservation of particles leads to:

$$\rho_+ = \frac{p}{I + p} \quad \text{and} \quad \rho_- = \frac{I}{I + p} \quad (2.27)$$

So overall the boundaries of the density regimes as well as the constant value of flow within the plateau regime (e.g. $F = \rho_+(I, p)[1 - \rho_+(I, p)]$) are given by the two hopping rates I and p .

Making use of the latter results the length l of the high-density regime can be calculated. For a total number of N particles one finds:

$$N = l\rho_+ + (L - l)\rho_- \quad \text{leading to} \quad l(\rho) = L \left(\frac{\rho - \rho_-}{\rho_+ - \rho_-} \right) \quad (2.28)$$

For $\rho < \rho_-$ the cluster length becomes negative. It reaches the system length for $\rho = \rho_+$. This is in analogy to a system with particlewise disorder where the leading particle becomes blocked as the platoon length reaches the system size. Overall the cluster-regime extends from $l(\rho_-) = 0$ to $\rho_+ = L$. Again the mean-field picture fails to incorporate fluctuations (see Fig. 2.13 right). With increasing defect rate I the measured cluster length at the boundaries of the cluster-regime is above zero and below the system size L .

As an extension also multiple impurity-sites can be treated. One also finds the same basic properties like particle-hole symmetry as in the previously discussed case (see Fig. 2.12 right). With increasing number of defect sites or defect-length in case of consecutive defects the plateau value decreases. A lower bound is given by the flow for a system with homogeneous hopping rate equivalent to the defect rate. Finally the plateau breaks down as approximately the TASEP case with hopping rate I is recovered.

Applying the same approach to multiple sites [81, 82] is also in good agreement with the simulations. As multiple shocks from ρ_- to ρ_+ exist the approximation is not as good as in the discussed case where only the increase for one shock has been neglected.

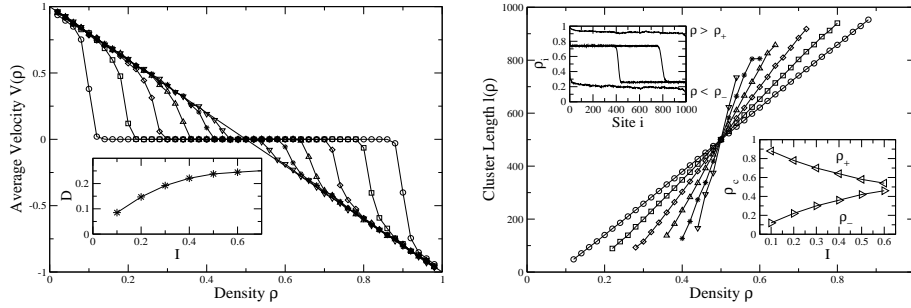


Fig. 2.13. Cluster-length and velocity of the second-class particle: ($Q = 1$, $I = 0.1$) (\circ), $0.2(\square)$, $0.3(\diamond)$, $0.4(\triangle)$, $0.5(*)$, $0.6(\nabla)$, 1 (solid line)). For intermediate densities $\rho_- < \rho < \rho_+$ the domain-wall separating ρ_- and ρ_+ performs no drift as $v = 0$. Nevertheless fluctuations occur with increasing defect rate as shown by the inset. The length of the high-density area is measured analogous to the preceding section. For $\rho_- < \rho < \rho_+$ a linear increase is found. The density profiles corresponding to that regime have the same value ρ_+ as shown in the inset. For $\rho < \rho_-$ and $\rho > \rho_+$ a flat density profile like in the TASEP is recovered (see upper inset).

3 The Unidirectional Model

Based on the *TASEP* we have developed models for traffic on preexisting uni- [16] and bidirectional ant trails [45, 56, 76]. Both cases will be discussed in the following two chapters. The plain *TASEP* has been extended such that the most important or universal features of real *ant-traffic* are captured. So the terms agent, particle and ant will be used interchangeably depending on the actual context. The model for uni- as well as the models for bidirectional traffic will be discussed in comparison to reality in chapter 5. The focus of the next two chapters therefore will be on the physics exhibited by the models. Generally the incorporated means of interaction induce some kind of disorder similar to the kinds already discussed (see chapter 2). This will be subject of the subsequent investigations which can be divided into two parts. In the initial state particles are distributed homogeneously on the lattice. Due to different mechanisms of particle-particle interaction they will form clusters. Like in the case of static particlewise disorder phase separation into low- and high-density areas namely the emergence of clusters is observed. The formation of clusters or equivalently the coarsening behaviour will be discussed. At the end of this process the system has evolved into the stationary state. This state will be characterised by the corresponding fundamental diagrams which are closely related to the spatial distribution of particles.

3.1 Definition

The unidirectional ant trail model (*ATM*) was introduced [16] as an extension of the *TASEP*. Ants move strictly in one direction on a lattice with L sites. Each site may be occupied by one of the N ants or is empty. Extending the *TASEP*, ants leave marks, so-called pheromones, at sites they occupy. So each site might also be marked or not by a pheromone (see Fig. 3.1). If a site is not occupied by an ant but by a mark also evaporation, namely the removal of the mark with rate f , takes place. Otherwise in presence of an ant at that site the mark is not removed. Unlike in the *TASEP*, the hopping rate p of particles is

not constant but depends on the presence or absence of pheromone marks at the next nearest neighbour site $i + 1$. If a mark is present, the hopping rate is $p = Q$, whereas in absence of a mark it is $p = q < Q$. So the presence of pheromone marks leads to an increase of the hopping rate from q to Q .

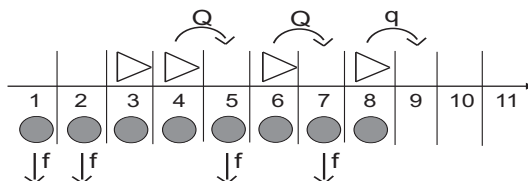


Fig. 3.1. Definition of the unidirectional ATM: The hopping probability p depends on the presence ($p = Q$) or absence ($p = q$) of a pheromone-mark at site $i + 1$. As $q < Q$ the presence of marks leads to some kind of particle-particle attraction. In comparison to the TASEP the marks induce different hopping rates, depending on the distance to the preceding particle. Generally particlewise disorder is induced dynamically.

For first investigations we use periodic boundary conditions. Employing the extremal principle (see (2.7) and (2.8)) one easily obtains the flow for the open system. It has been shown by direct numerical investigations [57] that the main feature of the unidirectional *ATM* does not depend much on the boundary conditions. For simplicity random-sequential dynamics are used due to the absence of update-induced correlations. But also here the main features are not much affected by the choice of an particular update procedure. This has been confirmed by direct numerical investigations for the case of a time-parallel update [16, 45].

3.1.1 Some Aspects Concerning Reality

This section gives a brief survey of some basic aspects of modelling employing the introduced unidirectional *ATM*. Most of the discussion is also valid for the other traffic models which are compared to the unidirectional *ATM*. Also the bidirectional *ATMs* are based on the unidirectional one (see chapter 4). For a more detailed discussion of the ant trail models vs. reality we refer to chapter 5. Finally the results will be used for constructing an experimental setup.

Trail Topology

The unidirectional *ATM* obviously assumes a preexisting trail with only one lane. So like in vehicular traffic a single lane road already exists. Although ant trails are known to be highly dynamic and generally have more than one lane [13, 21] quasi one-dimensional situations are found quite frequently on real trails [36].

Properties of the Moving Agents

Like in vehicular traffic the modelled agents namely the ants might differ quite strongly in size. This property of ant species known as *polymorphism* [36] can lead to much larger differences in size than encountered in vehicular traffic. Nevertheless an appropriate choice of cell-size with respect to reality can be made if the differences are not too large or the observed species is *monomorphic*. More severely with respect to reality a possible load is neglected. Depending on the carried load or the direction of movement (e.g. nestbound or outbound) different behavioural patterns are likely to emerge [11, 12, 36]. But for first investigations we will neglect this. The only kind of interaction besides mutual blocking is just the attraction via pheromone marks.

Velocity of the Moving Agents

Taking the *Nagel-Schreckenberg* model as some kind of prototype for modelling vehicular traffic some crucial differences become visible. In comparison to the *Nagel-Schreckenberg* model the *ATM* uses $v_{max} = 1$. As a result there is nothing like a velocity memory. Ants accelerate within one update to the desired velocity which is described by the hopping rate p . This incorporates the fact that ants can change velocity on much shorter time-scales than cars. For that reason the velocity distribution can be expected to be more narrow. The *Nagel-Schreckenberg* model as well as the *ATMs* both do not incorporate any overtaking. Like in vehicular traffic this is also reasonable for certain traffic scenarios found on ant trails.

Due to $v_{max} = 1$ the modeled ants perception can be limited to the next neighboring site. So with respect to reaction time the random-sequential update does not incorporate any time-latencies. In comparison to cars, ants tend to interact "bumper to bumper" [11, 31, 36]. One crucial difference is also the absence of a deterministic limit due to the random-sequential dynamics. But also velocity is modeled in a completely stochastic way. One reason is the uncertainty about the mechanisms involved. By employing stochastic hopping one expects some kind of behaviour on average but also some fluctuations around the expectation values. The second reason is the intrinsic stochasticity found in ant behaviour [6, 13].

3.1.2 Exact Mapping to Other Models

The crucial difference of the unidirectional *ATM* to the *TASEP* is the use of different hopping rates. But the evaporation probability f can be chosen such that the *TASEP* is recovered. In case of instantaneously evaporating pheromones ($f = 1$) all particles hop with rate $p = q$. For ($f = 0$) no evaporation takes place and all particles hop with $p = Q$ in the stationary state.

But also without restricting the choice of parameters an exact equivalence to a well-established model namely the *bus route model (BRM)* exists. After

reinterpreting the variables, the unidirectional *ATM* can be used for describing traffic of busses picking up passengers at a line of bus stops [68, 69] which constitute the L sites of a one-dimensional lattice. Passengers arrive at the bus stops with rate λ if no bus is already there. A bus reaching a site occupied by passengers has to stop and thus moves with a reduced hopping rate β . At an unoccupied site the hopping rate is $\alpha > \beta$. For simplicity no difference between the number of passengers waiting at a bus-stop is made.

The equivalence to the unidirectional *ATM* can be seen by identifying busses with ants and busstops as already mentioned with lattice sites (see Fig. 3.2). The absence of passengers at a site leads to a higher hopping rate α , unoccupied sites therefore correspond to a marked site in the *ATM*. So the arrival of passengers is equivalent to the evaporation of pheromone marks. Therefore the arrival rate λ of passengers is equivalent to the evaporation rate f of the pheromones.

Originally the bus route model was formulated with random-sequential dynamics and periodic boundary conditions. Due to the equivalence to the unidirectional *ATM*, also the effects observed in the *BRM* are stable against the particular choice of dynamics and boundary conditions (e.g. [45, 57]).

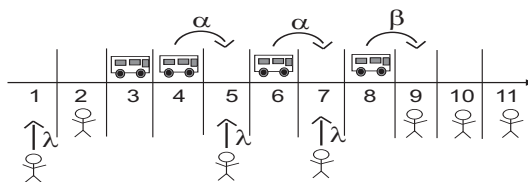


Fig. 3.2. Definition of the BRM: This figure shows the definition of the bus route model. In comparison to the unidirectional ATM hopping rates are related over $\alpha = Q$, $\beta = q$, $f = \lambda$. The presence of passengers leads to a lower hopping rate and is therefore equivalent to the absence of pheromone marks in the unidirectional ATM and vice versa.

Due to its simplicity one might wonder how realistic the BRM can be. For example no difference between the number of waiting passengers is made. The waiting-time and the hopping rates are independent from the number of waiting passengers. Although the construction was based rather on theoretical interest than on the intention to describe reality (stated in [68]) some basic features are already captured. One aim in that context is to have a minimal waiting time of passengers for all bus stops. This can be achieved only by a homogeneous distribution of busses. So one would like to avoid the clustering of busses emerging for a particular choice of arriving rate of passengers and number of busses. The same feature with a different interpretation is also exhibited by the *ATM* and will be discussed later on. In the context of ants clustering is a commonly observed phenomenon [21, 36]. Extensions of the bus route model

have been developed. One possibility is to incorporate the limited capacity of busses as well as the number of waiting passengers [40].

3.2 Properties of the Unidirectional ATM

For investigating the properties of the unidirectional *ATM* we start with the spatio-temporal distribution of particles. This is done for the system evolving out of a homogeneous distribution of particles and for the stationary state. The characteristic features of the model can already be observed. But also with respect to reality first empirical observations will concern with the directly observable traffic patterns (see chapter 5).

Therefore the discussion is divided into two parts. First a description of the time evolution towards the stationary state will be given. The stationary state itself will be characterised employing the same tools already used for investigating the *TASEP*.

3.2.1 Observed Patterns

Starting from the initial state particles are distributed homogeneously on the lattice (see Fig. 3.3 left). During time evolution particles form clusters while still moving. Those clusters are not compact with a local density of 1 as otherwise nearly no movement would be possible. The term "loose cluster" has therefore been established [66]. Particles finally form one large cluster comprising all particles of the system (see Fig. 3.3 right). As the number of particles is still finite, dissolving due to the stochastic nature of the system can be expected. Nevertheless only minor dissolving on short time scales are observed (see Fig. 3.3 right, inset).

Generally patterns resembling those known from the *TASEP* with particle-wise disorder are found [53,54]. The mechanism of cluster formation is obviously based on the different hopping rates induced by the pheromone marks. So one observes a decrease in the slope of the particles' trajectories catching up to preceding ones. This decrease corresponds to an increase of speed of the particles catching up. Finally particles will accumulate behind the one with the lowest hopping rate. During the coarsening process this obviously happens locally for few particles leading to small clusters. Finally at late times all small clusters have merged into one single cluster. From that point of view even a single particle behaves like a cluster of unit-length.

For the mechanism of inducing different hopping rates the following picture turned out to be useful. Each particle is followed by a trace of pheromones. As the pheromones are evaporated this trace is of finite length determined by the evaporation rate f . Due to the stochasticity of the process particles might even approach each other just like in the *TASEP* due to fluctuations. A particle i not perceiving a pheromone trace will move with average velocity $v_i = q$. If the directly following particle $i - 1$ gets close enough its average velocity is

increased to $v_{i-1} > v_i = q$ by the presence of the pheromones. Finally it will catch up with the slower one forming a platoon. Generally the velocity depends on the distance to the preceding cluster.

In a finite system this cluster can also dissolve due to fluctuations and reform at a different position.

As already mentioned the unidirectional *ATM* reduces to the *TASEP* for an appropriate choice of the evaporation rate. For $f = 1$ pheromones are evaporated instantaneously once the corresponding site has been chosen leading to $p_i = q \forall i \in \{1, \dots, N\}$. If no evaporation takes place ($f = 0$) all sites will be marked in the stationary state leading to $p_i = Q \forall i \in \{1, \dots, N\}$. The corresponding spatial distribution of particles is homogeneous as known from the *TASEP* (see Fig. 2.3 left). A similar effect can also be achieved by increasing density above a critical value for $f \neq 1$ or $f \neq 0$.

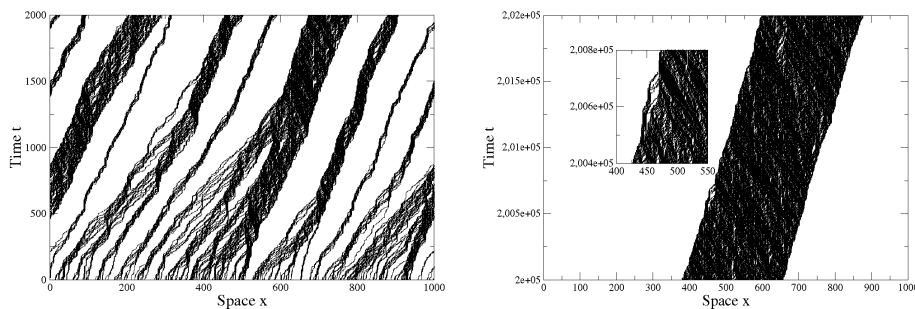


Fig. 3.3. Space-time plots for the unidirectional ATM ($Q = 0.9$, $q = 0.2$, $f = 0.002$): On the left the formation of small moving clusters can be seen. The plot on the right shows the stationary state. All particles are comprised in one large moving cluster. But also dissolving on short time scales is possible (see inset).

3.2.2 Coarsening Behaviour

A quantitative characterisation of the coarsening process is obtained from measuring equal-time *density-density correlations*. Following a method already used in [15] one defines

$$G(r, t) = \frac{1}{L} \sum_{i=1}^L \langle n(i, t) n(i+r, t) \rangle - \rho^2 \quad (3.1)$$

and evaluates the correlation function numerically by averaging over different initial conditions. Here $n(i, t) = \{0, 1\}$ denotes the occupation number of site i at time t . For a comparison of $G(r, t)$ at different densities ρ it is useful to work with the normalised correlation function $C(r, t)$:

$$C(r, t) = \frac{1}{G(0, t)}G(r, t) = \frac{1}{\rho(1 - \rho)}G(r, t). \quad (3.2)$$

The density-density correlation function will be used for gathering information about the *time-dependent coarsening process* and the *stationary state*. By definition deviations from the uncorrelated occupation of two lattice sites separated by distance r are measured. As no particular site or particle exists averaging is done over all particles.

Following [15] density-density correlations are measured at different densities under time evolution. For each density the *zero crossings* $R(t)$ of $C(r, t)$ are measured vs. time. Generally more than one *zero crossing* of $C(r, t)$ at an particular instance of time is observed. The *first zero crossing* $R_1(t)$ for a fixed density and time is interpreted as the minimum distance between uncorrelated high density areas. Generally such a crossing corresponds to a change of sign of $C(r, t)$. Within high-density areas $C(r, t) > 0$ is found whereas in low-density areas one observes $C(r, t) < 0$. During time evolution the high-density areas namely the already observed clusters form larger clusters. As a result the average distance between the clusters increases. This increase will be measured by the time evolution of the *first zero crossings* $R_1(t)$. Also the number of clusters is related to $R_1(t)$. This is indicated by taking into account the non-first-zero-crossings of the density-density correlation function. Using the *first zero crossings* one obtains the minimum average distance of uncorrelated clusters. This implies the existence of some kind of periodic structure. So in general, *zero crossings* can be expected at $R_n(t) = n(t)R_1(t)$ with $n \in [1, \frac{L}{2R}]$ ($R_n < \frac{L}{2}$), with n being interpreted as the average number of clusters at a given instance of time. So one finds $n(t) \sim \frac{1}{R_1(t)}$.

The density-density correlation function shows a strong time dependence. At early times (see Fig. 3.4 left) only short-ranged correlations are present as only high-density areas of short lengths exist. Under time evolution the range of correlations interpreted as the average length of clusters increases. Finally the constant minimal value $C_{min}(\rho) = C(l, t)$ is reached for distances larger than the cluster length ($r > l$).

Plotting the *first zero crossings* vs. time reveals that coarsening follows a power law (see Figs. 3.4 right, 3.5 right). As suggested in [15] coarsening is described by:

$$\begin{aligned} R_1(t) &= A_1 + B_1 t^{\frac{1}{3}} && \text{at early times,} \\ R_1(t) &= A_2 + B_2 t^{\frac{1}{2}} && \text{at later times.} \end{aligned} \quad (3.3)$$

Depending on the time scale one finds different dynamical exponents. The parameters are determined numerically by fitting the appropriate power law. In the initial state particles are distributed randomly. So averaging over different initial states at $t = 0$ will lead to $A_1 = 0$. The existence of a power law is also in accordance with the already observed self-similar spatio-temporal pattern (see Fig. 2.3 left). Independent of the actual time-scale no difference is made.

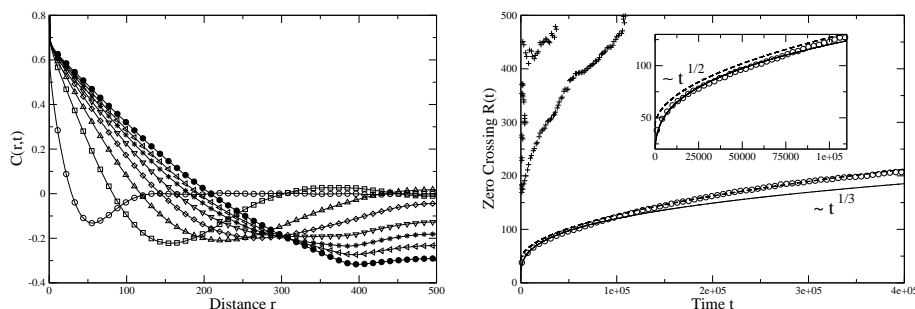


Fig. 3.4. Density-density correlation function of the unidirectional ATM ($Q = 1$, $q = 0.2$, $f = 0.005$ and $\rho = 0.3$) at different times t : $t = 1 \times 10^3$ (\circ), 30×10^3 (\square), 88×10^3 (\triangle), 146×10^3 (\diamond), 204×10^3 (∇), 262×10^3 ($*$), 320×10^3 (\leftarrow), 400×10^3 (\bullet). On the left, the time evolution of the density-density correlations is depicted. The figure on the right shows first zero crossings vs. time. Later crossings are also depicted. The inset shows the fitted power laws for different values of the dynamic exponent $z = \frac{1}{3}$ (solid line) and $z = \frac{1}{2}$ (dashed line).

Coarsening between single particles at early times follows the same principle as the merging of clusters at later times at least for the particular temporal regime with respect to the dynamical exponent. So even single particles can be treated as some kind of cluster with a length one.

From investigations of systems with static particlewise disorder [53,54] relations between the distribution of hopping rates and the dynamic exponent are known. In chapter 4 some additional features in comparison to the bidirectional model are discussed.

An explanation for the existence of two different dynamical exponents is given in [68]. At early times particles did not had enough time to form clusters. So the average distance between particles is small enough for the pheromones to induce particlewise disorder. At later times multiple small clusters have formed. The average distance between clusters now is so large that the pheromone marks have only little influence. The length of the pheromone trace following each cluster or particles is short in comparison to the average distance between the moving entities. Therefore cluster formation is mainly caused by random fluctuations which reduce the distance between two clusters or particles. Once the distance is small enough the pheromone marks will induce disorder finally leading to the coalescence of the two clusters. Iterating this scheme the system finally reaches the stationary state. All particles are comprised in one large cluster. So *zero crossings* become constant in time and are all of first order. The crossing separates distances $r < l$ within the cluster (high-density area $C(r, t) > 0$) from distances $r > l$ outside the cluster (low-density area $C(r, t) < 0$). Assuming a continuous behaviour of $C(r, t)$ only one zero-crossing exists. Since no other high-density areas outside of this cluster exist, $C(r, t)$ reaches its minimum

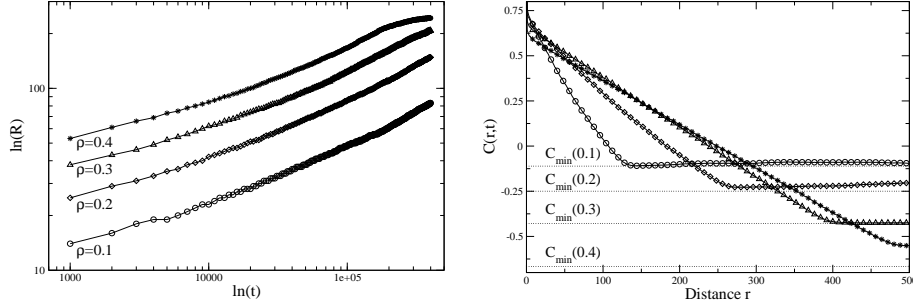


Fig. 3.5. Density-density correlation functions ($Q = 1$, $q = 0.2$ and $f = 0.005$): On the left double-logarithmic plots of the time evolution of $R(t)$ for different densities $\rho = 0.1$ (\circ), 0.2 (\diamond), 0.3 (Δ), 0.4 ($*$) are shown. The two constant slopes correspond to the two regimes of dynamic exponents. The right figure shows the density-density correlation function $C(r, t)$ in the stationary state for different densities. $C(r, t)$ in the stationary state. For $\rho = 0.4$ the beginning of the regime with $C(r, t) = C_{min}(\rho)$ does not correspond to the cluster length.

$$C_{min} = \frac{-\rho}{1 - \rho} \quad \text{for } r > l \quad (3.4)$$

for values of r larger than the cluster size l . But as $C(r, t)$ is symmetric with respect to $r = L/2$, this method is limited to cluster sizes $l < L/2$. An example is found in (see Fig. 3.5 left). For $\rho = 0.4$ the beginning of the interval with $C(r, t) = C_{min}$ does not correspond to $r = l$ as for the other densities. In the next section the cluster length will be measured according to the method introduced in chapter 2. In fact it turns out that the cluster length for $\rho = 0.4$ is larger than $\frac{L}{2}$.

3.2.3 The Stationary State

At the end of the described coarsening process the system finally settles into a stationary state. The particles have formed one single moving cluster. Nevertheless as the system size is finite this state has a finite lifetime. As no dissolving is observed the lifetime obviously is much larger than the times accessible by computer simulations. *Fundamental diagrams* are used to characterise the traffic-like properties. With respect to density two regimes can be distinguished (see Fig. 3.6) at least for an appropriate choice of the evaporation probability f . At low to intermediate densities velocity stays constant and is given by the minimal hopping rate $p = q$. This behaviour is analogous to systems with *static particlewise disorder* (see chapter 2). The flow shows the corresponding linear increase with density in accordance with the hydrodynamic relation. With increasing density a sharp but continuous increase exhibited by velocity as well as by flow is observed. Both quantities finally merge into the curves corresponding

to the *TASEP* with hopping rate $p = Q$. This behaviour is quite different from the one observed in case of static particlewise disorder where the transition to the *TASEP-regime* is not accompanied by a *non-monotonicity* in the average velocity.

The properties of the fundamental diagrams in each regime as well as the transition again can be understood employing the same tools invented for the case of static particlewise disorder. As already mentioned each particle is followed by a trace of pheromone marks. Due to evaporation the length is finite and depends on the evaporation rate f . So particles in general can be expected to have different hopping rates p_i . A mark which was set at a particular site will decay during T_i timesteps until it is renewed by the succeeding ant. Therefore the probability of finding a pheromone at a particular site depends on the time headway of two succeeding ants:

$$p_i(T_i) = q + (Q - q)(1 - f)^{T_i} \quad (3.5)$$

On the other hand, the time-headway T_i is given by the distance headway x_i of the i th particle to the preceding one:

$$T_i = \frac{x_i}{p_i}. \quad (3.6)$$

Basically the hopping rate of the i th particle p_i depends on the distance x_i to the preceding one:

$$p_i(x_i) = q + (Q - q)(1 - f)^{\frac{x_i}{p_i}} \quad (3.7)$$

So the particle i with the maximal distance x_{max} will also be the one with the lowest hopping rate:

$$p_{min} = \min_{i \in [1, N]} \{p_i = p(x_i)\} = p(x_{max}) \quad \text{with} \quad x_{max} = \max_{i \in [1, N]} \{x_i\} \quad (3.8)$$

The particles will follow the one with the largest gap in front of it forming a cluster (see Fig. 3.3 right). Since hopping rates p_i depend only on the gap-size x_i a mapping to the *Zero-Range Process* is possible, as in the case of static particlewise disorder [57, 68, 69].

LCA Approximation

Also a phenomenological approach has been developed [66]. One assumes that the system has reached the stationary state and all particles are comprised in one single loose cluster. Therefore the approach has been named "*Loose Cluster Approximation*" (*LCA*). The leading particle is characterised by a large gap of length $x_1 = L - l$ in front of it. For determining its hopping rate $p_1 := h$ the corresponding time headway $T_h = \frac{L-l}{h}$ is used. Particles within the cluster are assumed to have all the same hopping probability H ($p_i := H \forall i \in \{2, \dots, N\}$).

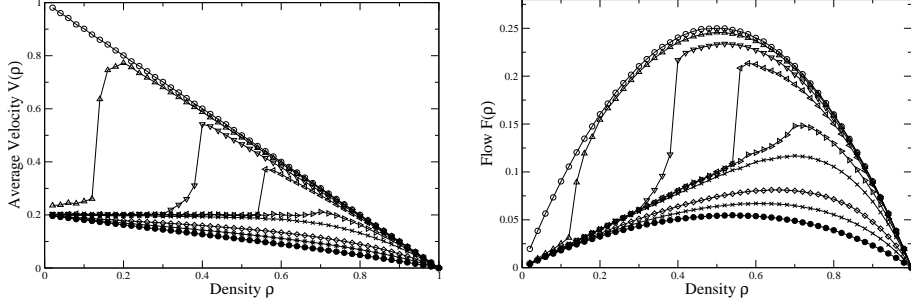


Fig. 3.6. Fundamental diagrams for the unidirectional ATM ($Q = 1$, $q = 0.2$ and $f=0(\circ)$, $0.0002(\triangle)$, $0.0008(\nabla)$, $0.002(\triangleleft)$, $0.008(\triangleright)$, $0.02(\times)$, $0.08(\diamond)$, $0.2(*)$, $1(\bullet)$). For $f = 1$ and $f = 0$ the TASEP with hopping probabilities $p = q$ and $p = Q$ is recovered. Depending on the particular choice of f one observes a regime with constant average velocity and a corresponding linear increase in flow.

Like in case of static particlewise disorder (2.22) is applied. Again all particles have to move with the same average velocity $(1 - \rho_i)H = h$. So the distance headway x_i within the cluster is given by $x_i = \frac{h}{H}$. Thus the corresponding time headway is $T_H = \frac{h}{H^2}$. Together with (3.7) T_h and T_H lead to:

$$h = q + (Q - q)(1 - f)^{\frac{L-1}{h}} \quad \text{and} \quad H = q + (Q - q)(1 - f)^{\frac{h}{H^2}}. \quad (3.9)$$

The LCA obviously assumes a flat density profile within the *moving system* due to the use of (2.22). Measuring the density profile seen from the *second-class particle* one also observes a flat density profile within the cluster (see Fig. 3.7 right, upper inset). At the boundaries of the profile the LCA obviously is not valid as no flat profile is observed. In analogy to the *TASEP* the approximation is strictly valid only for the bulk of the cluster.

Like in the case of *static particlewise disorder* an analogy to the *TASEP* with open boundary conditions can be drawn. Holes are injected into the cluster at the head with rate h by exchanging the position with that one of the leading particle. All other particle exchange their positions with holes at rate H . So the density of holes is given by $\alpha = h \approx q$ leading to $\rho_i^{hole} = \frac{h}{H} \approx \frac{q}{Q}$. With respect to the *TASEP* the moving system is in the low-density phase where the density of holes and thus also the one of particles is determined by the injection rate α . The ejection rate is given by $\beta = H$. So in general no flat density profile can be expected. This is also observed directly by measuring the density profile of the moving system (see Fig. 3.7 right, upper inset). But the bulk density is in good agreement with $\rho_i = 1 - \frac{h}{H} \approx 1 - \frac{q}{Q}$.

Evaluating (3.9) numerically also shows good agreement with the simulations [66]. With increasing density the TASEP-like regime is reached where particlewise disorder dissolves. From (3.9) one finds that h depends on the sys-

tem size L whereas l only depends on the number of particles N (2.24). So the density where the cluster dissolves depends on the system size. This has also been observed directly in computer simulations ¹.

HMFA Approximation

For densities above the critical value all particles can be assumed to be homogeneously distributed. So a "Homogeneous Mean-Field Approximation" (HMFA) is applied [16, 66]. In contrast to the LCA, distance headways for all particles are assumed to be the same $x = \frac{L-N}{N}$ and are just given by the average number of empty sites in front of each particle. Therefore also the hopping rates p are assumed to be the same, leading to $T_p = (\frac{L-N}{N})\frac{1}{p}$ and finally to:

$$p = q + (Q - q)(1 - f)^{\left(\frac{L-N}{N}\right)\frac{1}{p}} \quad (3.10)$$

The employed picture is also in agreement with the behaviour observed for the second-class particle. In the cluster regime only drift is present (see Fig. 3.7 left). At increasing density pheromones increase the velocity of the leading particle and also drift-velocity is increased to $h > q$. At sufficiently high densities pheromones become present at every site leading to a translational invariant state of the lattice. With respect to the second-class particles drift is replaced by diffusion according to (2.10).

3.3 Discussion

A model for *unidirectional traffic* on preexisting ant trails has been introduced. Although it is quite simple the characteristic features of ant traffic have been incorporated (see Fig. 3.1). Differences and similarities to already established models were discussed. The main feature is the formation of a single *moving particle cluster*. This feature is based on *dynamically* induced particlewise disorder due to pheromone marks. The formation of the cluster namely the *coarsening* and the *stationary state* have been investigated. Power laws with different dynamic exponents depending on the time scale were found to describe the coarsening process (see Fig. 3.4).

In the stationary state analogies to systems with *static particlewise disorder* are drawn. Unlike in systems with static particlewise disorder the transition from the cluster regime to the homogeneous distribution takes place at lower densities. The cluster length in the *ATM* is still below L and the density within the cluster is still below the global density $\rho = \frac{N}{L}$ (see Fig. 3.7 right, upper inset) when the homogeneous distribution of particles is reached. In the static case (see chapter 2) that transition takes place for $l = L$ at $\rho_c = \frac{N}{L}$. The upper inset of (see Fig. 3.7 right) shows the growth of the extend of the density profile in the moving system. From (2.23) it is clear that this extend is equivalent to

¹ Observed during investigations for [41], unpublished

the cluster length. Finally the homogeneous distribution (grey line) is reached. Obviously the global density ρ is still below the density ρ_i within the cluster. This is a crucial difference to the results for static particlewise disorder. The increase of the cluster length is still well described by using $I := q$ and $p = Q$ (see Fig. 3.7 right) as in the static case.

Obviously the *pheromones marks* lead to the formation of the cluster in a way very similar to the one which would emerge in a system with static particlewise disorder ($I := q, p := Q$). The homogeneous regime is reached at lower densities which is a result of the pheromones. With increasing global density or decreasing evaporation rate the distance between the leading particle and the pheromone trace becomes smaller. Finally it is small enough to dissolve the particlewise disorder. In the static case this is achieved for higher densities by mutual blocking as $\rho_i \rightarrow \rho$. The *non-monotonicity* observed for the *ATM* which does not exist in case of static particlewise disorder originates just from the two different hopping rates. In the cluster regime particles move with constant average velocity q . This is equivalent to the case of static particlewise disorder. In the homogeneous regime particles hop at an increased rate Q due to the pheromones causing a *non-monotonicity* in the average velocity. Like in the case of static disorder particles are homogeneously distributed, finally recovering the *TASEP* case. Depending on the critical density the non-monotonicity can be completely suppressed.

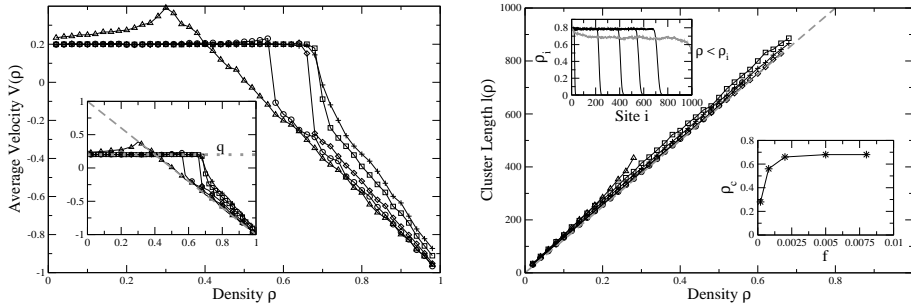


Fig. 3.7. Cluster properties for the unidirectional ATM ($Q = 1, q = 0.2$ and $f = 0.0002 (\triangle), 0.0008 (\circ), 0.002 (\diamond), 0.005 (+), 0.008 (\square)$). On the left the average velocity of the second-class particle is shown. Clearly the change from drift to diffusion indicating the change in the spatial distribution of particles can be observed. On the right the measured cluster length is compared to the one calculated according to (2.24) in case of static particlewise disorder (dashed line). For different evaporation rates, ρ_c extracted from simulations is shown on the lower inset. In a system with static particlewise disorder one would expect $\rho_c = 0.8$. According to this the upper inset shows the growth of length $l(\rho)$ of the density profile with $\rho_i > 0$. In the homogeneous regime the global density ρ (grey) is still below the density ρ_i within the moving cluster.

4 The Bidirectional Models

For extending the unidirectional model to the bidirectional case several variants have been proposed [43, 56]. As a common feature they should reduce to the unidirectional model in absence of *counterflow*. Overall three variants of the bidirectional model appear to be useful. They share common features with each other as well as with the unidirectional one. Nevertheless each model might be most realistic for a particular trail topology within a certain ecological context.

A brief survey over the different variants including their common and particular features will be given. It will turn out that the generic features of all variants are basically the same. They emerge for different sets of parameters depending on the choice of the model. Generally they do not depend much on the complexity of the employed model itself. So a detailed discussion will be given only for one particular variant. Nevertheless for modelling a certain trail topology leading to the emergence of a particularly preferred pattern it is still necessary to distinguish between the models.

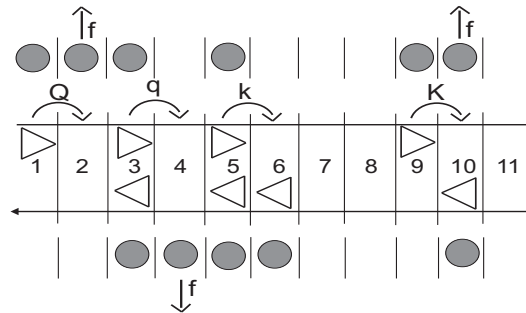
Generally all bidirectional models are the first step towards extending the unidirectional model to the multi-lane case. In *vehicular traffic* two lanes in the same direction would be chosen (e.g. [3, 19]). But unlike in vehicular traffic there is also interaction with ants moving in counterdirection [11, 12, 21]. This has great similarity to behaviour observed in pedestrians dynamics. Analogies between ants and *pedestrians* with respect to the coupling of lanes in opposite directions for example in narrow corridors have already been drawn [25, 26, 77]. So the extension to bidirectional lanes will be proposed. A more detailed discussion with respect to reality is given in chapter 5.

4.1 Definitions and Properties

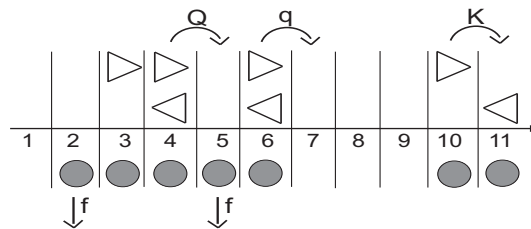
The bidirectional models being discussed in the following differ basically in two ways. One is the way ants facing each other in opposite directions pass by (see Fig. 4.1). This can be done in an *asynchronous* (ATMs 1 and 2) [41, 43] or an *synchronous* (ATM 3) [43, 56] way. The second difference between the

models is the interaction with the pheromone marks. Also here two choices are possible. Ants moving in both directions can share a common trail for pheromones (ATMs 2 and 3) or they have an own trail for each direction (ATM 1). The first two models assume two kinds of pheromones whereas the last one assumes just one kind. So overall four models can be expected. A model with synchronous exchange of ants and separated lattices for pheromones will not be considered. Although one could in principle define such a model severe difficulties arise with respect to reality.

ATM 1



ATM 2



ATM 3

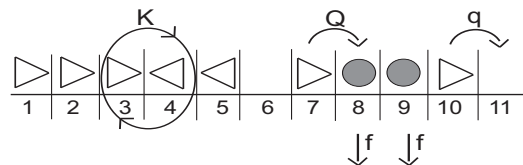


Fig. 4.1. Survey of bidirectional models: In the first two models ants moving in opposite directions exchange their positions in an asynchronous way at different update-steps. This would not be possible in the third model in order to preserve the simple-exclusion principle. Ants moving in both directions share one common lattice. So two ants have to exchange positions at the same time (update step). Regarding the pheromones only the first model uses two different kinds depending on the direction.

All models will be discussed with respect to the emerging spatial patterns and the fundamental diagrams. For first investigations the same number of ants

will be used for each direction. Also the hopping rules are the same for each direction. Results for different particle numbers and hopping rates are briefly discussed at the end of this chapter.

4.1.1 Bidirectional Trail with Separated Pheromone Lattices

This model is probably the most natural extension of the unidirectional one. It consists of two coupled full unidirectional models [41]. Ants in each direction have their own lattice for moving and for pheromone marks (see Fig. 4.1 ATM 1). Coupling is achieved by incorporating the occupation of the lattice for ants in counterdirection. Again only the occupation of the nearest neighboring site $i + 1$ in hopping direction is important. If there is an ant in counterdirection two additional hopping probabilities are used. In presence of an ant in counterdirection and also of a mark on the lattice for pheromones in the own direction hopping takes place with hopping rate K . In case of counterflow and absence of a pheromone mark, the hopping rate is set to k . Obviously ants facing each other in opposite directions exchange their positions at different update-steps and thus at different times. Mutual blocking is still incorporated but only by ants moving in the same direction.

With respect to real trails this model corresponds to a species employing at least two kinds of *trail-pheromones*. Even in case of counterflow the interaction via pheromones leading to *particlewise disorder* still exists [85, 86]. This will be the dominating form of interaction in this model. Generally hopping rates in case of *counterflow* k and K are smaller than in the unidirectional case. So the mutual slowing down by counterflowing ants is also incorporated.

Spatial Patterns

In absence of counterflow hopping takes place with rates q and Q depending on the presence of pheromone marks. So the same mechanism of cluster formation known from the unidirectional model is present. In case of counterflow an additional mechanism is found. Both ant clusters moving in opposite directions will have to pass each other. As the hopping rates are reduced by counterflow the clusters generally get deformed (see Fig. 4.2). The counterflow disturbs the *particlewise disorder* known to be the mechanism for the formation of the cluster in the strictly unidirectional case. As the cluster can be completely destroyed this process has been named "*shredding*" [56]. Nevertheless under certain conditions a reformation or recoarsening is still possible (Fig. 4.2).

As in the unidirectional case the cluster comprises all particles in one direction. So an increase of density leads to an increase of the cluster length l . On the other hand the time between the passing of the clusters is roughly given by

$$T = \frac{\frac{1}{2}L - l}{v} \quad (4.1)$$

Here L denotes the length of the lattice and v is the average velocity in absence of counterflow. Like in the unidirectional model one finds $v = q$. During

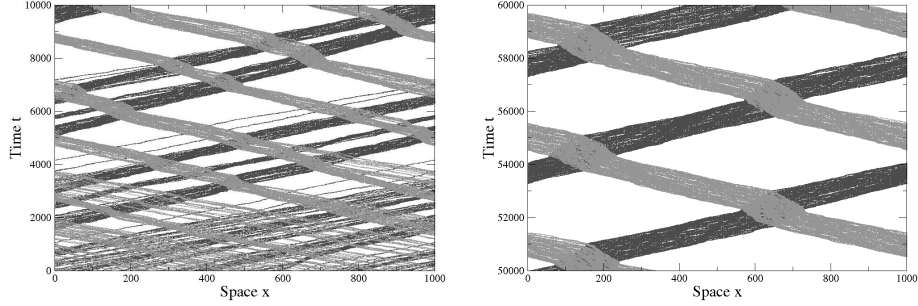


Fig. 4.2. Space-time plots for ATM 1 ($Q = 1$, $q = 0.6$, $K = 0.5$, $k = 0.2$, $f = 0.002$ and $\rho = 0.1$): The formation of moving clusters at low densities is shown on the left. Counterflow obviously disturbs the formation. Under certain conditions finally one moving cluster with the same properties known from the strictly unidirectional case is formed for each direction. The figure on the right shows the shredding and recoarsening of this cluster.

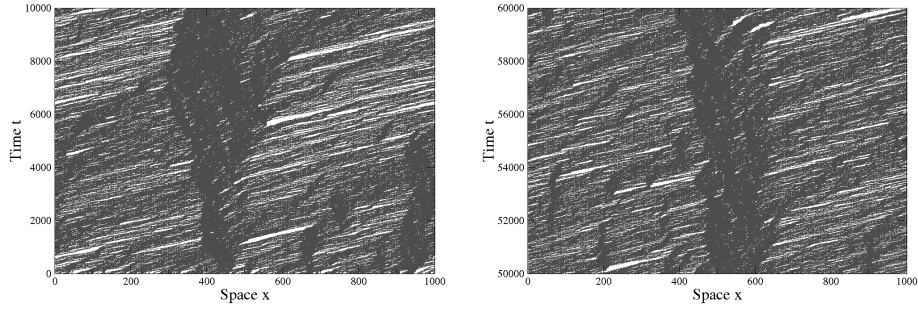


Fig. 4.3. Space-time plots for ATM 1 ($Q = 1$, $q = 0.6$, $K = 0.5$, $k = 0.2$, $f = 0.002$ and $\rho = 0.33$): On the left the formation of localised clusters is shown. Ants moving in opposite directions effectively form an extended defects for the other direction shown on the right. For clarity only the occupation for the LR-direction is shown.

the time T recoarsening takes places. For simplicity the time for recoarsening is assumed to be independent of density. So an increase of density reduces the time for recoarsening due to $l \sim N$. As a result the time T between two encounters of the clusters is not sufficient anymore for the recoarsening of a single unidirectional cluster. So the system is in a permanent state of *coarsening* and *shredding* without being able to form a single moving cluster for each direction. The particle distribution resembles that one found during the coarsening at very low densities (Fig. 4.2 left). At intermediate densities multiple small but moving clusters exist [56].

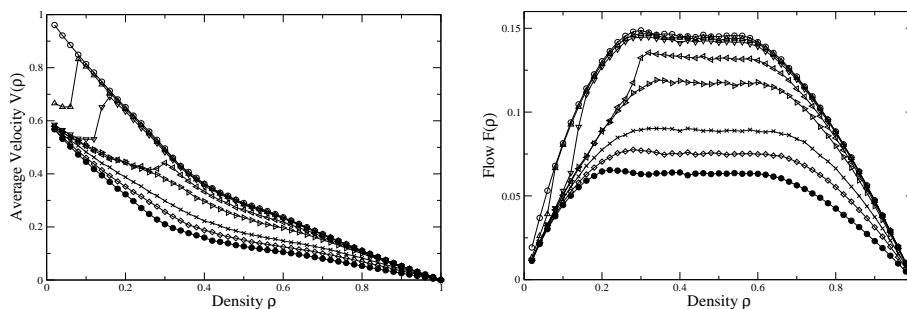


Fig. 4.4. Fundamental diagram for ATM 1: ($Q = 1$, $q = 0.6$, $K = 0.5$, $k = 0.1$ and $f = 0(\circ)$, $0.0008(\Delta)$, $0.002(\nabla)$, $0.008(\triangleleft)$, $0.02(\triangleright)$, $0.08(\times)$, $0.2(\diamond)$, $1(\bullet)$). At low densities roughly the same behaviour known from the unidirectional model is found. For intermediate to high densities flow shows a plateau known from systems with latticewise disorder.

With increasing density the pheromone marks cannot induce particlewise disorder anymore. They become present at any site with the same probability. Effectively only two hopping rates depending on the presence or absence of counterflow exist. Obviously this induces effectively quenched latticewise disorder with ants moving in the opposite direction forming the defects (see Fig. 4.3). The emerging clusters now are localised high-density areas. This is also true in the case where the counterflow even increases the hopping rate. Then holes in counterdirection form the defects for particles moving in the opposite direction.

Fundamental Diagram

The fundamental diagrams exhibit properties reflecting the observed spatio-temporal patterns. At low densities velocity shows a *non-monotonicity* (Fig. 4.4 left). This is in accordance to the moving clusters already discussed. The corresponding density regime is comparably small. At intermediate to high densities velocity shows a strictly monotonic decrease. The reason is the increasing mutual hindrance by counterflow which also affects the mutual blocking by ants moving in the same direction. Overall one observes three distinct regimes of flow. In accordance to the formation of localised clusters namely defects flow exhibits a *plateau* (Fig. 4.4 right). The value of constant flow obviously depends on the evaporation probability f .

4.1.2 Bidirectional Trail with Common Pheromone Lattice

Modifying ATM 1 leads to the second possible bidirectional model [45, 76]. Instead of using an own pheromone lattice for each direction both directions share a *common* lattice for pheromones (see Fig. 4.1 ATM 2). Therefore only one additional hopping rate K is needed. In presence of an counterflowing ant

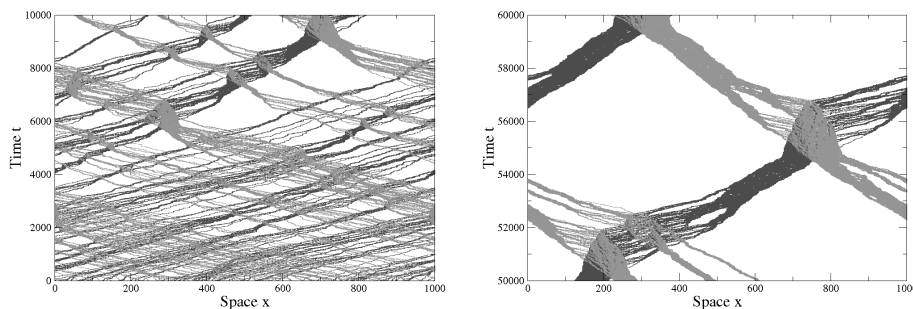


Fig. 4.5. Space-time plots for ATM 2 ($Q = 1$, $q = 0.2$, $K = 0.2$, $f = 0.002$ and $\rho = 0.08$): The left plot shows the formation of moving clusters. Finally one cluster for each direction has formed. In comparison to ATM 1 the density is very small.

at the nearest neighboring site $i + 1$, hopping takes place with rate K . As the presence of an ant at site $i + 1$ always implies the existence of a pheromone-mark at the same site, the case leading to hopping probability k (see ATM 1) does not exist. Again ants in opposite directions exchange their positions *asynchronously*. In absence of counterflow the unidirectional case with rates q and Q depending on the presence or absence of pheromones is recovered.

With respect to reality counterflow is dominating over the ant-pheromone interaction. The presence of an ant at a particular site prevents the pheromone at that site from being evaporated. So the effective lifetime of pheromones is higher than in ATM 1 as ants in both directions renew the same kind of pheromone. Therefore particlewise disorder can only be induced at very low densities. But in case of unidirectional traffic ant-pheromone interaction is still present. So this model would be employed for species with only one kind of trail-pheromone [36].

Spatial Patterns

Ants from both directions set their marks on the same lattice. So the mean time till reoccupying a particular site and thereby renewing or setting a pheromone mark is only half of the time of ATM 1. Therefore the translational invariant state of the pheromone lattice is reached for comparably low densities. Unlike in ATM 1 this induces a second kind of coupling between the opposite directions. Nevertheless moving clusters are formed (see Fig. 4.5 left). If the time for recoarsening is sufficient finally one single moving cluster emerges (see Fig. 4.5 right). Again the cyclic process of recoarsening and shredding is found.

At sufficiently high densities small localised clusters emerge (see Fig. 4.6 left). They exist at the same sites for each direction. Obviously their lifetime depends on the cluster size. In the stationary state only one large localised cluster exists. Unlike in the unidirectional model not all particles are comprised in this kind of cluster (see Fig. 4.6 right).

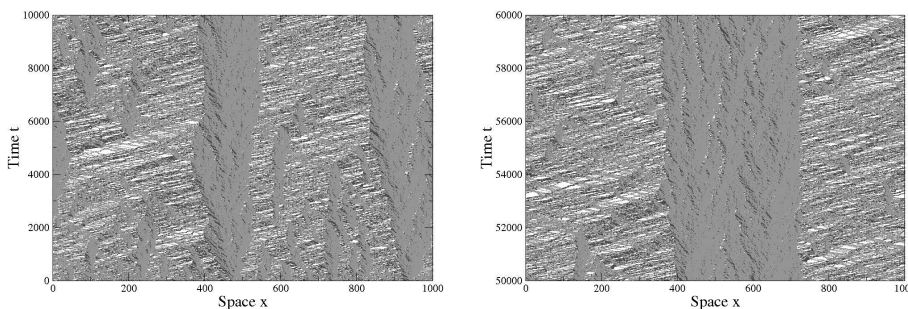


Fig. 4.6. Space-time plots for ATM 2: ($Q = 1$, $q = 0.2$, $K = 0.2$, $f = 0.002$ and $\rho = 0.3$): The left plot shows the formation of small localised clusters. On the right one large localised cluster is shown.

Fundamental Diagram

Again the a non-monotonicity of the average velocity is found at low densities (see Fig. 4.7 left). Due to the common pheromone lattice the translational invariant state depending on the pheromones is reached at very low densities. One also observes the occurrence of density regimes with constant flow (see Fig. 4.7 right). The value of constant flow again depends on the evaporation rate f . But also the boundaries of the regime depend on f . At low evaporation rates the regime begins at lower densities than for higher evaporation rates. This is also in analogy to systems with *lattice-wise disorder*. At intermediate to high densities effectively only two hopping rates exist. The rate in case of counterflow does not depend on the pheromones. But in absence of counterflow the hopping rate is determined by f . Overall one finds:

$$p \approx \begin{cases} Q > K & \text{for } f \rightarrow 0 \\ q < K & \text{for } f \rightarrow 1 \end{cases} \quad (4.2)$$

In the first case ($f \approx 0$) ants in counterdirection form the defects. On the other hand for ($f \approx 1$) holes in counterdirection act as defects. So the evaporation probability is used to choose between the impact of counterflow. This can also be used to reducing the coupling to counterflow ($f = 0.08$).

4.1.3 Single-lane Bidirectional Ant Trail Model

A further reduction of the model's complexity is possible if one also uses just one common lattice for both directions of ant movement [56]. Unlike the first two models already discussed it basically consists of just one unidirectional model. As an extension to the unidirectional case ants moving in both directions share one common lattice (see Fig. 4.1 ATM 3). In case of vanishing ant-pheromone coupling the so-called *bridge-model* introduced in the context of spontaneous

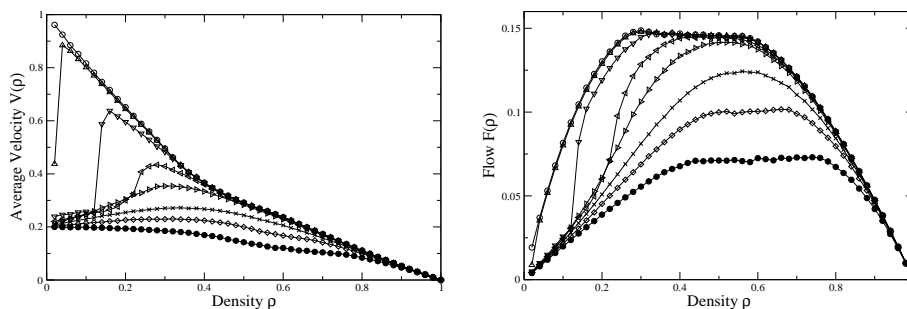


Fig. 4.7. Fundamental diagrams for ATM 2: ($Q = 1$, $q = 0.2$, $K = 0.5$ and $f = 0$ (\circ), 0.0002 (Δ), 0.002 (∇), 0.008 (\triangleleft), 0.02 (\triangleright), 0.08 (\times), 0.2 (\diamond), 1 (\bullet)). On the left average velocity shows the characteristics known from the moving cluster regime. Flow exhibits plateaus which are characteristic for systems with static latticewise disorder. Depending on the evaporation rate f particles or holes form some kind of dynamic latticewise defect.

symmetry breaking in one-dimensional non-equilibrium systems is recovered [28]. As basically two kinds of particles (left- and right-moving ants)¹ share the same lattice the total density is given by:

$$\rho = \frac{N_R + N_L}{L} \quad \text{and} \quad \rho_i = \frac{N_i}{L} \quad i \in \{L, R\} \quad (4.3)$$

Each lattice site still can be occupied only by one ant. In case of counterflow ants facing each other in opposite directions exchange their positions with rate K . Like in the unidirectional model, mutual blocking is achieved by ants moving in the same direction. Pheromone marks are also set on the same lattice used by the ants. So each lattice site can either be occupied by a right- or left-moving ant or a pheromone mark. In comparison to the unidirectional model one observes that the unidirectional model makes use of an extra lattice for pheromones. This is in principle not necessary and originates just from the original definition of the unidirectional model with time-parallel dynamics [16].

As a consequence of using only one lattice for ants and preserving the hardcore exclusion principle, ants facing each other in opposite directions have to exchange their positions at the same time. The movements of one ant thus automatically forces the other ant to move either. A separate lattice for pheromone marks like in *ATM 2* would not make any difference between directions in that case as hopping rates could not be chosen independently. One would have to distinguish between four possible cases for the synchronous exchange depending on the possible local configurations (sites i and $i + 1$) of the three lattices.

The *synchronous* exchange of counterflowing ants appears to be a very special case. Nevertheless in situations with limited space this model is applicable

¹ not incorporating holes and pheromone marks



Fig. 4.8. Both photographs show a trail which is defined by spatial restrictions. On the right two platoons pass each other. As there is only little space available one platoon moves to the right and the other one to the left. After passing by both platoons will move back to the centre of the cable. The left photograph shows an extremer example. If space is even too little for the latter scenario ants move temporally to the downside of the cable to make way (upper left corner of the right photography).

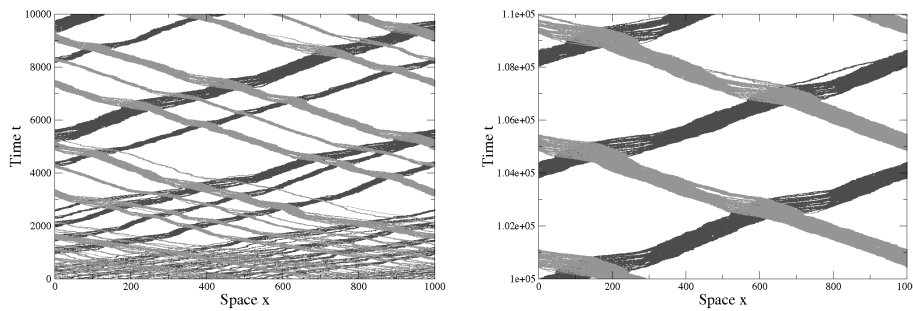


Fig. 4.9. Space-time plots for ATM 3 ($Q = 1$, $q = 0.2$, $K = 0.05$, $f = 0.002$ and $\rho = 0.1$): The left plot shows the formation of small but moving clusters out of the homogeneous distribution of particles in the initial state. At late times single and moving cluster have formed in each direction.

(see Fig. 4.8). Recent investigations show [25] that this situation is also of practical interest in other systems [43, 56]. An analogy can be drawn to the movement of pedestrians for example in a narrow corridor. In that case the platoon formation bears some advantages arising from some kind of *follow-the-leader* behaviour (e.g. [25, 48]).

Spatial Patterns

Also here moving clusters are formed at sufficiently low densities. As pheromones are dropped on a common lattice the translational invariant state for the marks again is reached at very low densities (see Fig. 4.9) .

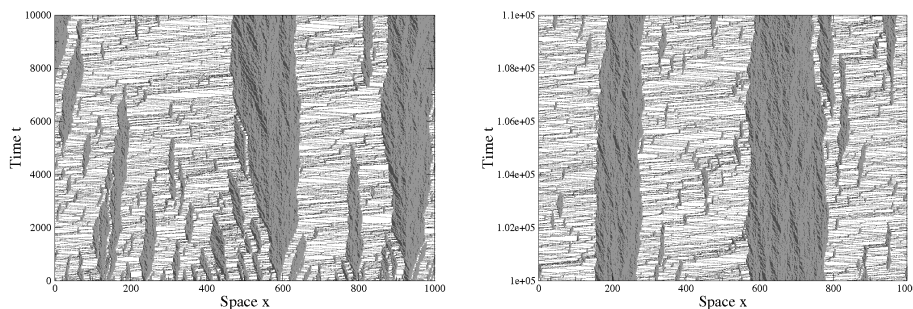


Fig. 4.10. Space-time plots for ATM 3: ($Q = 1$, $q = 1$, $K = 0.05$, $f = 0$ and $\rho = 0.4$): On the left the formation of multiple small and localised clusters is shown. In the stationary state only a few large clusters exist shown on the right.

Like in ATMs 1 and 2 *localised clusters* emerge (see Fig. 4.10) for higher densities. But the stationary state consists of two large localised clusters. Also the choice of $K = 0.05$ is quite extreme in comparison to the other models. Overall due to the synchronous exchange blocking by counterflow is not the dominating mechanism even at very high densities. Thus coarsening and shredding turn out to be the main features of the model. Both processes have been studied in great detail in [56].

Fundamental Diagram

At low to intermediate densities the average velocity is independent from density. So the characteristics of the *moving clusters* are also found here. Additionally the *non-monotonic* behaviour of the average velocity is found which is caused by dissolving particlewise disorder. But also for vanishing ant-pheromone coupling, e.g. for $f = 0$, one observes a strictly monotonic increase of velocity. Unlike in the other models also ants share a common lattice. So at very high densities pairwise exchange of counterflowing ants dominates over mutual blocking by ants moving in the same direction. Finally at $\rho = 1$ the *TASEP-case* for each direction is recovered. Generally ants moving in one direction are equivalent to holes for the ants of the opposite direction:

$$F_i(1) = \rho_i(1 - \rho_j)K \quad i, j \in \{L, R\} \quad (4.4)$$

But also a mean-field description neglecting the ant-pheromone coupling has been developed [56]. Except for the cluster regime the results are in good agreement with the fundamental diagrams obtained from computer simulations.

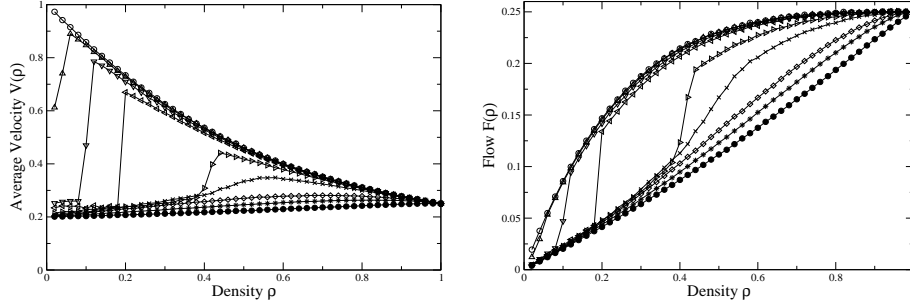


Fig. 4.11. Fundamental diagrams for model 3: ($Q = 1$, $q = 0.2$, $K = 0.5$ and $f = 0(\circ)$, $0.0002(\triangle)$, $0.0008(\nabla)$, $0.002(\triangleleft)$, $0.008(\triangleright)$, $0.02(\times)$, $0.08(\diamond)$, $0.2(*)$, $1(\bullet)$). Even for $\rho \approx 1$ velocity and flow are non-vanishing. The reason is just the recovering of the TASEP.

4.2 Common Features

The three bidirectional ATMs basically exhibit the same two features. As already observed they emerge for different choices of parameters depending on the model. Also each model has a preference towards a particular feature. The first one is the *coarsening* and *shredding* at low densities. By construction all bidirectional models reduce to the unidirectional ATM in absence of counterflow. So at sufficiently low densities ants form moving clusters. Clusters passing by are mutually affected by the cluster of counterflowing ants. Especially ATM 3 exhibits that feature even at comparably high densities.

The second common feature emerges at intermediate to high densities. As already noticed flow exhibits *plateaus*. These plateaus are known from models with static latticewise disorder. The corresponding spatial pattern is a large *localised cluster* forming the defect for the opposite direction. The first two models have a preference toward that pattern. As ants in opposite directions facing each other pass by asynchronously hindrance is increased by counterflow. This obviously leads to the formation of large localised clusters. This is quite different from ATM 3 where even for a very low exchange rate K hardly such patterns can be produced.

Like for the unidirectional model the coarsening behaviour as well as the stationary state are investigated for both features in the following. Effects of shredding have already been investigated extensively for ATM 3 [56]. The formation of the localised cluster is known from ATMs 1 and 2 [41, 44]. Both models become completely identical for $f = 0$ and $f = 1$. Especially the formation of localised clusters originates from mutual hindrance by counterflow and does not originate from the ant-pheromone coupling. So (re)coarsening and shredding as well as the coarsening and the stationary state of the localised clusters are studied for ATM 2 in the following.

4.2.1 Moving Clusters

One of the main results from the discussion in chapter 2 it is that the moving clusters are formed due to the *dynamic particlewise disorder* induced by the pheromones. As already observed this mechanism are also present in case of counterflow at sufficiently low densities. In case of counterflow the cluster structure becomes disturbed. As ATMs 2 and 3 are closely related the effects of *(re)coarsening* and *shredding* will be investigated for ATM 2. Nevertheless the same techniques would also work out for the other models.

(Re)coarsening and Shredding

At low densities pheromones induce particlewise disorder leading to the formation of moving clusters. Counterflowing ants disturb this coarsening process. First by affecting the hopping rate directly due to $p = K$. A second kind of coupling to ants in counterdirection is the pheromone lattice. Two clusters passing by each other in opposite directions are followed by their own pheromone trace on a common lattice. So the ant at the head of the cluster finds pheromone. Obviously the passing by of clusters temporally dissolves the particlewise disorder which is crucial for the cluster formation. As a result the shredding prevents the formation of one single moving cluster. This is also observed in the *first zero crossings* (see Fig. 4.12, left). Even in the stationary state strong fluctuations occurred. The clusters are in a permanent state of recoarsening and shredding. If clusters already exist in the initial state these *oscillations* are even stronger. Two clusters pass each other and recoarse to one single cluster for each direction after shredding. The zero crossings reflect this *periodicity* (see Fig. 4.12, right). Although shredding prevents the formation of the single cluster it does not prevent the recoarsening once a single cluster has been prepared in the initial state.

From these observations it is very likely that also for a random initial configuration of particles a single cluster for each direction will emerge. Correspondingly the *Fourier transform* $S(T)$ of $C(r, t)$ exhibits a peak (see Fig. 4.12 right, inset). The reason why this is observed only for a particular initial configuration is just the limitation of the observed period of time.

4.2.2 Localised Clusters

At sufficiently high densities the large localised cluster emerges for each direction at the same sites. The main mechanism is *dynamically* induced latticewise disorder by counterflowing ants. So the mechanism basically does not depend on the pheromones. Previous investigations showed that also for $f = 1$ and $f = 0$ localised clusters are formed. In that case only two different hopping rates depending on the presence or absence of counterflow exist. So for further investigations the ant-pheromone coupling can be neglected.

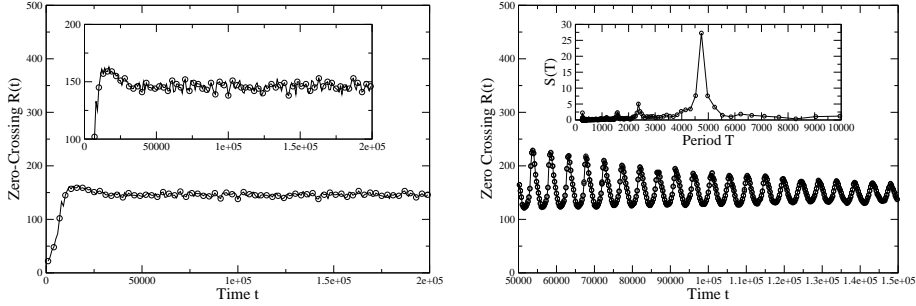


Fig. 4.12. Density-density correlation function of ATM 2 ($Q = 1$, $q = 0.2$, $K = 0.2$, $f = 0.002$ and $\rho = 0.1$): Both figure show the first zero-crossings at a low density for different initial conditions. On the left the density-density correlation function was averaged over different initial states. On the right particles were already set to one single cluster for each direction in the initial state. The inset shows the Fourier transform $S(T)$ of $R(t)$.

Coarsening Behaviour

The formation of the localised cluster is investigated analogous to the unidirectional case. Two-point equal time density-density correlations were measured under time evolution towards the stationary state. As the *density-density correlation function* is taken at an particular instance of time, no difference is made between moving and localised high-density areas. So one roughly observes the same behaviour (see Fig. 4.13) as for the unidirectional case.

At early times only short ranged correlations exist (see Fig. 4.13, left). The correlation function is non-zero only for *short distances*. With increasing time the correlation function becomes non-zero for a growing range of distance r . Overall this reflects the fact that the high-density areas grow with increasing time. This is also in accordance with the behaviour observed in the space-time plots of the preceding section. Finally the stationary state is reached. The correlation function shows the same behaviour as observed for the unidirectional case. One also observes a qualitative change in the behaviour for $t > t_m = 20 \times 10^3$. Before t_m the minima of the correlation functions at different times are nearly the same. For times later t_m the minimum values start to decrease further. The functions $C(r, t)$ with $t > t_m$ shows a linear decrease with increasing r and a minimal value C_{min} which is independent of r is finally reached.

Like in the unidirectional model *zero crossings* were measured (see Fig. 4.13, right). Again the first zero crossings separate the length scales of high- and low-density areas. Also power laws describing the time evolution of $R(t)$ according to 3.3 are observed. At early times one finds $z = \frac{1}{3}$ and for late times $z = \frac{1}{2}$. This is exactly the same result as for the unidirectional model. The constant value for the zero crossing namely the stationary state is reached comparably

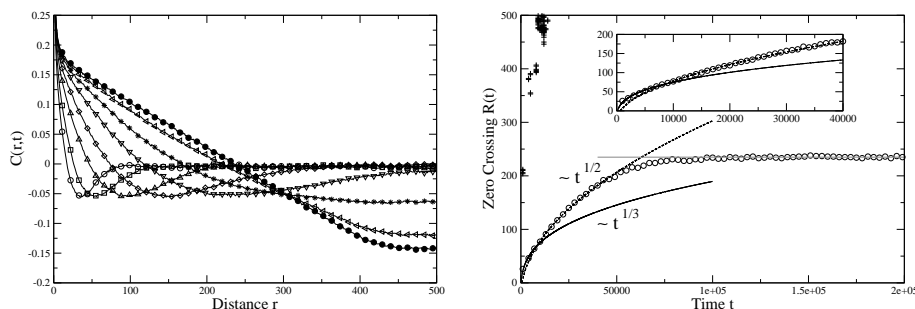


Fig. 4.13. Density-density correlation function of the bidirectional model 2 ($Q = 1$, $q = 0.2$, $K = 0.2$, $f = 0.002$ and $\rho = 0.4$) at different times: $t = 1 \times 10^3$ (\circ), 2×10^3 (\square), 5×10^3 (\triangle), 10×10^3 (\diamond), 20×10^3 (∇), 35×10^3 ($*$), 66×10^3 (\leftarrow), 300×10^3 (\bullet). On the left, the time evolution of the density-density correlations is depicted. The figure on the right shows first zero crossings vs. time. Later crossings are also depicted. The inset shows the fitted power laws for different values of the dynamic exponent $z = \frac{1}{3}$ (solid line) and $z = \frac{1}{2}$ (dashed line). Finally a constant value is reached (grey line).

fast. Also the higher order zero crossings being interpreted as small localised clusters vanish faster.

This can be explained by the nature of the coarsening process which basically relies on *mutual hindrance* by counterflow. Particles in opposite directions get stuck at each other due to the reduced hopping rate $K < Q$. This happens for different particles at different times. Due to fluctuations succeeding particles in the same direction accumulate behind a particle slowed down in counterdirection. Even if that one passes by the accumulated particles still have to pass. In comparison to the unidirectional model the density is effectively twice as high which accelerates the coarsening process.

But still the dynamic exponents of the power laws are the same for the uni- as well as for the bidirectional ATM 2. As already mentioned this cannot be explained by the pheromones². So the different exponents might be due to some kind of memory effect arising from the initial state which would be present in both models. But as averaging of $C(r, t)$ was done over about 1000 different initial states this is very unlikely. In comparison to the unidirectional model an additional lattice for ants is used. So a memory effect would be much stronger as more initial states are possible. More reasonable seems to be that the different exponents are related to the different qualitative behaviour observed for the density-density correlation function with respect to $t_m = 20 \times 10^3$. The two regimes of the dynamical exponents are roughly separated by t_m (see Fig. 4.13 right, inset). So $z = \frac{1}{3}$ describes the coarsening of multiple small localised clusters. At later times $z = \frac{1}{2}$ corresponds to the coarsening of the single large localised cluster. This is also in accordance to the explanation given for the

² since the same results are obtained without pheromones.

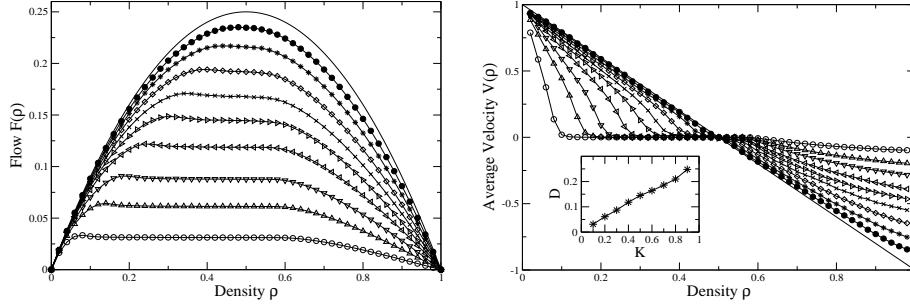


Fig. 4.14. Flow vs. density and velocity of the second-class particle: dynamic lattice-wise disorder ($Q = 1$, $I = 0.1$ (\circ), 0.2 (\triangle), 0.3 (∇), 0.4 (\triangleleft), 0.5 (\triangleright), 0.6 (\times), 0.7 (\diamond), 0.8 ($*$), 0.9 (\bullet)). On the left flow vs. density exhibits plateaus known from static lattice-wise disorder. Obviously flow does not exhibit particle-hole symmetry anymore. Different regimes again can be characterised by the velocity of the second-class particle. The regime of phase separation namely that one of the localised cluster corresponds to the vanishing of the average velocity. One also observed that roughly at $\rho = 0.54$ independently from K the cluster dissolves which is indicated by $v < 0$.

unidirectional model [68]. There the density-density correlation function also shows a qualitative different behaviour for $t < t_m$ and $t > t_m$. At *early times* multiple small moving clusters exist. The average distance is low so coarsening is affected by pheromones. At *later times* few large moving clusters exist. The average distance between clusters therefore is also large. So clusters coalescent due to fluctuations. This finally corresponds to the growth of the single moving cluster.

The Stationary State

Like in the case of static lattice-wise disorder the traffic-like properties of the stationary state are characterised by the fundamental diagram (see Fig. 4.14, left). Again flow exhibits characteristic *plateaus* which are caused by the formation of *dynamically induced* high-density areas. As already pointed out the high-density areas in one direction act like a localised defect for particles moving in the opposite direction. In case of static lattice-wise disorder one observes a *particle-hole symmetry* (see chapter 2). Therefore the plateaus appear for $\rho \geq \rho_-$ and vanish again for $\rho \geq \rho_+ = 1 - \rho_-$. Obviously the symmetry is broken in the dynamic case. For measuring the extend of the plateau regime again second-class particles are employed (see Fig. 4.14, right). In the plateau regime $\rho \in [\rho_-(K), \rho_+(K)]$ the second-class particle's effective velocity is zero corresponding to the emergence of a localised high-density area. As a new crucial feature $\rho_+ = \frac{1}{2}$ is independent from K . Unlike in the static case the upper boundary is nearly independent from the impurity hopping rate K . The diffusion

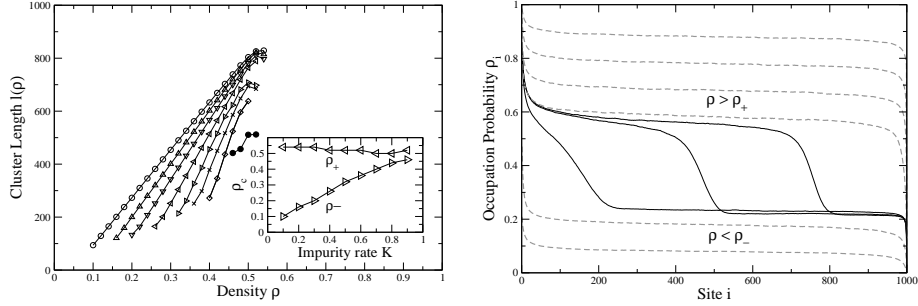


Fig. 4.15. Cluster length for $Q = 1$, $K = 0.1$ (\circ), 0.2 (Δ), 0.3 (∇), 0.4 (\diamond), 0.5 (\triangleright), 0.6 (\times), 0.7 (\diamond), 0.8 (\bullet). On the left a linear increase of the cluster length for $\rho \in [\rho_-, \rho_+]$ is found. This is also observed for the static case. But independent from the impurity rate K the cluster dissolves at $\rho_+ \approx \frac{1}{2}$ (see inset). The beginning of the cluster regime ρ_- shows a linear dependence on the impurity rate K . On the right the density profiles for the LR-direction at different global densities is shown. In the cluster regime the high- and the low-density areas are of constant density like in the static case.

constant D characterising the fluctuations (see Fig. 4.14 right, inset) shows a linear dependence on K . This is also different from the static case.

Like for static disorder the cluster length is defined as the number of consecutive sites with $\rho_i > \rho = \frac{N}{L}$. Again a linear increase is observed (see Fig. 4.15 left). Correspondingly the length of the high-density area grows linearly (see Fig. 4.15 right). As already indicated by the behaviour observed for the second-class particles the cluster breaks down for $\rho > \frac{1}{2}$. Like for static disorder the cluster-length should reach the system-size L at $\rho_c = \frac{1}{2}$. But obviously fluctuations play a role so that the measured cluster length effectively never reaches the system size at ρ_c (see Fig. 4.15 left).

Due to the absence of *particle-hole symmetry* the same approach as in the static case cannot be applied (see chapter 2). Therefore a closer investigation of the cluster structure becomes necessary. This is done by investigating the density profile seen from the same second-class particles for both directions (see Fig. 4.16 left). As already observed in the space-time plots one single high-density area exists for each direction at the same sites for each direction. As indicated by the vanishing effective velocity of the second-class particle this areas are localised besides minor fluctuations (see Fig. 4.14 right). Like in the case of static disorder phase separation is observed. The density-profile for the low-density area is flat at a constant value ρ_- . But the density-profiles for the high-density areas exhibit a slope (see Fig. 4.16 left). Employing the TASEP picture the high-density areas exhibit density profiles corresponding to those found on the coexistence-line $\alpha = \beta$. Overall the average density within the cluster can be calculated using the cluster length l and the number of particles N_+ inside the cluster $\rho_+ = \frac{N_+}{l}$.

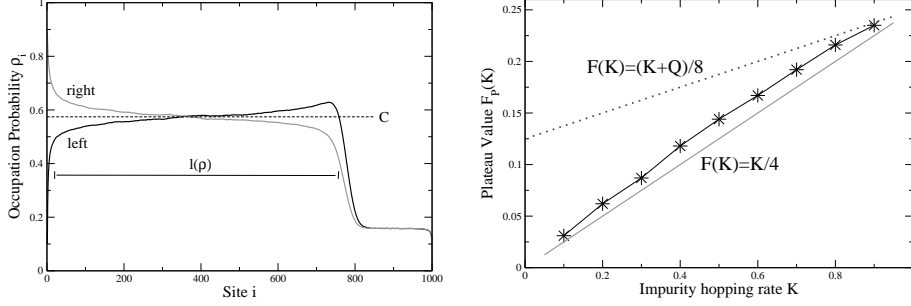


Fig. 4.16. Density profile and flow measured in the plateau regime: On the left the density profile for both directions seen from the same second-class particle is shown. Again phase separation into a high- and a low-density area is observed. Within the high-density area additionally two symmetries exist. On the right flow within the plateau region $F_p(K)$ depending on K is shown (*) for $Q = 1$. The solid grey line corresponds to $F = \frac{1}{4}K$ whereas the dotted line describes $F = \frac{1}{8}(K + Q)$.

A *point symmetry* to the middle of the clusters can be expected. This symmetry arises from two other underlying symmetries. As observed the slopes of the density profiles $m_{R/L}$ for both directions are related by $m_R = -m_L$. Generally particles in counterdirection decrease the hopping rate of particles moving in the other direction. Therefore a high-density area in one direction leads to a low-density area in the opposite one:

$$C = \rho_+^R(i) + \rho_+^L(i) \quad (4.5)$$

If an occupied site i in one direction would exactly lead to an unoccupied site i in the opposite direction a perfect particle-hole symmetry corresponding to $C = \frac{1}{2}$ would be found. This is obviously not exactly the case but later calculations will show that assuming a perfect particle-hole symmetry is a good approximation. The second symmetry arises from the fact that both directions are completely equivalent. Therefore the spatial patterns should exhibit a symmetry to the middle i_0 of the high-density area:

$$\rho_+^R(i_0 - i) = \rho_+^L(i_0 + i) \quad (4.6)$$

Overall both symmetries give rise to a point ($i = i_0$) symmetry of the density profiles:

$$\rho_+^R(i_0 - i) = C - \rho_+^R(i_0 + i) \quad (4.7)$$

This is also observed directly (see Fig. 4.16 left) in the density profile. Making use of the two symmetries one derives the flow F^R within the high-density region say for the RL-direction. Again a mean-field picture is employed.

Although the density-profile is not flat we work with average densities within that region:

$$F^R = \rho_+^R(1 - \rho_+^R)p = \rho_+^R(1 - \rho_+^R)[\rho_+^L K + (1 - \rho_+^L)Q] \quad (4.8)$$

The hopping rate p is decomposed into the probabilities of finding a particle in counterdirection or not. Depending on those probabilities the hopping rate is K or Q . Obviously no coupling between both directions is assumed. Due to the previous investigations of the density profile we assume $\rho_+^R = \rho_+^L \approx \frac{1}{2}$ to be valid. Then flow is given by:

$$F^R = \frac{1}{4}p = \frac{1}{8}(K + Q) \quad (4.9)$$

A comparison with the measured values of flow confirms the already observed symmetry (see Fig. 4.16 right). Using (4.9) obviously is not a good approximation. Using the hopping rate p , given by $p = \rho_+^L K + (1 - \rho_+^L)Q$, does not incorporate the symmetries of the cluster. The density profile shows that a high-density area in one direction leads to a low-density area in the other one and vice versa. Therefore the following local configurations of sites i and $i + 1$ in both directions are favoured (see Tab. 4.1).

Configuration $(i i+1)$	1.	2.	3.	4.
RL-direction	(1 0)	(0 1)	(0 0)	(1 1)
LR-direction	(0 1)	(1 0)	(1 1)	(0 0)

Table 4.1. Due to the symmetries within the cluster certain configurations are favoured on average. Here all relevant configurations which have to be taken into account for particle hopping are shown. Especially configurations 1 and 2 are important. A particle not blocked by another one in the own direction will probably find a particle in counterdirection. Therefore its hopping rate is $p = K$.

Obviously the case that a particle at site i is not blocked is equivalent to an occupied site $i + 1$ in counterdirection. The hopping rate therefore is $p = K$ and flow is given by $F = \frac{1}{4}K$. Incorporating the symmetries leads a good approximation of flow (see Fig. 4.16 right). Also some similarity to ATM 3 for $N_R = N_L = \frac{1}{2}L$ is observed.

Measurements of the density profile (see Fig. 4.16 left) show a flat profile in the low-density region. Using the conservation of flow and neglecting the coupling to counterflow one assumes $\frac{1}{4}K = \rho_-(1 - \rho_-)Q$, finally leading to:

$$\rho_-^1 = \frac{1}{2} + \frac{1}{2}\sqrt{1 - \frac{K}{Q}} \quad \text{and} \quad \rho_-^2 = \frac{1}{2} - \frac{1}{2}\sqrt{1 - \frac{K}{Q}} \quad (4.10)$$

As $\rho_- < \rho_+ = \frac{1}{2}$ has been observed only $\rho_- = \frac{1}{2} - \frac{1}{2}\sqrt{1 - \frac{K}{Q}}$ is a valid solution. Overall one obtains the flow for all density regimes:

$$\begin{aligned}
F(\rho) &= \rho(1 - \rho)Q \quad \text{for } \rho \leq \rho_- \\
F(\rho) &= \frac{1}{4}K \quad \text{for } \rho \in [\rho_-, \frac{1}{2}] \\
F(\rho) &= \rho(1 - \rho)K \quad \text{for } \rho \geq \frac{1}{2}.
\end{aligned} \tag{4.11}$$

4.3 Extending the Parameter Regime

The variety of bidirectional models turned out to exhibit basically the same features. Depending on the employed model a particular feature is dominating. The same is also true for some extensions of the models leading to additional parameters. The investigations thus far made no difference between the two directions of movement. So two extensions are possible. Assuming that different directions have different behavioural patterns one introduces different hopping rates depending on the direction [2]. Further differences may arise just by the number of ants travelling in one particular direction [42].

4.3.1 Different Hopping Rates

Different hopping rates are most likely to occur if some asymmetry between directions can be expected. This might be at the end or beginning of a swarm raid or migration when a particular direction is favoured. But also in an intermediate state like the exploitation of a food source an asymmetry can be expected. Ants carrying prey probably move differently from ants without any load [10–12, 36]. An extension to different hopping rates with respect to counterflow is only possible for models with an asynchronous exchange of positions like in ATMs 1 and 2. The choice of a synchronous exchange always implies the same hopping rate K in case of counterflow. Nevertheless one still could assume different rates for the unidirectional case.

4.3.2 Different Particle Numbers

For simplicity an equal number of ants for both directions was used for the previous investigations. In general this cannot be expected in a natural scenario. So different densities ρ_R and ρ_L for each direction are introduced.

The hopping rates are the same for each direction. Therefore flow F only depends on the densities $(\rho_L, \rho_R) \in [0, 1] \times [0, 1]$:

$$\begin{aligned}
F(\rho_L, \rho_R) &= F_L(\rho_L, \rho_R) \\
F(\rho_R, \rho_L) &= F_R(\rho_L, \rho_R)
\end{aligned} \tag{4.12}$$

So it is sufficient to measure flow say $F(\rho_L, \rho_R) = F_L$ in one direction for all densities. The corresponding flow in the opposite direction say $F(\rho_R, \rho_L) = F_R$

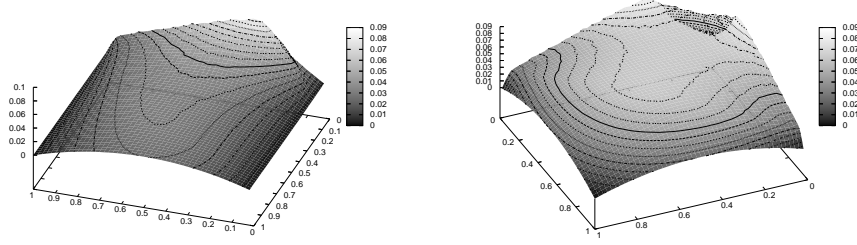


Fig. 4.17. Fundamental diagrams for ATM 2 ($Q = q = 1$, $K = 0.1$ and $\rho_L, \rho_R \in [0, 1]$): The figure on the left shows the flow in one particular direction say F_R for different densities (ρ_L, ρ_R) . On the right the total flow is shown for different densities (ρ_L, ρ_R) .

is found in the same diagram (see Fig. 4.17 left). Like in the special case $\rho_R = \rho_L$ already discussed flow shows only a slight density dependence. Although not exactly a constant plateau is attained the main feature of the counterflow model still exists.

As a consequence of using the same hopping rates for both directions the total flow $F_T = F_L + F_R$ is symmetric under the exchange of ρ_L and ρ_R :

$$F_T(\rho_L, \rho_R) = F(\rho_L, \rho_R) + F(\rho_R, \rho_L) = F_T(\rho_R, \rho_L) \quad (4.13)$$

This symmetry is also observed directly in the fundamental diagram (see Fig. 4.17 right). The total flow will be of interest especially in the ecological context of collective transport like foraging [10, 12].

4.4 Discussion

This chapter introduced different extensions of the unidirectional ATM to the *multilane* case. Unlike for example in vehicular traffic an extension to the bidirectional case was chosen. Depending on the particular kind of trail different bidirectional models are introduced (see Fig. 4.1). All models exhibited the features known from the unidirectional ATM at sufficiently low densities. Incorporating counterflow leads to additional features namely the *recoarsening* and *shredding* of the *moving cluster* (see Fig. 4.12). This feature was exhibited by all three models. At intermediate densities especially the models with asynchronous exchange of particles exhibited a new feature. Due to the mutual hindrance by counterflow one large *localised cluster* emerged (see Fig. 4.15). It was shown that this feature does not originate from the pheromone-marks. Again coarsening follows power laws with the same dynamical exponents as for

the unidirectional model (see Fig. 4.13). The stationary state exhibited phase separation similar to the case of static latticewise disorder.

Analogies to systems with static latticewise disorder (see chapter 2) were drawn. Unlike in the static case high- and low-density areas exhibit no particle-hole symmetry (see Fig. 4.14). Instead the high-density areas for both directions exhibit *particle-hole symmetry*. Making use of the symmetries within the localised cluster a mean-field description was developed. Unlike in the static case a common threshold density $\rho_+ \approx \frac{1}{2}$ was found. Again the cluster length showed a linear increase. The constant density ρ_+ within the clusters is independent from the impurity rate K . Therefore the cluster length is not used for indicating the transition to the homogeneous distribution for $\rho > \rho_+$.

Generalisations of the bidirectional models with asynchronous exchange of counterflowing particles were introduced. They also exhibited the same characteristic features discussed for the special case of equal particle numbers in both directions.

5 Empirical Results

The preceding chapters gave a survey over different models for traffic- and traffic-related systems. Those models made several qualitative and also quantitative predictions for traffic on real ant trails. This chapter seeks to draw a comparison between the models' predictions and the behaviour of the real system at least for one particular species based on empirical investigations.

5.1 Experimental Scenario

The models being discussed are quite simple as they incorporate only the most important (basic) features of the real system. So in comparison to the more complex reality they are quite restrictive [21, 36, 62]. For example they do not describe the trail formation itself. Also ants moving on the already existing trail are assumed to have all the same properties like the size of load or behavioural patterns. These properties are completely neglected in the following (see chapters 3 and 4). As no functional difference in the behaviour is incorporated the term "ant" will be used to refer to all moving agents in the system.

Also the choice of an *ecological context* for the observations has to be quite specific. A natural scenario was supposed to be less difficult to establish than a scenario that has to be built up artificially in a laboratory. If some kind of evolutionary generated optimisation is assumed it is more likely to be found in a natural situation [10, 85, 86].

On the other hand a natural system is more susceptible to disturbances which could be excluded in a laboratory. Nevertheless a key feature of *self-organised* systems in biology is some kind of robustness of patterns [6, 7, 13]. So a suspected optimisation pattern should be quite stable against natural disturbances. But in general the situation can be assumed to be more complex than in an experiment performed in a laboratory. As a compromise between a completely controlled artificial environment and a completely free natural environment we have focused on specific natural situations. They should already incorporate the main features of traffic organisation. Additionally they can be

treated even by simple models which can be extended later on once the key features have been identified.

5.1.1 Observed Species

The choice of the observed species appears to be the most important part. Meeting the already described requirements we used the trails of *Leptogenys processionalis* for our observations. Belonging to the so called *army ants* (in the broader sense) a whole set of features is associated with that species. Following [36] one definition would be:

Army ant: *Any species of ant that goes out in search of food in companies, particularly the driver and legionary ants.* (Webster's New International Dictionary 2nd ed., taken from [36])

Although the real behaviour is found to be more complex with respect to raiding and migration this definition will be sufficient as more detailed properties of that species are not used. Our species belongs to the *processionalis* group within the subfamily *ponerinae* which exhibits army-ant behaviour in a broader sense [36]. Till now especially the topological structure of the trails has been investigated [32].

Swarming behaviour in army ants is known to be a highly coordinated process [24, 36, 86]. Means of interaction are tactile as well as chemical ones. The system of trail pheromones is quite complex and yet not completely understood [86]. One main property is that the trails are defined by some of those pheromones. But the high degree of dynamics exhibited by the coordination of swarming can not be understood by incorporating just one kind of pheromone [13, 85, 86]. Extensive studies have been carried out for *Leptogenys distinguenda* [85, 86] but most results can be assumed to be also valid for *Leptogenys processionalis*¹. Another species close to *Leptogenys mutabilis* which also belongs to the *processionalis* group consists of approximately 30×10^3 workers per colony. Up to two third of them are known to take part in foraging raids [36]. Those raids are not controlled by leader-ants or scouts.

As one common feature the described species are nomadic. If one assumes some kind of evolutionary optimised traffic pattern this is most likely to be found in a species which frequently performs migrations. In fact swarm raids have been found to turn into migrations [86]. For that reason experiments inside a lab are nearly impossible and would influence the natural behaviour [86].

5.1.2 Environment and Ecological Context

Most of the advantages of observing in a natural environment have already been pointed out. Nevertheless there are also some disadvantages. One might

¹ R. Gadagkar and T. Varghese, personal communication

be the climate. As trails are known to be defined by *chemical marking*, heavy rainfall will destroy them. A prominent example is known from the army ants species *Labidus praedator* [36] where a larger group of workers was cut off from the trail system through rainfall. The group kept on moving, forming a circular mill and died finally due to starvation. So during periods of heavy rainfall hardly any trails of *Leptogenys processionalis* could be observed. Also movement along the trail appeared to be less coordinated when the ground was still wet. Additional requirements would be that the surface should be as smooth as possible. Leafs and tweaks are found quite frequently on the ground. They are leading to additional patterns like bifurcation into two different routes which have already been investigated extensively [6–8, 26]. Also bottleneck-situations are found which have also been investigated [25] drawing analogies to pedestrians dynamics. Although interesting both situations disturb the traffic situation we want to observe. For the same reason also surfaces with slopes defining a preferred direction were avoided.

The described lack of control in a natural situation can partially be compensated by the choice of an appropriate environment. Only environments with as less disturbances as possible were used for data collection.

The actual situation of the colony is also part of the observation. Ants on raiding trails have been observed to exhibit different behavioural patterns from those observed on migration trails [10, 86]. Additionally the trail structure is known to be highly dynamic in response to new requirements (e.g. [36, 85, 86]). The purpose of the trails can be shifted quite continuously from raiding to migration. So for data collection only trails exhibiting some constant temporal patterns were used. An additional characterisation was tried by distinguishing the trails by the carried load. Workers were carrying pieces of termites in a raid or larvae or pupae while migrating.

Observations were carried out on three different colonies living on the campus of the *Indian Institute of Science* (IISc) in Bangalore, India. The colonies were separated by more than three kilometres each. With respect to the distances a colony moves within the raid-migration cycle [36] it was ensured that three different colonies were observed independently.

5.1.3 Mapping the Model to Real Trails

Employing the latter restrictions mapping a real trail to the models becomes possible. At a first step this can even be done without any simplification. The trail itself might exhibit some curvatures and therefore appears to be topologically two dimensional (see Fig. 5.1 left). Nevertheless movement itself takes place in just one dimension although possibly in opposite directions along the trail. For describing the position of the ants, we follow the standard mapping also employed in vehicular traffic [22, 27]. The trail is subdivided into sections of equal length. Each section corresponds to a cell in the cellular automaton. The section length is approximately of one body length to ensure the *hard-core exclusion* principle (see Fig. 5.1 right). As *Leptogenys processionalis* is monomorphic with a body size of approximately 15 – 20mm this can be done quite

easily (see Fig. 1.1 right). More sophisticated considerations would be needed in case of highly polymorphic species like for example leaf-cutting ants. They differ in size even stronger than cars from trucks [12, 36]. But for *Leptogenys processionalis* all ants have the same physical abilities. This is obviously quite different from *vehicular traffic*. Different vehicles exhibit different behaviour due to construction or just caused by the driver (see chapter 2). In our case the "cars" are all identical and the "driving-behaviour" can be expected to be cooperative instead of being competitive [7, 11, 36]. Unlike in vehicular traffic the lanes can be supposed to be quite flexible. Depending on the actual situation they might just change their shape. As only the position along the lane itself is incorporated into the models this should not lead to any major difficulties. Nevertheless observations were carried out on trail-sections exhibiting a stationary shape.

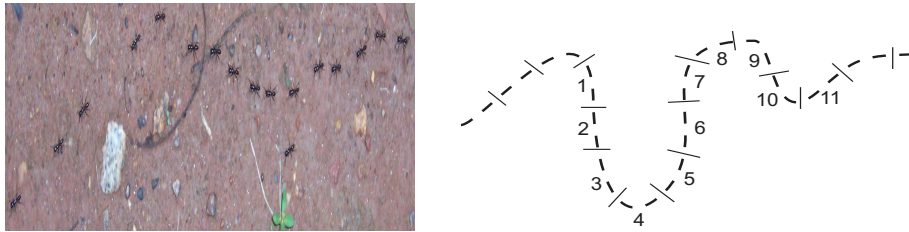


Fig. 5.1. The photograph (not drawn to scale) on the left shows an unidirectional single-lane trail. Obviously movement takes place along a one-dimensional chain. On the right the corresponding sectioning is shown. Each section is of the same length and equivalent to one cell in the cellular automaton model.

For implementing the model in a computer simulation, one also has to treat both ends or boundaries of the simulated trail section. Extensive empirical as well as theoretical investigations have been carried out. In vehicular traffic the boundaries would be equivalent to on- and off-ramps on a highway system [71]. But also in simulations of the ASEP and derived traffic models based on it, a severe influence of the boundaries on the whole system is found [1, 52, 72]. As a common feature the boundaries effectively set the density realised by the bulk of the system. Investigations of the ASEP showed that the bulk of the open system (see chapter 2) is characterised by a ring-like behaviour (periodic boundary conditions) for an appropriate choice of boundary conditions. So for the empirical measurements on real trails only the bulk of the system was used (see Fig. 5.2 up). Also intersections with other trails which would effectively act as on- and off-ramps were excluded from the observed section (see Fig. 5.2 down).

All properties of ant traffic discussed so far in case of *Leptogenys processionalis* did not make use of any approximations besides assigning the ants' position along the trail to a certain cell. But still some underlying properties

of the models need empirical validation first. None of the models incorporates overtaking. Also the mechanisms of interaction have to be extracted from empirical observations. The uni- as well as the bidirectional model assume some kind of *pheromone-mediated* interaction. Additionally some coupling to counterflowing ants via *tactile stimuli* is assumed in the bidirectional case. Additionally the choice of an appropriate update procedure is part of the models and is known to be connected to the way of incorporating different kinds of perception [11, 12, 36, 62]. All of these mechanisms will be subject to first observations discussed in the following section.

5.2 Methodology of Observations

Qualitative as well as quantitative observations were carried out on the traffic flow of ants moving on the kind of trail fulfilling the discussed requirements. Qualitative observations mainly serve for two purposes. First they give a clue towards the main mechanisms of interaction which will have to be incorporated by the models. Also the feasibility of the necessary assumptions regarding the trail topology are investigated. The second purpose is just the observation of certain traffic patterns which should also be reflected in the subsequent more detailed quantitative measurements.

5.2.1 Qualitative Observations and Preliminary Results

First observations concerned with the trail itself which is obviously defined by some kind of marking. Generally curvatures were observed (see Fig. 5.1 left) so ants are not just moving in a straight line say from A to B . Although some kind of "follow the leader" behaviour has been found, this is very unlikely to define the trail in the sense that ants form some kind of continuous chain. Even if the trail has been empty for up to one minute, ants were following exactly the same path as their predecessors. Also spatial restrictions forcing a trail of the observed particular shape have not been observed. So nearly all other possibilities like learning e.g. by tandem recruiting [31] or visual clues known from other species [36] can be excluded. Obviously the trail itself is defined by chemical marking employing the so-called *trail-pheromones* from the highly evolved pheromone system known in *Leptogenys* [36, 85, 86].

Multi- as well as single-lane trails have been found (see Fig. 5.3 left). Characterising them by the carried load (nesting material, larvae or pupae) multi-lane trails seems to occur during migration. Nevertheless also raids can shift to migration [85] so a final characterisation is difficult. As one common feature different lanes seems to be roughly independent from each other. For example no hopping between lanes was observed. But sometimes ants moving on one lane temporarily jumped into a gap on one of the other neighboring lanes. In order to minimise complexity we focus here on single-lane situations. In case of bidirectional traffic this means one lane for each direction.

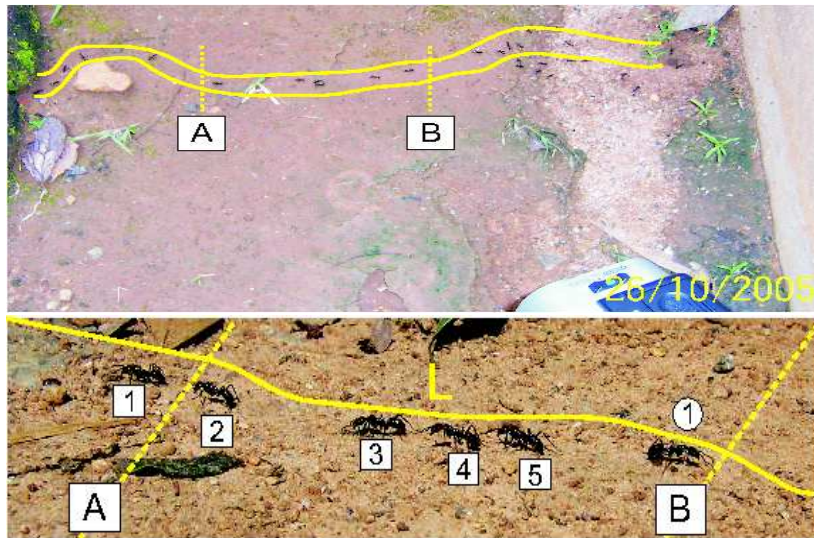


Fig. 5.2. The upper photography shows a whole trail including the observed section within points *A* and *B*. For data-collection the section was chosen to lie within the bulk. On the lower photography the observed section itself is shown. Ants entering the section in a particular direction say from right to left (\square) were labelled with the corresponding number of entering. The same was done for ants moving from left to right (\circ).

The Unidirectional Case

Already the single-lane unidirectional trails show a variety of interesting behaviour. One is the apparent absence of overtaking. Even at a high density of ants no *overtaking* has been observed. Under certain conditions ants might just slow down, probably due to a lack of orientation and temporarily leave their lane. In that case the succeeding ant(s) might just pass the preceding one. Nevertheless such events were mainly observed at low densities and are comparably rare. Also abandoning the trail completely appears to happen similarly rare. A second interesting phenomenon is the occurrence of *platoons* of ants (see Figs. 5.2 down, 5.1 left). Platoons of several workers, separated by roughly up to three body-lengths on average were entering the observed section and left it in the same structure. Also solitary ants have been observed, but predominantly movement in platoons was found. A more precise definition of a platoon used for quantitative measurements will be given in the next section. One also observes events of platoon formation. Single or multiple ants move at a speed allowing them to catch up with a preceding platoon or a single ant. Generally those ants did not seem to form a platoon by themselves but preferred to join an existing one. Once they managed to catch up they slowed down and followed as a part of the already existing platoon. In case of slowing down of a preceding



Fig. 5.3. The left photograph shows an unidirectional multi-lane trail. Only little interaction between the different lanes was observed. An empty gap in one lane might temporarily be filled with an ant of one of the two neighboring lanes. On the right the main form of communication on bidirectional trails is shown. So called head-on encounters happen almost anytime two workers face each other in opposite directions. Information is exchanged via the so-called antenna language using tactile stimuli.

ant the following ones also slowed down and increase speed again, preserving the platoon. So distances within the platoons can be expected to be fluctuating.

The Bidirectional Case

The bidirectional trail shows all the behavioural patterns and properties of the unidirectional one. In absence of counterflow the full unidirectional behaviour is recovered. So the bidirectional trail can be regarded as a superposition of both cases. But in presence of counterflowing ants some additional behavioural patterns emerge. The most important one is the occurrence so-called *head-on encounters*. Ants facing each other in opposite directions slow down and exchange information via their antennae (see Fig. 5.3 right). This was predominantly observed for any encounter of counterflowing ants and has been investigated in the context of ant-traffic for leaf cutting ant *Atta cephalotes* [11, 12]. The resulting slowing down affects the structure of the platoons. One additional feature completely different from unidirectional traffic seems to be the occurrence of *U-turns*. Ants moving in one direction suddenly reverse their course and join the movement into the opposite direction. The number of such events is comparably small but will also be subject of further investigations.

5.2.2 Quantitative Observations

For a comparison with traffic flow in other systems like for example vehicular traffic or pedestrians more detailed data is desirable. Also the already described behavioural patterns need some quantitative validation. Due to the obvious similarities to vehicular traffic, techniques from *traffic engineering* [34, 60, 83] will be employed for characterising the traffic flow of ants on a preexisting trail.

At a first step single-ant velocities and the actual number of ants within the observed section will be measured. Derived from time headways and single-ant velocities, distance headways will be calculated. The corresponding distributions of distances and velocities will also be of interest. As mutual blocking can be assumed to depend on the number of ants within the observed section, also fundamental diagrams will be extracted.

For observations video recordings of a particular trail section are used. So analysis can be repeated in order to avoid major errors ensuring the reproducibility of data. Also the investigation of directly observable macroscopic traffic patterns and individual behaviour is possible. In addition the carried load can be analysed as well, which will be helpful for identifying the ecological context [85, 86]. A direct comparison between the measured or derived quantities and the observed patterns finally concludes the discussion. As various automatic video tracking systems failed, measuring which is basically reduced to counting, had to be done by hand.

Cumulative Counting

For measuring so-called *cumulative counting* is used (e.g. [63]). An ant entering the observed section (see Fig. 5.2 right) was assigned to the time of passing say at point A . One obtains a data point (t_+, n) for the time of entering $t_+(n)$ and the actual number n . The same is done when the n th ant leaves the observed section again say at point B producing a datapoint (t_-, n) . If no overtaking or U -turns occur, the n th ant entering is also the n th ant leaving. Obviously the labelling of datapoints depends on the number $(n - 1)$ of ants which have already passed (see Fig. 5.4). Thus labelling by counting is done cumulatively. Based on the two datapoints for one ant all other quantities will be calculated. Nevertheless some correction of systematical errors had to be done. A discussion of systematical (see App. A.1) and statistical (see App. A.2) errors can be found in the appendix.

Travel Time and Single-Ant Velocity

Single-ant travel times and velocities are calculated for each ant passing the observed section. The n th ant entering at $t_+(n)$ leaves the section at $t_-(n)$. So one obtains the time $dT(n)$ it took the n th ant for travelling through the observed section (see Figs. 5.4, 5.5 left):

$$dT(n) = t_-(n) - t_+(n) \quad (5.1)$$

Incorporating the known length L of the section one obtains the average single-ant velocity between points A and B :

$$v(n) = \frac{L}{dT(n)} = \frac{L}{t_-(n) - t_+(n)} \quad (5.2)$$

In the succeeding discussions some averaging over individual measurements will be done. For the average velocity two definitions have been established in traffic engineering [60]. The *space-mean speed* is basically defined as the average over n_0 travel times:

$$V_S = \frac{L}{T_{av}} = L \left(\frac{1}{n_0} \sum_{n=1}^{n_0} dT(n) \right)^{-1} \quad (5.3)$$

As an alternative averaging over n_0 single-ant velocities leads to the *time-mean speed*:

$$V_T = \frac{1}{n_0} \sum_{n=1}^{n_0} v(n) = \frac{1}{n_0} \sum_{n=1}^{n_0} \frac{L}{dT(n)} \quad (5.4)$$

A comparison of both definitions shows that the average over travel times $dT(n)$ is related to the average over velocities $v(n)$. An exact relation between both, depending on the variance of the *space-mean speed* has been shown (e.g. [60]). In case of vanishing variance, like in the discussed computer simulations (see chapters 3 and 4) both velocities turn out to be exactly the same. Although this is not the case in our experiments we will make use of the *time-mean speed*. As one advantage of using time-mean speed one directly calculates flow making use of the *hydrodynamic relation*. In case of cooperative traffic, flow appears to be a crucial quantity related to a system optimum (see chapter 1). Travel times instead are related to a user optimum (see chapter 1). A brief discussion of the different quantities in the context of ant-traffic is given in [12, 41, 45].

Instantaneous Number of Ants

The method employed for measuring travel times makes use of the observation, that the n th ant entering the observed section will also be the n th one leaving it. But determining the instantaneous number $N(t)$ of ants between points A and B at a particular time t only makes use of particle- or mass conservation. Thus $N(t)$ is just given by the difference between the number of ants which have entered $n_+(t)$ and left $n_-(t)$ the section at time t (see Figs. 5.4, 5.5 right):

$$N(t) = n_+(t) - n_-(t) \quad (5.5)$$

Obviously $N(t)$ stays constant till $n_+(t)$ or $n_-(t)$ is changed. An ant entering at $\tilde{t} > t$ leads to $n_+(\tilde{t}) = n_+(t) + 1$ therefore increasing $N(t)$ by one unit. In the same way a leaving ant at $\tilde{t} > t$ will decrease $n_-(t)$ by one unit leading to $N(\tilde{t}) = N(t) - 1$.

For determining the fundamental diagram one is interested in the relation of the single-ant velocities vs. density or equivalently flow vs. density. The n th ant passing from A to B spends the period $dT(n)$ between $t_+(n)$ and $t_-(n)$ within the observed section. This ant will be affected by various changing instantaneous particle numbers $N(t)$ (with $t \in [t_+, t_-]$). Therefore it is necessary

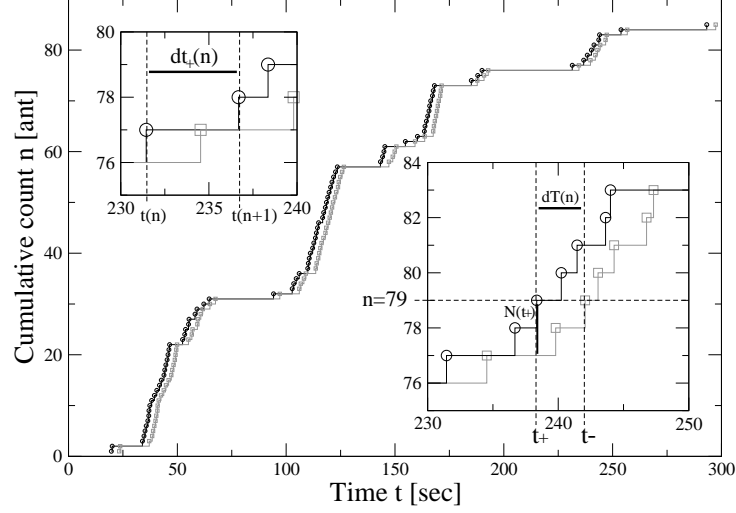


Fig. 5.4. Cumulative counting (video 13): The figure shows the cumulative counting of entering (\circ) and leaving (\square) ants. The times of entering $t_+(n)$ and leaving $t_-(n)$ for each ant n are shown. Based on this, the time for crossing the observed section $dT(n)$ as well as the instantaneous number of ants in the section $N(t)$ can be calculated (see lower inset). The time headway $dt_+(n)$ for the n th ant is shown on the upper inset.

to incorporate those changes by using a time average over $N(t)$ rather than using the instantaneous number of ants at time t_+ within the observed section.

$$N_{av}(n) = \frac{1}{dT(n)} \sum_{i=i_+}^{i_-} N(t_i)(t_{i+1} - t_i) \quad \text{with} \quad dT(n) = \sum_{i=i_+}^{i_-} (t_{i+1} - t_i) \quad (5.6)$$

Summation is done over all instantaneous particle numbers $N(t)$ and the time-period of their existence $t_{i+1} - t_i$. Hereby t_i denotes the time at which one particle number $N(t)$ is attained. At time t_{i+1} one ant leaves or enters the trail changing $N(t)$ by one unit². By summing up $N(t)$ like this one obtains the area enclosed by both curves between t_+ and t_- . The sum is finally averaged over the travel time $dT(n)$. So for each ant one obtains a velocity $v(n) = \frac{L}{dT(n)}$ and a corresponding particle number $N_{av}(n)$ both averaged over the same time-interval $dT(n)$. Other approaches using instantaneous particle numbers and

² Data points for entering (t_+, n) and leaving (t_-, n) are collected. Sorting them by time leads to a chronological order of entering and leaving events (t_i, n_i) changing $N(t)$ by one unit.

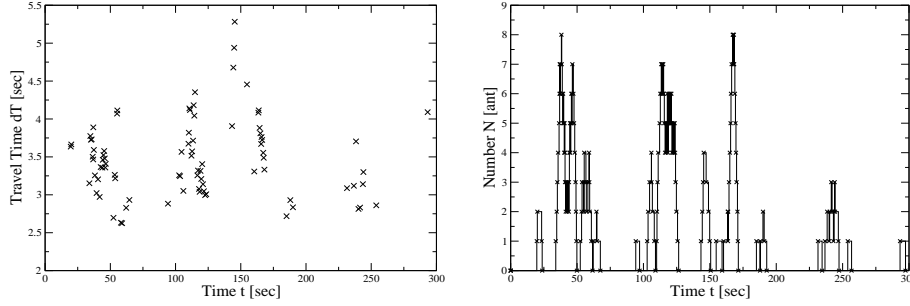


Fig. 5.5. Derived quantities (video 13): Both figures show the directly derived quantities. On the left the travel time $dT(n)$ for the n th ant entering the observed section at $t_+(n)$ is shown. The average of dT is given by $dT_{av} = \frac{1}{V_s}$. On the right the instantaneous number of ants $N(t)$ within the observed section is shown. Each ant entering or leaving the section changes $N(t)$ at time t_i . Hereby t_i denotes the actual time of that event $t_i = \min\{t_+(n), t_-(n)|n \in [1, N]\}$ with $t_i \geq t_{i-1}$ and $t_1 := t_+(1)$.

single-ant velocities hardly showed any functional relation between single-ant velocities and density [12, 47].

Measuring Lengths and Densities

For determining *time-mean-speed* and densities, the length of the observed section L had to be measured. As the trail and also the observed section exhibit some curvature direct measurements appear to be quite difficult. One would have to measure a still populated trail. Also marking the underground (e.g. [29]) for making the trail visible permanently would affect the ants' behaviour and probably destroy the observed part of the trail. So measuring the length of the observed section is based on the videos using the body-size of the ants as a natural scale (see Fig. 1.1). Tracing the path of one single ant, sections of one body length ($1bl$) were marked (see Fig. 5.1 right). Making use of the fact that *Leptogenys processionalis* is monomorphic one obtains the section length in units of the body size which can easily be converted into other length scales ($1bl \approx 18mm$ with $L \approx 19bl$). One additional advantage of this method is, that it is free from errors arising from the perspective of the camera.

Without converting lengths one easily obtains the density of ants within the observed section:

$$\rho(n) = \frac{N_{av}(n)}{L} \quad (5.7)$$

Again the average number of ants $N_{av}(n)$ is used (see 5.6). In the *fundamental diagram* single-ant velocities and flow are plotted vs. density. For the n th ant density and velocity are both averaged over the same time-interval given by the travel time $dT(n)$.

Time- and Distance Headways

For characterising traffic patterns time- and distance headways have proved to be very useful [60]. The time difference of two succeeding ants passing the same point say at the entrance of the observed section at point A is given by:

$$dt_+(n) = t_+(n+1) - t_+(n) \quad \text{and also} \quad f = \frac{1}{dt_+} = \frac{1}{t_+(n+1) - t_+(n)} \quad (5.8)$$

Also instantaneous flow f is given by the time headway which can directly be observed as the local slope of the cumulative plot $n(t)$ (see Fig. 5.4). Under the assumption that the single-ant velocity $v(n)$ stays constant within the observed section one directly derives the corresponding distance headway:

$$d_+(n) = dt_+(n)v(n-1) = [t_+(n) - t_+(n-1)]v(n-1) \quad (5.9)$$

5.3 Results of Quantitative Observations

Videos from several trails were recorded. Those fulfilling the requirements already discussed in the preceding section were chosen as some kind of prototype. The observed behavioural patterns will also be found on the other trails belonging to the same class. Therefore it is most likely that all trails belonging to the same class will exhibit similar properties also reflected in the quantitative measurements.

We start by investigating an ideal unidirectional trail (*video 13*). No error correction had to be done. But traffic flow ceases after only five minutes. A more complex situation is found for the second investigated unidirectional trail (*video 19*). The observed time-period extends up to 13 minutes. Due to the comparably large number of ant-countings slight error correction had to be done. The third class of trails will finally be a bidirectional trail which was observed over 25 minutes (*video 6A, B, C*). Nevertheless also periods of unidirectional traffic exist. Due to U-turns extensive error correction became necessary.

5.3.1 The Simple Unidirectional Trail (Video 13)

Although only 85 ants have been passing the observed section, some of the main features of unidirectional traffic are already visible. As no disturbances occurred they emerge very clearly. Also some basic techniques for investigating will be exemplified in this less complex case.

Single-ant Velocities

Measuring velocities vs. time shows oscillations around the average value (see Fig. 5.6 left). Some kind of clustering of datapoints in time is found which

results from the already observed feature that ants tend to move in platoons. In accordance with the already described behaviour no overtaking occurred. Like in vehicular traffic [34, 60] a normal distribution of single-ant velocities can be expected:

$$P(v) = \frac{1}{\sigma\sqrt{2\pi}} \exp\left(-\frac{(v(n) - V)^2}{2\sigma^2}\right) \quad (5.10)$$

Fitting (5.10) to the single-ant velocities one obtains the mean velocity $V = 6.40[bl/sec]$ with a standard deviation of $\sigma = 0.94[bl/sec]$ (see Fig. 5.6 right). A slight asymmetry towards small densities is found. This can be explained by directly observing the ants behaviour during the measurements. At low densities ants struggling to stay on the trail are found. Those ants had to slow down moving temporarily at a lower speed. This illustrates one advantage of extracting data from videos as measured data can be compared directly to the observable behaviour later on.

In this case the observed behaviour is also reflected in the dynamics of the single-ant velocities (see Fig. 5.6 left). A few datapoints show a strong deviation from the mean value. Although the deviations are comparably rare (see Fig. 5.6 right) they seem to be contradicting the fact that no overtaking has been observed. But this can be explained by incorporating the clustering of datapoints (see Fig. 5.6 left). Ants with a small time headway also show little differences in their velocities. So the velocity of the whole platoon deviates from the mean value. Ants within the platoon itself obviously do not overtake each other. Also the observed section is of finite length. So single-ant velocities are only measured for a comparably short time. Ants with velocities strongly deviating from the mean value might attain V again outside the observed section without any events of overtaking.

Distance Headways

Single-ant velocities can be assumed to be constant at least within one cluster of ants characterised by small time headways. From (5.9) this might also indicate some spatial clustering. Distances between ants, namely the distance headways $d(n)$, should reflect the already observed spatial clustering of ants to platoons. A first sign of platoon formation are the peaks observed for the instantaneous particle number $N(t)$ vs. time (see Fig. 5.5 right). Ants moving within a platoon lead to a sharp increase while entering and lead to a sharp decrease of $N(t)$ while leaving the observed section.

By measuring time headways at the entrance of the observed section one obtains the distance headway of the n th ant (see Fig. 5.7 left). While crossing the observed section distance headways are only slightly changed. So the platoons are quite stable regarding their structure like the length or the number of ants forming the platoon. A small time headway obviously also leads to a small distance headway due to the narrow distribution of velocities (see 5.9). From (5.9) the distance headway distribution is obviously dominated by the distribution

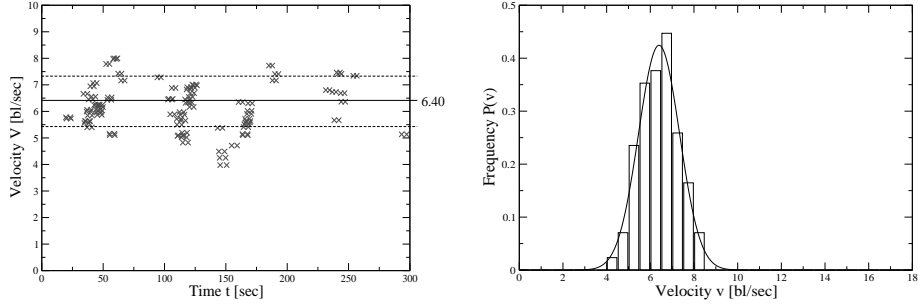


Fig. 5.6. On the left single-ant velocities as a function of time are shown. Some clustering of datapoints is observed. Ants with a small time-headway roughly move at the same speed. On the right the distribution of single-ant velocities $v(n)$ is shown. Velocities $v(n)$ exhibit a normal distribution with $V = 6.40 \frac{bl}{sec}$ and a variance of $\sigma = 0.94 \frac{bl}{sec}$ ($\frac{\chi^2}{\nu} = 2.25^{-4}$, $bin = 0.5$) depicted on the right. A small asymmetry towards lower velocities is found.

of time headways. The time headways are the inverse of the instantaneous flow and are therefore mainly controlled by the in- and outflow at the boundaries of the observed section (see Fig. 5.4). Overall no normal distribution is found (see Fig. 5.7 right). Due to the lack of datapoints this is observed more clearly in video 19 (see Fig. 5.12 right).

Basically two regimes can be distinguished. The distribution of small distances of ants within (*intra*) a platoon and the distribution of large distances between (*inter*) platoons themselves. The intra-platoon distances show a small average value in comparison to their large asymmetric variance. As distance-headways cannot become negative this gives rise to a so-called skewed distribution [9, 58]. This was to be expected as ants can not come arbitrarily close to each other. On the other hand large inter-platoon distances are found. One common choice for fitting in such a case is the *log-normal* distribution:

$$P(d) = \frac{1}{d\sigma_L\sqrt{2\pi}} \exp\left(-\frac{(\mu_L - \log(d))^2}{2\sigma_L^2}\right) \quad (5.11)$$

Due to its close relation to the normal distribution one obtains the mean-value D and the variance σ^2 as log-transformed quantities:

$$D = \exp\left(\mu_L + \frac{\sigma_L^2}{2}\right) \quad ; \quad \sigma^2 = (\exp(\sigma_L^2) - 1) \exp(2\mu_L + \sigma_L^2). \quad (5.12)$$

For the larger inter-platoon distances the *negative-exponential* distribution is applied. In traffic-engineering this distribution corresponds to the *random-headway state* (e.g. [60]):

$$P(d) = \frac{1}{\lambda} \exp\left(-\frac{d}{\lambda}\right) \quad (5.13)$$

The movement of the platoons is assumed to be uncorrelated when distances are large. Therefore the probability-density $P(d)$ decays with a constant λ .

Overall two kinds of ants can be distinguished. Ants with a short distance headway are moving inside a platoon whereas ants with a large distance headway are at the head of it. This is also true if only one ant forms the platoon. The term platoon therefore applies for all ants with a large distance headway.

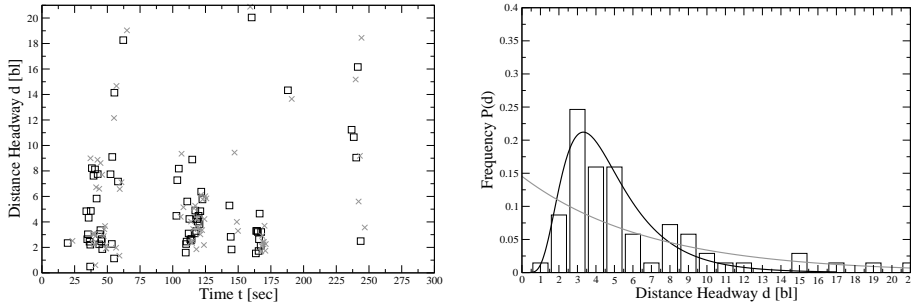


Fig. 5.7. On the left distance headways vs. time are shown. Headways were measured for entering \square and \times leaving ants. Obviously distances do not change much while passing the observed section ($L = 21bl$). As already suspected ants with a small time headway are very likely to have also a small distance headway. On the right the distance headway distribution is shown. Although there are only few datapoints two regimes can be distinguished. At low distances a skewed distribution is found. Larger distances show a different kind of distribution.

For investigating intra- and inter-platoon headways a cut-off distance d_c for assigning distances to one of the two regimes is used. Ants with $d(n) \leq d_c$ are assigned to the inside of a platoon whereas ants with $d(n) > d_c$ are not. The number of those ants with $d(n) > d_c$ corresponds to the number of platoons even if that one is formed by one single ant. The choice of the cut-off d_c depends on the average distance of the actual number of ants in the section (A.3). For practical reasons also an upper bound for large distances is used which is twice of the length of the observe section. Making use of that classification one finds $N_{platoon} = 49$ ants within platoons and $N_{ant} = 27$ outside (see Tab. 5.2). So each cluster consists of 1.43 ants on average. Obviously there are several solitary ants separated by large distances (see Fig. 5.7 left).

Fundamental Diagram

The previous discussion dealt with distributions of microscopic quantities like single-ant velocities and distance headways. As established in traffic engineering

effects like mutual blocking or other kinds of interaction can be assumed to depend on the average distance of the moving agents or equivalently on density. The functional relation between average velocity $V(\rho)$ or flow $F(\rho)$ vs. density ρ , known as the *fundamental diagram*, is widely used for characterising traffic flow. Due to the *hydrodynamic relation* $V(\rho) = \rho F(\rho)$ both descriptions V vs. ρ and F vs. ρ are basically equivalent. Nevertheless as already observed in the previous chapters 2 and 3 particular features (e.g. like the plateau in flow) are clearly visible only in one of the two descriptions.

The already observed patterns in the distributions of single-ant velocities and distance headways should also be reflected in the fundamental diagram. Although only small densities $\rho_{max} \approx 0.33 \frac{ant}{bl}$ are found for the investigated trail section (video 13) some basic features already emerge. Velocities stay nearly constant and show a decreasing width of scattering around the average value with increasing density. As a consequence flow shows a linear dependence on density (see Fig. 5.8).

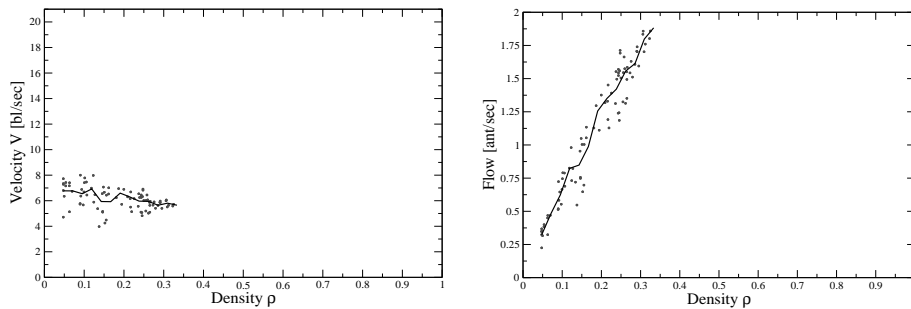


Fig. 5.8. The figures show the fundamental diagram obtained for the observed section of video 13. The single ant-velocities on the left show nearly no density dependence. The width of scattering around the mean-value nevertheless depends on density. In accordance to the hydrodynamic relation flow increases linearly with density. The solid line corresponds to the average value in each description.

As velocities stay nearly constant one might assume the traffic system to be in the so-called *free-flow* state. In vehicular traffic this state also exhibits a nearly constant single-vehicle velocity at low densities. Vehicles are separated at distances such that they are able to drive at their desired speed. In the case of ant-traffic investigated here this seems to be quite different. The previous investigations of distance headways and direct observations revealed the movement in platoons. Nevertheless some analogies can be drawn (see chapter 6).

A more detailed description could be obtained from the "*Optimal Velocity (OV)*"-curve. Single-ant velocities vs. distance headways are investigated. This is mainly done as any kind of interaction is assumed to depend on the distance

headway. For investigating ant-ant interaction the OV-curve will be used in Sec. 5.4.

5.3.2 The Complex Unidirectional Trail (Video 19)

The previous trail showed only light traffic with little interaction. As a result only datapoints within a limited density regime were obtained. In order to investigate the density dependence of the average velocity or flow a trail with heavy traffic ($\rho_{max} \approx 0.8 \frac{ant}{bl}$) was chosen. The exhibited pattern are more complex than in the previous case and some error correction became necessary (see A.1). But the number of datapoints is sufficient for more detailed analysis (see A.1).

Single-ant Velocities

Investigating single-ant velocities vs. time one observes strong oscillations (see Fig. 5.9 left). Especially at early and later times velocities lie above the confidence interval. For those times only few ants are moving on the trail (see A.1). At the beginning of the observed period of time only little but non-vanishing flow is observed. This is indicated by the slope of the cumulative count. Approaching the end of the observed time flow continuously vanishes (see A.1). Obviously some density dependence of velocities exists. But still a clustering of datapoints in time is found (see Fig. 5.9 left). So again no overtaking takes place.

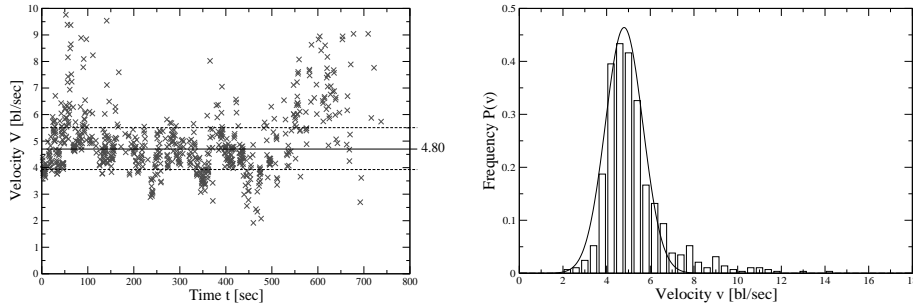


Fig. 5.9. The left figure shows strong oscillations around the mean values of single-ant velocities vs. time. The centre of oscillation is somewhat shifted to velocities larger than the average value. Therefore the corresponding distribution on the right shows a slight asymmetry towards larger velocities. $V_{tot} = 4.80 \frac{bl}{sec}$, $\sigma = 0.86 \frac{bl}{sec}$, $\frac{\chi^2}{\nu} = 5.77 \times 10^{-4}$ and $bin = 0.4$

The strong oscillations of velocities in time are also found in the distribution of single-ant velocities (see Fig. 5.9 right). For some times the centre of

oscillation is slightly shifted above the average value $V_{tot} = 4.80 \frac{bl}{sec}$. Although the corresponding distribution is approximately symmetric a slight asymmetry towards very high single-ant velocities is found. As a threshold value velocities above $V_{th} = 2V_{tot} = 9.8 \frac{bl}{sec}$ can be considered to be unrealistic. They most probably arise from some kind of error (see A.1). But still the number of velocities above the threshold value is comparably small (see Fig. 5.9 right). So for further investigations they will be neglected.

Fitting a normal distribution leads to the already used average velocity $V = 4.80 \frac{bl}{sec}$ and a variance of $\sigma = 0.86 \frac{bl}{sec}$. In comparison to the simple unidirectional trail the average velocity is significantly lower whereas the variance is nearly the same. Overall this might indicate a density dependence of single-ant velocities or flow on density. So velocity distributions were measured for three different density regimes (see Tab. 5.1).

$\rho \in$	$n[ant]$	$V[blsec^{-1}]$	$\sigma [blsec^{-1}]$	$\frac{\chi^2}{\nu}$
$[0, 0.8]$ (complex)	721	4.80	0.86	5.77×10^{-4}
$[0, 0.2]$	125 (17.3%)	6.20	1.58	7.37×10^{-4}
$[0.2, 0.4]$	329 (45.6%)	5.10	0.95	2.00×10^{-4}
$[0.4, 0.8]$	267 (37.0%)	4.64	0.60	0.88×10^{-4}
$[0, 0.3]$ (simple)	85	6.40	0.94	2.25×10^{-4}

Table 5.1. Single-ant velocities were measured for three different density regimes of the complex unidirectional trail. The regimes are roughly found in the corresponding fundamental diagram (see next section). Average velocity decreases slightly with density. Also the variance decreases with density. The last line shows the data obtained for the simple unidirectional trail.

The regimes were chosen such that they can roughly be distinguished in the fundamental diagram (see Tab. 5.1) which will be discussed in the next section. With increasing density the average single-ant velocity V decrease slightly. More striking is the decrease of variance with increasing density (see Fig. 5.10). At low to intermediate densities again a slight asymmetry to higher velocities is found which does not exist in the very narrow distribution at high densities. So this feature already observed for the total distribution (see Fig. 5.9 right) originates from the ants' behaviour at low to intermediate densities. The total average velocity V_{tot} is determined by the ants behaviour at intermediate to high densities. Average velocities in these regimes are nearly the same as $V_{tot} = 4.80 \frac{bl}{sec}$ (see Tab. 5.1). At very low densities the average velocity of the complex and the simple trail are nearly identical. Negligible differences arise from the slightly different density regimes used for measuring. This might also account for the comparably large difference in the variance which shows a stronger density dependence than the average velocity.

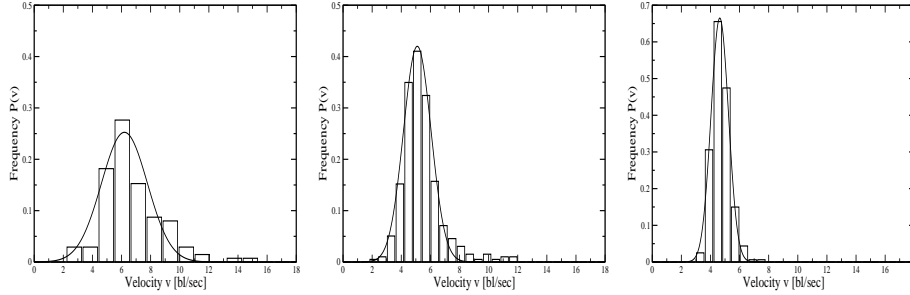


Fig. 5.10. From left to right the velocity distributions of the three density regimes for the complex unidirectional trail are shown. Normal distributions were fitted. At very low densities $\rho \in [0, 2]$ (left) variance is quite high. At intermediate $\rho \in [0.2, 0.4]$ (middle) and high $\rho \in [0.4, 0.8]$ (right) densities, the mean value of velocity is nearly the same. Note that for very high densities (right) the scale of the y-axis has been changed. The most striking feature is obviously the strong density dependence of variance. The average velocity shows only little density dependence for intermediate to high densities.

Fundamental Diagram

The fundamental diagram gives a more detailed picture of the density dependence of the single-ant velocities or flow. From velocity one identifies the three density regimes already used for the previous discussion of velocity distributions (see Fig. 5.11 left). At low densities the average velocity and variance are quite high. For intermediate to high densities the average velocity stays nearly constant. Only the variance changes significantly with density (see Tab. 5.1).

As already indicated by the velocity distributions the average velocity decreases slightly with increasing density (see Fig. 5.11 left). Also flow shows a nearly linear increase (see Fig. 5.11 right). At very high densities flow exhibits some non-linearity. But the number of datapoints in that regime are quite low. Nevertheless a slight curvature is visible. This might indicate that effects of mutual blocking start to set in.

Concerning the variance, single ant velocities show an asymmetric scattering to higher values of velocity especially at low densities. With increasing density the width of scattering decreases and becomes symmetric.

Overall the fundamental diagram shows two interesting effects. In comparison to vehicular traffic velocity stays nearly constant. Even at high densities only slight effects arising from mutual blocking are found. As a second feature variance exhibits a strong density dependence. The asymmetry of the single-ant velocity distributions to higher values clearly depends on density.

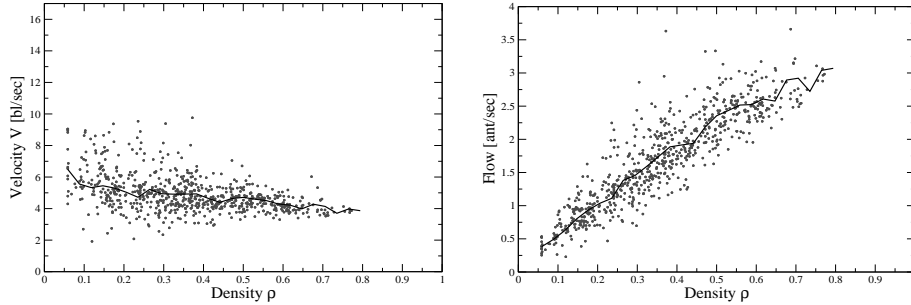


Fig. 5.11. Single-ant velocities and flow vs. density are shown. The solid black line corresponds to the average value. Unrealistic velocities $v(n) > 2V_{tot}$ were not incorporated. The average velocity shows only a slight decrease with increasing density. Flow exhibits a slight curvature at high densities indicating slowing down due to mutual blocking.

Distance Headways

The discussed properties exhibited by the fundamental diagram can be assumed to originate from the spatial distribution of ants within the observed section. So distance headways are measured according to (5.9).

Distance headways vs. time show the same properties already observed for the simple trail (see Fig. 5.12 left). Most datapoints for entering and leaving ants cluster at low distances. Comparably few datapoints are found at larger distances. The headways for entering and leaving differ stronger than in the simple case. Obviously the spatial structure of the platoons is changing while passing the observed section. Nevertheless platoons exist which is also indicated by the peak-like structure of the instantaneous particle number $N(t)$ (see Fig. A.1).

The total headway distribution clearly shows a division into two parts (see Fig. 5.12 right). For low distances a skewed distribution is found. Variance is high in comparison to the low mean value. Analogous to the preceding section a log-normal distribution (5.11) appears to be appropriate. Unlike in the simple case a continuous distribution of the larger distances is found, which is a consequence of the larger amount of datapoints. Following the argumentation of the preceding section a negative-exponential distribution (5.13) can be assumed.

For a more detailed investigation of the spatial distribution distance headways are measured for each of the three density regimes (see Fig. 5.13). At low densities a very broad distribution is found. The average distances between ants are so large that hardly any interaction takes place. Therefore the random headway state can be expected. Correspondingly the negative exponential distribution instead of the log-normal distribution fits best for all distances. At intermediate densities the distribution can be divided into smaller and larger distances. Smaller distances follow a log-normal distribution whereas larger

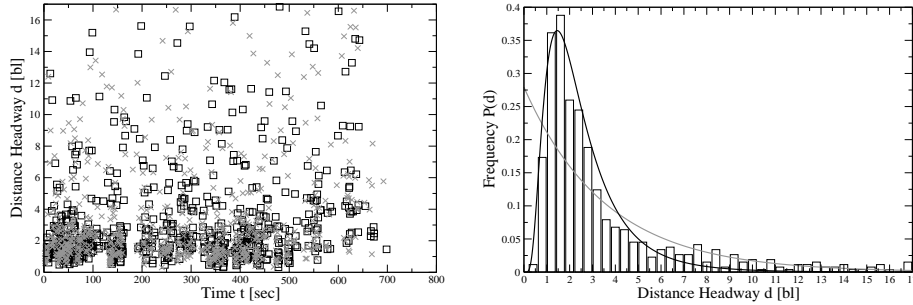


Fig. 5.12. The left figure shows distance headways vs. time. Unlike on the simple trail entering + and leaving \square ants can have quite different headways. Nevertheless most headways are clustered at small distances. On the right the distribution of distance headways shows a peak at low distances and an exponential decay at growing distances.

distances are distributed according to the random-headway state. At very high densities a narrow log-normal distribution is found for all distances. Distance headways obviously are highly correlated indicated by the vanishing of larger distances leading to the random-headway state.

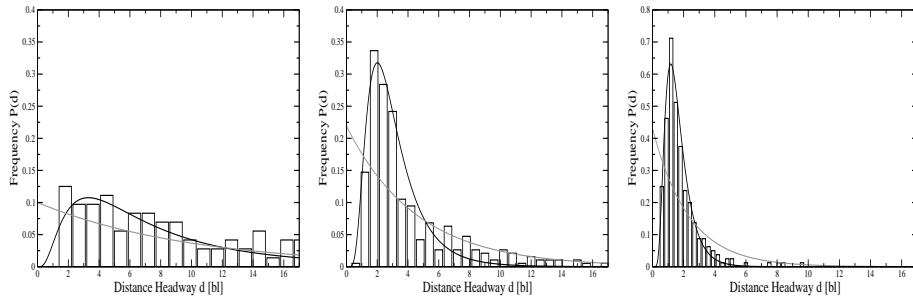


Fig. 5.13. For different density regimes distance headway distributions are shown. A broad distribution (left) is found for low densities. At intermediate densities (middle) the distribution gets sharper. For high densities (right) only short distances are found. Depending on the particular density regime the distributions follow a negative exponential- or a log-normal distribution.

Quantitative measurements also confirm the clustering of ants to platoons (see Tab. 5.2). The average available distance per ant decreases with increasing density (see A.3). Therefore at low densities only half of the ants move in platoons. At intermediate densities this does not change much. But for high densities nearly all ants are moving in platoons. The mean value of the dis-

tance headways D extracted from the log-normal distributions also decreases with increasing density. Nevertheless this value generally does not correspond to the average distance of ants within a platoon. The intra-platoon distance depends on the mechanism of platoon formation. But as already observed distance headways show some clustering at small values (see Fig. 5.12 left) which is obviously independent from density. At high densities all ants can be assumed to be affected by moving in platoons. Therefore the average distance headway within a platoon is given by $D = 1.66[bl]$ in that case. This is also in accordance with the observations from Fig. 5.12 left.

$\rho \in$	d_c	N_{ant}	$N_{platoon}$	$D[bl]$	$\sigma[bl]$	$\lambda[bl]$
$[0, 1]$ (complex)	2.45	394(56.0%)	309(44.0%)	2.59	1.77	3.58
$[0, 0.2]$	8.34	59(54.6%)	49(45.4%)	8.83	8.50	10.00
$[0.2, 0.4]$	2.60	167(50.9%)	161(49.1%)	3.11	1.81	4.56
$[0.4, 0.8]$	0.68	26(9.7%)	241(90.3%)	1.66	0.84	2.32
$[0, 3]$ (simple)	5.8	49(64.5%)	27(35.5%)	4.83	2.57	6.88

Table 5.2. Quantities extracted from fitting log-normal- and negative-exponential distributions are shown for different density-regimes of the complex trail. The last line shows the values for the simple trail. Overall the mean-value and the variance of the log-normal distribution decrease with increasing density. Also the constant λ describing the decay of the probability density in the random-headway state decreases. Nevertheless each distribution only applies for a certain regime of distance headways depending on density.

5.3.3 The Bidirectional Trail (Videos 6a, b, c)

The previous investigations all concerned with unidirectional trails. For further investigations *multi-lane traffic* is the obvious choice. Basically the same arguments apply as for the multi-lane extension of the unidirectional ATM (see chapter 4). So two-lane *bidirectional traffic* will be investigated in the following section.

Quantities like velocity and flow generally depend on the density of ants in one particular direction or lane. But due to the coupling between lanes also the density in counterdirection can be expected to have some influence. Basically the density in counterdirection determines the number of ants being encountered by one ant passing the observed section in the opposite direction. This is a consequence of the observation that ants passing each other in opposite directions nearly always slowed down during a *head-on encounter*. Unlike for the unidirectional case no microscopic quantity like a distance headway for counterflowing ants is available. Therefore only density will be used for distinguishing between uni- and bidirectional traffic on a macroscopic scale.

Unidirectional traffic still can be found on the bidirectional trail. When the flow in one particular directions temporarily ceased periods of unidirectional traffic are found (see Figs. A.2, A.3, A.4). So the subsequent analysis will distinguish between the uni- and bidirectional case of a basically bidirectional trail.

Analogous to the previous investigations the number of ants within the observed section during the crossing of the n th ant is averaged according to (5.6). For each crossing one obtains the average number of ants in the own $N_{av}(n)$ and in counter direction $N_{av}^{cf}(n)$. Densities are defined correspondingly. For $N_{av}(n) \leq 1$ traffic is assigned to the unidirectional case otherwise the bidirectional case applies:

$$N_{av}^{cf}(n) \begin{cases} \leq 1 & \text{unidirectional case; } v(n) = v(\rho) \\ > 1 & \text{bidirectional case; } v(n) = v(\rho, \rho^{cf}) \end{cases} \quad (5.14)$$

Obviously this choice is somewhat arbitrary. It seems to be more reasonable to require $N_{av}^{cf} = 0$ for strict unidirectional traffic. But a single ant in counter direction will not have much impact. So the threshold was chosen such that effects of counterflow can be identified quite clearly. More detailed data could be obtained by distinguishing between the total occupation of the trail $(\rho_{av}(n), \rho_{av}^{cf}(n)) \in [0, 1] \times [0, 1]$ leading to $v(n) = v(\rho_{av}(n), \rho_{av}^{cf}(n))$. But obviously the number of datapoints required for such an analysis is quite high.

Basic traffic data were measured for the uni- and bidirectional case. Three consecutive observations (video 6, parts a, b, c) of the same trail section (see Figs. A.2, A.3, A.4) were carried out. Each observation is separated from the preceding one by approximately 60 seconds.

Single-ant Velocities

Single-ant velocities exhibit a normal distribution for both directions. Generally the RL-direction shows a larger variance (see Figs. 5.14, 5.15). Like for the complex unidirectional trail (video 19) some asymmetry depending on the particular direction is found. For the uni- as well as for the bidirectional case the variance is higher than for the strictly unidirectional trail. This was to be expected especially in the bidirectional case as velocity depends on densities in both directions (see 5.14).

On a qualitative level one can only distinguish between directions but hardly between the uni- and the bidirectional case (see Figs. 5.14, 5.15). The reason is the finite length of the observed section. Basically the whole trail exhibits bidirectional traffic. Ants passing the observed section without any counterflow might have nevertheless been affected by counterflow on the outside of the section. If the travel time $dT(n)$ for passing the section is small in comparison to the time it takes for the unidirectional pattern to emerge the unidirectional case still will resemble the bidirectional one.

Depending on the particular direction different features are found in the velocity distributions. The distributions for the LR-direction are more narrow

than those for the RL-direction (see Figs. 5.14, 5.15). Also the average velocities differ slightly. The distributions for the LR-direction show slight asymmetries towards higher velocities whereas slight asymmetries towards lower velocities are found for the RL-direction.

Overall the features of each direction are visible more clearly on a quantitative level. The average velocities for both directions are nearly the same in the unidirectional case (see Tab. 5.3). Also the average velocities for the unidirectional case are somewhat larger than those for the strictly unidirectional trails of the previous section (see Tab. 5.1). The variance of the strictly unidirectional trails is smaller than the one for the bidirectional trail especially for the RL-direction. In case of bidirectional traffic the average velocity is lower than the one for the unidirectional case. Especially for the RL-direction the difference is significant. But variance obviously depends more on the particular direction than on the kind of traffic.

	$n[ant]$	$V[blsec^{-1}]$	$\sigma [blsec^{-1}]$	$\frac{\chi^2}{\nu}$
LR	935	5.83	1.16	3.98×10^{-4}
	<i>uni</i> 726 (77.65%)	5.87	1.14	6.16×10^{-4}
	<i>bi</i> 209 (22.35%)	5.68	1.17	1.44×10^{-4}
RL	368	5.45	1.70	0.84×10^{-4}
	<i>uni</i> 201 (55.62%)	5.86	1.73	2.08×10^{-4}
	<i>bi</i> 167 (45.38%)	4.92	1.55	1.82×10^{-4}

Table 5.3. Normal distributions were fitted for single-ant velocity distributions extracted for both directions. Generally both directions exhibit particular features. The average velocity in the unidirectional case is nearly the same. For the bidirectional case the RL-direction shows a stronger decrease of the average velocity. Also the variance of the velocity distributions in RL-direction is higher than in LR-direction.

Overall the LR-direction is not affected as much by counterflow as the RL-direction. The reason is probably the comparably heavy traffic flow in LR-direction. This is also indicated by the time-series analysis of the basic traffic data (see Figs. A.2, A.3, A.4). At the beginning of the first part (A) ($t \leq 200sec$) and during the whole last part (C), flow in both directions is nearly the same. Beginning from the second third of the first part (A) and during the whole second part (B) flow in LR-direction increases finally leading to the dominance of that direction. Therefore 45% of the ants in the RL-direction experience bidirectional traffic whereas only 22% of the ants in the LR-direction are affected by counterflow (see Tab. 5.3).

Fundamental Diagrams

The already observed dominance of the LR-direction is also found in the fundamental diagrams. This is most clearly seen for the bidirectional cases which

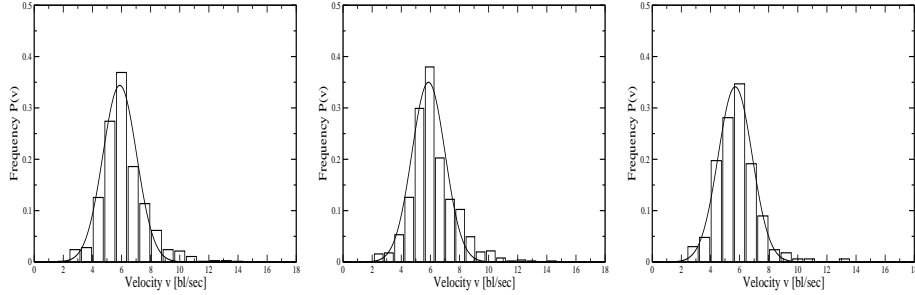


Fig. 5.14. The velocity distributions for the LR-direction are shown. On the left the broad total distribution and in the middle the less broader unidirectional one is shown. Finally variance is quite low for bidirectional traffic depicted on the right.

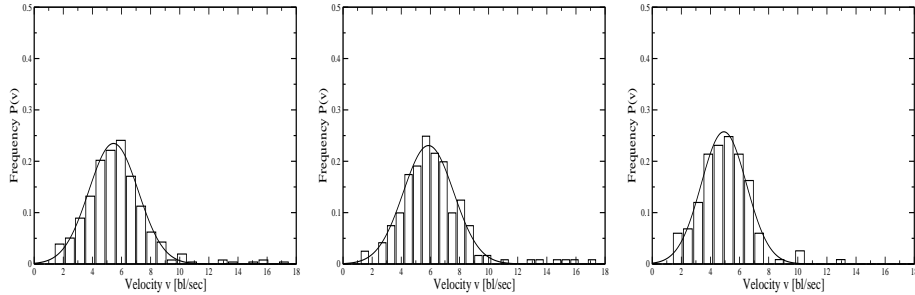


Fig. 5.15. The velocity distributions for the RL-direction are shown. The variance of the total distribution is much higher than for the LR-direction. For unidirectional traffic variance decreases further. Finally the distribution on the right for bidirectional traffic has the smallest variance.

will be discussed later on. In comparison only slight differences are observed for the unidirectional case. The fundamental diagrams for that case of the bidirectional trail exhibit the same features found for the strictly unidirectional case at least in LR-direction.

For the LR-direction the average velocity shows only a slight density dependence. At low densities single-ant velocities are scattered with an asymmetry towards higher velocities (see Fig. 5.16). In comparison to the strictly unidirectional case the same features are found (see Fig. 5.11). For the RL-direction the average velocity shows fluctuations depending on density (see Fig. 5.18). Even a decrease with increasing density is observed. Also variance is higher as for the LR-direction and the scattering of velocities shows an asymmetry towards lower values. These features are quite different from the unidirectional case of the LR-direction and also from the features of the strictly unidirectional trail.

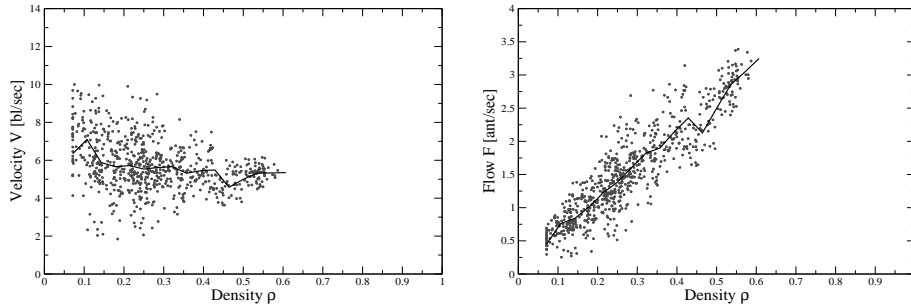


Fig. 5.16. Single-ant velocities and flow vs. density are shown for the unidirectional case of the LR-direction. Nearly the same behaviour as for the strictly unidirectional trails is found. The average velocity stays constant. Correspondingly flow shows a linear increase. Single-ant velocities show a density-dependent scattering towards higher velocities.

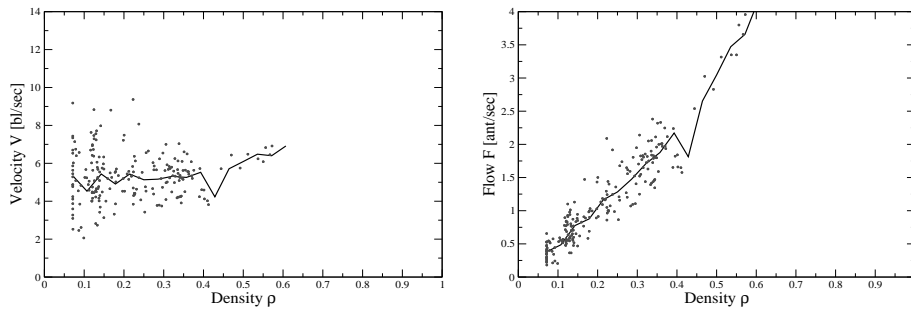


Fig. 5.17. Single-ant velocities and flow vs. density are shown for the bidirectional case of the LR-direction. At very high densities even a slight increase of the average velocity and flow is observed. Although only few datapoints for high-densities are found the scattering around the average value is quite low. Therefore the observed increase is most likely a consequence of the suppression of counterflow.

Even stronger differences between the directions are found for the bidirectional case. Especially flow exhibits different features. For the LR-direction flow increases linearly (see Fig. 5.19). At higher densities flow increases even non-linearly. Although only comparably few datapoints exist for those densities they exhibit only very slight scattering around the average value of flow. Therefore this is most likely a generic feature of the trail instead of being a consequence of random fluctuations. On the other hand flow in RL-direction decreases non-linearly (see Fig. 5.19). Again only few datapoints are available close to the maximum of the attained density. Nevertheless a quantitatively different behaviour is observed. Unfortunately datapoints are too few to confirm whether flow really attains a constant value (see Fig. 5.19).

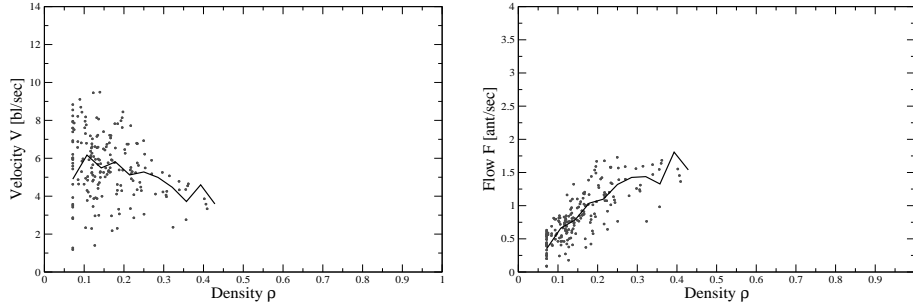


Fig. 5.18. Single-ant velocities and flow vs. density are shown for the unidirectional case of the RL-direction. Even in absence of counterflow no constant value of the average velocity is attained. The average velocity decreases with increasing density. Variance is quite high and scattering is slightly asymmetric towards lower velocities. Overall the observed features differ strongly from the unidirectional case of the LR-direction and the strictly unidirectional trail.

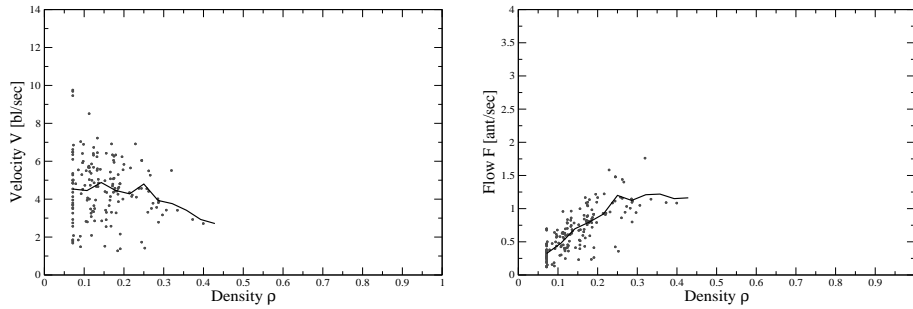


Fig. 5.19. Single-ant velocities and flow vs. density are shown for the bidirectional case of the RL-direction. Average velocity and flow decrease with increasing density. Unlike for the bidirectional case of the LR-direction flow reaches roughly a constant value. Again only few datapoints are available. Nevertheless scattering is quite low which indicates that the observed plateau is a generic effect of counterflow.

Overall flow in the RL-direction seems to be suppressed by the heavy counterflow in the LR-direction. The unidirectional case resembles the one for the strictly unidirectional trail. But the features found for the RL-direction like the platoon formation are hardly visible. As already mentioned this is a consequence of the finite length of the observed section. Therefore the patterns found for the bidirectional case differ even stronger. An increase in flow for the LR-direction at high densities is observed whereas flow in the RL-direction decreases with density. This might indicate some kind of "follow the leader" behaviour. High densities lead to an increase of flow in that direction and to a

suppression of flow in the opposite one. This can also be observed directly on the videos. A nearly uninterrupted stream of ants in one direction passes the observed section. Ants moving in the opposite direction have to leave the centre of the trail. Besides head-on encounters this leads to an additional slowing down as the ants have to find back to the centre of the trail. But still another interesting feature can be observed. For higher densities flow reaches a constant value (see Fig. 5.19). Due to the lack of datapoints it is hard to decide whether this is a generic effect of counterflow or just caused by random fluctuations. As the scattering around the constant value is quite low this might indicate a generic effect.

Distance Headways

Distance headways are in accordance with the different features already observed. Basically they indicate a change in the spatial patterns known from the unidirectional trails. For the LR-direction different distributions depending on the actual case (see Fig. 5.20) emerge. For the unidirectional case clearly the deviation into a log-normal- and a negative-exponential distribution is visible. As discussed for the strictly unidirectional trails this is a characteristic feature of the spatial distribution in that case. Ants are moving in platoons which is also confirmed by direct observations. In the bidirectional case the log-normal distribution exhibits an increased variance (see Tab. 5.4). Also the average distance between ants increases. Qualitatively the threshold distance separating the regimes of the two distributions has shifted to lower distances (see Fig. 5.20). Also the number of ants above the threshold distance has increased (see Tab. 5.4). The spatial pattern corresponding to a random-headway state is dominating at intermediate to large distances. In the unidirectional case about 50% of the ants were moving with a large distance headway. For the counterflow case about 60% have a large distance headway. Together with direct observations this indicates a change in the spatial distribution of ants in case of counterflow. Obviously a more homogeneous spatial distribution is favoured.

As already emphasised the impact of counterflow is even stronger for the RL-direction. Qualitatively no difference can be made between the uni- and the bidirectional case. The average value D and the variance σ of the log-normal distribution are so large that for nearly all distances no difference to the negative-exponential distribution can be found (see Fig. 5.21). Quantitative measurements show that more than 60% of all ants move outside of platoons. Together with direct observations this confirms the total suppression of clusterformation. Therefore the random-headway state described by the negative-exponential distribution is found.

5.4 Discussion

The previous sections gave an introduction to the experimental setup and the employed techniques for extracting *ant-traffic data*. Observations were carried

	d_c	N_{ant}	$N_{platoon}$	$D[bl]$	$\sigma[bl]$	$\lambda[bl]$	
LR	2.99	424	435	3.45	2.55	3.53	
	<i>uni</i>	2.99	353(52.2%)	323(47.8%)	3.24	2.18	3.13
	<i>bi</i>	2.99	71(38.8%)	112(61.2%)	4.50	3.84	3.58
RL	4.02	101	183	6.78	6.75	5.32	
	<i>uni</i>	4.02	53(34.0%)	103(66.0%)	6.11	8.50	5.35
	<i>bi</i>	4.02	48(37.5%)	80(62.5%)	7.77	6.81	5.28

Table 5.4. Quantities extracted from fitting log-normal- and negative-exponential distributions are shown for the uni- and the bidirectional case. Generally the average value and variance are quite high for the RL-direction. Overall the RL-direction is in a random-headway state for the uni- as well as for the bidirectional case. But the LR-direction shows a clear deviation into the uni- and the bidirectional case.

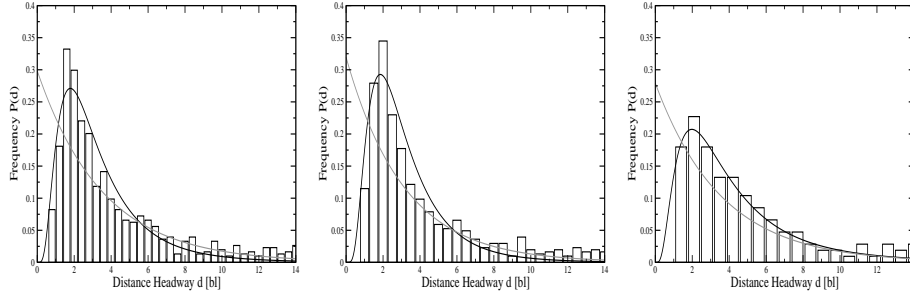


Fig. 5.20. The distance headway distributions for the LR-direction are shown. For this direction slight differences in case of uni- and bidirectional traffic are found. In absence of counterflow (middel) the same features as in the strictly unidirectional case are found. Counterflow (right) obviously disturbs the platoon formation.

out for a species exhibiting a certain set of behavioural patterns known as *army-ant* behaviour. For the investigated trails some restrictions were necessary. Nevertheless it has been shown that these restrictions are not essential and arise mainly out of practical reasons. Qualitative and quantitative data were extracted from video observations. Directly observable patterns have been identified which were also subject to quantitative measurements. Basically three kinds of trails have been investigated. The complexity of the observed traffic patterns ranged from a simple unidirectional trail with low traffic to a complex highly populated bidirectional trail. Although the three trails appear to be quite different the complex bidirectional trail shares elementary features with the simpler trails. Overall a step-like structure by increasing the complexity of the investigated trail is used. Depending on the particular trail characteristic features were identified. So the validity of identifying the particular features of each trail is ensured as they should also be visible for the more complex trails.

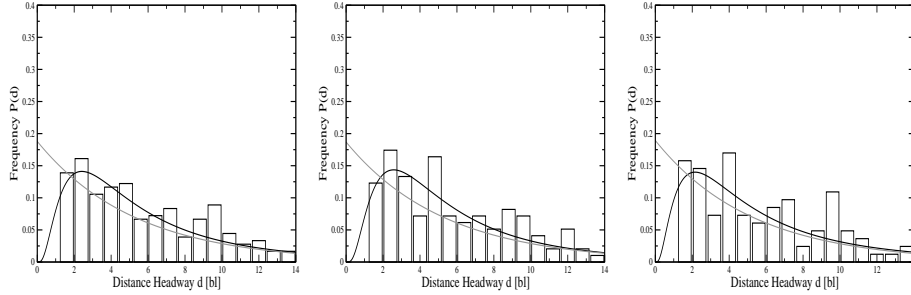


Fig. 5.21. The distance headway distributions for the RL-direction are shown. The distributions are nearly the same for all cases. Ants moving in this directions are obviously in the random-headway state.

5.4.1 The Simple Unidirectional Trail (Video 13)

The simple unidirectional trail (see Sec. 5.3.1) showed only little traffic at quite low densities $\rho_{max} = 0.33$. Nevertheless some elementary patterns of unidirectional traffic are already visible. The basic data like the instantaneous particle number shows some peaks (see Fig. 5.5 right). This is a first sign of the tendency of ants to move in platoons. The distribution of single-ant velocities shows a comparably narrow normal-distribution (see Fig. 5.6 right). This is in agreement with the qualitative observation that ants on this trail did not overtake.

5.4.2 The Complex Unidirectional Trail (Video 19)

A unidirectional trail with heavy traffic was used to investigate the density-dependence of the already observed features like platoon formation or the absence of overtaking. The maximum of attained densities is quite high $\rho_{max} = 0.8$. Overall the average velocity showed only a weak density dependence (see Fig. 5.11). Even at very high densities no significant decrease of the average velocity is observed. This feature is quite different for example from vehicular traffic [34, 60] where an increasing density is always accompanied by a noticeable decrease of the average velocity due to mutual blocking. One exception is the so-called *free-flow* state. Nevertheless the variance of single-ant velocities exhibits a strong density dependence (see Fig. 5.10). Additionally one observes an asymmetry in the velocity distribution towards higher velocities. Nevertheless no overtaking is observed. As discussed in more detail later on this is part of the mechanism of *platoon formation*.

Distance headway distributions exhibit a strong density dependence (see Fig. 5.13). Basically one distinguishes inter- and intra-platoon distances. Intra-platoon distances exhibit a skewed distribution (see Fig. 5.12 right). Due to the low average distance headway and the comparably large variance a log-normal

distribution was assumed. Although variance changes with density a constant average intra-platoon distance can be identified (see Fig. 5.12 left). Also the position of the peaks of the log-normal distributions does not change much with density (see Fig. 5.13). So for very small intra-platoon distances a normal distribution might be more appropriate. The intra-platoon structure is obviously independent from density. For larger inter-platoon distances a negative-exponential distribution is used. Platoons themselves are distributed according to the random-headway state. For distinguishing between ants within platoons and platoons themselves the average distance headway depending on density was used (see A.3). Fitting distributions according to the distance-regimes leads to quite high uncertainties due to the lack of data. Therefore both kinds of distributions were fitted over the whole range of distance headways. Overall the density dependence of the *spatial distribution* of ants allows them to keep on moving at an approximately constant average velocity which is nearly independent from density.

5.4.3 The Bidirectional Trail (Videos 6a, b, c)

The investigations of the bidirectional trail were divided into the uni- and the bidirectional case. Basically the LR-direction was the dominating one which lead to additional features depending on the direction. For the LR-direction the unidirectional case exhibited the same features already observed for the strictly unidirectional trails. This is indicated by the fundamental diagrams (see Fig. 5.16) as well as by the distance headways (see Fig. 5.20) and velocity distributions (see Figs. 5.14).

The bidirectional case of the LR-direction exhibits crucial differences to the unidirectional one. With increasing density the average velocity also increases. This is most clearly visible in flow 5.17). The distributions of single-ant velocities and intra-platoon distances are broader than in the unidirectional case. Counterflow obviously affects the characteristic features of unidirectional traffic.

For the RL-direction the effect is even stronger. The fundamental diagram shows an decrease of the average velocity with density. Also the distributions of single-ant velocities (see Figs. 5.15) and distance headways (see Fig. 5.21) are comparably broad. Hardly any difference between the uni- and bidirectional case can be made. Overall this is explained by the dominance of the flow in LR-direction. As a result the RL-direction is in a permanent bidirectional state even in absence of counterflow. Due to the finite length of the observed section only slight differences are detectable. One observes that the main lane of the trail is predominantly occupied by ants moving in the LR-direction. Therefore ants moving in RL-direction have to move off the trail centre. The corresponding spatial pattern is the random-headway state. As no platoon formation is possible velocity decreases with density. The velocity in LR-direction on the other hand increases with increasing density as ants in the opposite direction are less frequently encountered on the central part of the trail.

5.4.4 Mechanisms of Platoon Formation

The striking feature of unidirectional traffic is the independence of the average velocity from density. Even at high densities nearly no decrease was observed. Flow therefore increases linearly up to high densities. From other systems like freeway traffic one would expect a monotonic decrease with increasing density. As effects like mutual blocking generally depend on density (average distance headway) this is quite surprising. The investigated ant species obviously employs mechanisms preventing such a decrease. Additionally the spatial distribution of ants in platoons originates from these mechanisms.

For the complex unidirectional trail (see Sec. 5.3.2) and the unidirectional case (LR-direction) of the bidirectional trail (see Sec. 5.3.3) platoons are found. Direct investigations of the time-series also indicate some change in distance headways while passing the observed section. Therefore also platoon formation is found. Direct observations from videos showed ants catching up to preceding ones. After catching up they move with the same velocity as the preceding ant.

This behaviour is also reflected in the single-ant velocity distributions and the fundamental diagrams. Although the average velocity V_{av} stays nearly constant density-dependent scattering of single-ant velocities towards higher velocities is found.

Both observations can be explained by assuming some kind of collective velocity V_{av} for ants moving within platoons and a higher velocity for ants catching up V_{ct} to a platoon. When encountering a slow ant, the succeeding one reduces speed in order not to overtake. As a result the succeeding ant follows the slower one as part of the platoon with velocity V_{av} . Due to the finite length L of the observed section this leads to a dependence of measured velocities on the initial distance headway $d(n + 1)$ of the two ants (see Fig. 5.22).

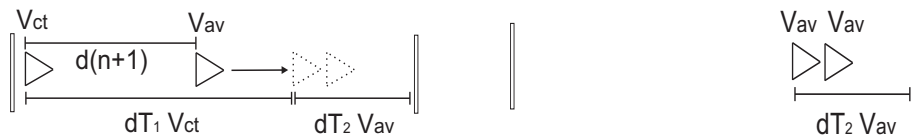


Fig. 5.22. This figure illustrates the mechanism of platoon formation. Initially two ants are separated by a distance headway $d(n + 1)$. The $n + 1$ th ant catches up with the n th one moving with velocity $V_{ct} > V_{av}$. If the initial distance headway is not too large, catching up takes place within the observed section. As a result the velocity of the $n + 1$ th ant while passing the observed section decreases from V_{ct} to the measured value $v(n + 1)$.

Overall one assumes two constant intrinsic velocities. The lower one is the average velocity V_{av} measured in the fundamental diagrams and the single-ant velocity distributions. For ants catching up a higher velocity V_{ct} is assumed. As already shown due to the slowing down by ants moving at V_{ct} this velocity

cannot be observed directly like V_{av} . Nevertheless an experimental validation is possible.

The whole process of catching up can be divided into two parts. During the time interval dT_1 the $n + 1th$ ant is catching up. Obviously both ants have to move at different velocities $V_{ct} > V_{av}$. After catching up both ants move with the same velocity during the time-interval dT_2 .

$$dT_1 = \frac{d(n+1)}{V_{ct} - V_{av}} \quad , \quad dT_2 = \frac{L - (dT_1 \cdot V_{ct})}{V_{av}}. \quad (5.15)$$

Overall one calculates the travel-time $dT(n+1) = dT_1 + dT_2$ of the $n + 1th$ ant. Therefore the measured non-constant velocity of the $n + 1th$ ant is given by:

$$v(n+1) = \frac{L}{dT(n+1)} = V_{av} \left(1 - \frac{d(n+1)}{L} \right)^{-1} \quad (5.16)$$

This result could have already been guessed in advance. The whole process starts with the n th ant entering the observed section and ends with the $n + 1th$ ant leaving the section again (see Fig. 5.22).

In order to detect the catching up it has to take place within the observed section. So the $n + 1th$ ant may not leave the section before having caught up. This is equivalent to $dT_1 \cdot V_{ct} \leq L$ leading to an upper threshold value d_{th} for the initial distance headway:

$$d(n+1) \leq d_{th} = L \left(1 - \frac{V_{av}}{V_{ct}} \right) \quad (5.17)$$

The measured data are found to be in accordance with (5.16). Especially for the unidirectional trails single-ant velocity vs. distance headway shows the behaviour expected from (5.16). At very short distances ant-ant interaction is quite strong leading to a scattering of datapoints (see Fig. 5.23). Also for the bidirectional trail strong scattering is found (see Fig. 5.24). As already pointed out the platoon formation is affected by counterflow. By fitting (5.16) to the traffic data one obtains the average velocity V_{av} (see Tab. 5.5).

	Video 13	Video 19	Video 6-LR	Video 6-RL
$V_{av}[bl/sec]$	4.75(uni)	4.14(uni)	4.7(uni), 4.7(bi)	4.36(uni), 3.78(bi)

Table 5.5. Average velocities are obtained by fitting (5.16) to the traffic data. Especially the unidirectional trails show even a quantitative agreement with the data extracted from measuring velocity distributions.

Also the existence of a maximum velocity V_{ct} is observed. For initial distance headways $d > d_c$ velocity $v(n+1)$ shows oscillation around a mean value.

This is most clearly visible for the unidirectional trails (see Fig. 5.23). For the bidirectional case roughly the same feature is found (see Fig. 5.24).

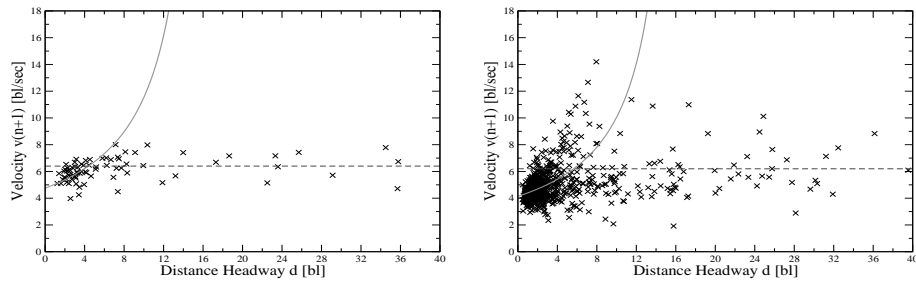


Fig. 5.23. The figures shows distance headways vs. velocity for the unidirectional trails. On the left the curve for the simple trail (video 13) is shown. The same pattern is less clearly visible for the more complex situation shown on the right (video 19). The horizontal lines correspond to the average velocity at low densities. At low densities the average distance headways can be expected to be above d_{th} . Therefore ants will approximately move with V_{ct} .

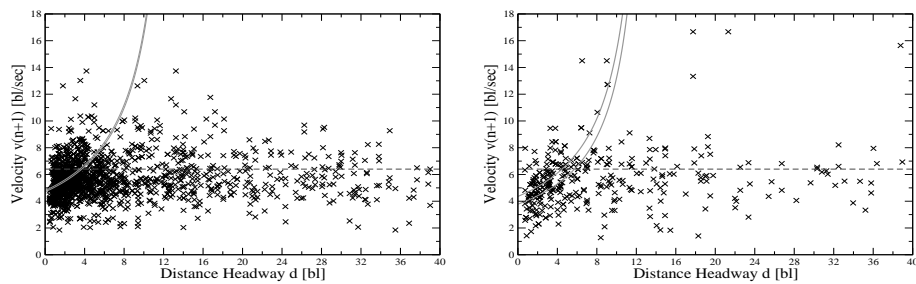


Fig. 5.24. The figures show distance headway vs. velocity for the uni- and bi-directional case of video 6. The LR-direction (left) shows heavy traffic. Therefore the pattern emerges less clearly. As already shown the platoon formation is suppressed by counterflow.

6 Conclusions

6.1 Summary and Discussion of Results

The main aim of the present work is the investigation of the dynamical properties of traffic on preexisting ant trails. It is mainly divided into two parts which are based on the interplay between theory and experiment. Both parts are developed independently and compared later on in the succeeding discussion.

Methods from statistical and non-equilibrium physics were employed for theoretical studies. New models for bidirectional traffic on preexisting ant trails were introduced [45,56]. Also the understanding of the already existing unidirectional ant trail model was improved [16,43].

The results of the empirical studies are compared with the models predictions. Ant-traffic data are extracted using methods from traffic engineering and behavioural biology. Similar approaches have already been employed successfully in the context of vehicular traffic. Nevertheless crucial differences between the already investigated systems and ant-traffic are the main motivation of the present study [43,46].

6.1.1 Theoretical Results

Based on stochastic non-equilibrium systems of particle flow models for traffic on preexisting ant trails are constructed. Therefore *chapter 2* gives an introduction to driven non-equilibrium systems in the context of traffic flow. As an elementary example the *TASEP* is discussed (see 2.2). Although quite simple many models are actually based on the TASEP. One of the TASEP-based models is the *Nagel-Schreckenberg model* for freeway traffic (see 2.2.1). This model can be regarded as some kind of prototype for cellular automaton based traffic models. The discussions shows that the introduced ant trail models are quite different due to the different properties of the moving agents (see 3.1.1 and 5.1.3). It turns out that the ant trail models exhibit more similarity to the *TASEP* with static disorder (see chapters 3 and 4). Therefore *static particlewise* (see 2.3.1) and *lattice-wise* disorder (see 2.3.2) are discussed. The main features

are being identified already employing some new techniques developed for investigating the ant-trail-models [15,44]. Generally phase-separation is observed. As established for investigating the TASEP the density-profile contains nearly all the necessary information. By definition so-called second-class particles will follow high-density areas. The density profile seen from the second-class particle is measured. Especially in the case of particlewise disorder analogies to the phases found in the TASEP are drawn as now density-profiles are available even in the case of particlewise disorder (see 2.3.1).

Chapters 3 and 4 introduce models for uni- and bidirectional traffic on preexisting ant trails. For the unidirectional model introduced in *chapter 3* pheromone marks are the main mechanism of interaction between ants. The pheromone marks lead to some kind of dynamically induced particlewise disorder (see 3.3). Unlike in the disordered TASEP hopping rates depend on the distance headway to the preceding ant [57,68]. Therefore disorder emerges *dynamically* depending on the particular choice of parameters. A moving particle *cluster* emerges and average velocity vs. density shows a non-monotonicity. As pointed out this effect is based on the pheromone marks when particlewise disorder is *dissolved* with increasing density (see 3.3). A phenomenological theory namely the "*Loose Cluster Approximation*" is discussed (see 3.2.3) and compared to the case of *static* particlewise disorder. A crucial difference in the critical density is found. Due to the pheromone marks the jamming transition generally occurs at lower densities than for static particlewise disorder [54]. Generally the cluster length instead of the cluster density is the crucial quantity for determining the transition (see 3.2.3). Employing the method of measuring the density-profile seen from the second-class particle the cluster length is obtained. As hopping rates depend on the pheromone marks, the second-class particle has been modified in accordance to (see 2.2).

The coarsening process leading to phase-separation was investigated numerically by measuring density-density correlation functions. In analogy to the *Bus Route Model* coarsening follows a power law with two different dynamical exponents depending on the particular regime with respect to time (see 3.2.2). The same exponents as in the already investigated case of time-parallel update are found [15]. This indicates the universality of the observed exponents. The techniques for measuring the coarsening process were extended such that also the number of moving clusters can be estimated [44]. Also the cluster length can be measured for a certain parameter regime.

In chapter 4 the extension of the unidirectional ant trail model to the multilane case is discussed [43,45,56]. Several extensions especially the use of bidirectional instead of unidirectional multilane models are discussed. The bidirectional models being introduced basically can be divided into two classes. Models with *synchronous* or *asynchronous* exchange of counterflowing ants are distinguished (see 4.1). In case of asynchronous exchange the main feature does not depend on the pheromone marks. Like on real ant trails counterflowing ants lead to a lower hopping rate due to mutual slowing down. Caused by fluctuations this effectively induces *dynamic latticewise disorder*. In contrast to the

unidirectional model one now observes a large *localised* particle cluster. The coarsening behaviour is investigated analogous to the unidirectional model. Although the models are quite different the same dynamic exponents are found (see 4.2.2). Obviously the dynamics of phase separation in the discussed cases is independent from particular features like the choice of the update procedure or the origin of dynamic disorder [44]. For the stationary state a phenomenological description based on *symmetries* observed in the density profile of the localised cluster is developed (see 4.2.2). As no pheromone marks are incorporated the effect is just based on an extension of the plain TASEP to counterflow. Therefore this extension might also be of interest for other models incorporating the same basic mechanism [43, 46]. At very low densities an additional feature namely the alternation of *coarsening* and *shredding* is found (see 4.2.1). The moving particle cluster is shredded by counterflowing ants. Obviously this feature depends on the pheromones. Although this has already been investigated extensively for the model with synchronous particle exchange [56] a new technique for measuring the periodicity of the process is introduced (see 4.2.1).

6.1.2 Empirical Results

In chapter 5 finally an experimental setup for measuring traffic data on real ant trails is proposed. It is designed such that measured quantities allow a direct comparison to the models' predictions. The assumed improvement or even some kind of optimisation of traffic flow by evolution is most likely to emerge within a natural *ecological context*. With respect to the measurements quantities and techniques from traffic engineering have been used (e.g. [34, 60, 83]). Due to the nature of ant trails some modifications were necessary. Making use of the fact that nearly no overtaking is observed so-called cumulative counting was used for extracting the average velocity and density. As one crucial difference to vehicular traffic also the agents moving in counterdirection interact with each other [12, 45] and therefore had to be taken into account (see 5.2.2).

The measured quantities allow a qualitative and quantitative comparison to the models' predictions. On a more technical level it was shown that techniques from traffic engineering can successfully be adapted and applied to ant-traffic. This has been doubtful and only few studies concerned with the organisation of traffic flow itself [12, 47]. For example it was concluded in [47] that no functional relation between the average velocity (or flow) and density exists. In that particular case heavy bidirectional traffic has been investigated without taking into account the density in counterdirection.

Even the existence of a somehow ordered traffic stream appeared to be doubtful. From the point of view of behavioural biology this is less surprising. Even without having a direct proof like the present field study (see chapter 5) this was to be expected from the collective nature of ants [36]. Also the lacking of self-consciousness in contrast to other multi-agent systems [19, 65] is a vital part (see 3.1.1 and [43, 45]). Cooperativity is a consequence of natural selection. To an ant colony traffic flow is probably as much as vital as to human

societies and analogies have been proposed recently [10] for leaf-cutting ants. Nevertheless the selective pressure for foraging situations can be expected to be quite high. A colony suffering from traffic jams will most probably just starve. Especially nomadic species like *Leptogenys processionalis* frequently have to move to new raiding-grounds [32, 85, 86]. An inefficient transport of the nesting material or the brood would most probably be fatal. Spending more energy on retrieving prey back to the nest than gaining by consuming it obviously is inefficient. Overall traffic is crucial to survival for most ant colonies and can therefore be expected to exhibit evolutionary generated optimisation [6, 7, 32].

For the present study data collection itself turned out to be highly non-trivial as *automatic* digital image processing devices failed. The videos of the observed section were recorded in a natural environment. Therefore even monomorphic ants are difficult to detect as the underground changes colour or twigs are blocking a direct view. Depending on the duration of observation also light conditions are changing (see 5.2.1).

6.1.3 A Comparison between Theory and Empiricism

The main result of the present experimental and theoretical study is the detection of certain patterns found in ant-traffic at least for one particular species. By choosing an ant species exhibiting army ant behaviour the observed patterns are most likely also found for a larger number of other species.

The Unidirectional Case

Ants on an unidirectional trail tend to move in platoons. Succeeding ants catching up to preceding ones were observed. This is reflected in the distance headway distribution which shows two distinct regimes (see 5.3.2). Short distances exhibit a skewed distribution. Overall observations are consistent with a *log-normal* distribution. Ants within the platoons move at a constant average distance independent from density. Hardly any distances smaller than that are found. But platoons themselves can be separated by very large distances. Overall this induces some kind of asymmetry. At very large distances platoons can be assumed to be uncorrelated leading to a *negative-exponential* distribution of the larger distance headways. No clear threshold between both regimes of short and large distances could be identified. Generally density determines the average distance headway (see A.3). Using this average distance headway as some kind of threshold the number of ants inside and outside of the platoons was determined.

Unlike in vehicular traffic hardly any events of overtaking are observed. As a result the velocity distribution is comparably narrow for all density regimes (see 5.3.2). Also the fundamental diagrams reflect this behaviour (see 5.3.2). Overall the observations in case of unidirectional traffic show the characteristic features of particlewise disorder. Ants moving at the lower average velocity correspond to the defect-particle. Faster ants catch up with the slower ones forming a

platoon (see 5.4.4). Some asymmetric scattering to higher velocities is also observed. The velocities of upcatching ants V_{ct} have been measured. Finally the observations justify the assumptions made for constructing the unidirectional ant-trail-model (see 3.1.1). Therefore overtaking is not incorporated and two intrinsic velocities corresponding to the parameters Q and q are used.

Finally the question regarding the advantage of organising traffic in the observed way arises. In the unidirectional case the average velocity has been observed to be nearly independent from density over a large regime (see 5.3.2). As demonstrated by the models and also observed empirically this is a consequence of platoon formation (see 3.2). The platoons move roughly as uncorrelated entities along the trail indicated by the random-headway distribution for larger distances. As a result *mutual blocking* is suppressed in contrast to a homogeneous distribution of ants.

Further investigations will have to address the structure of the platoons themselves. One important point is the number of ants within a platoon depending on density. Obviously the platoons cannot reach an arbitrary size without any mutual blocking. If a large number of ants would be comprised by one platoon a nearly homogeneous distribution would be reached. Also very high densities showed first signs of mutual blocking (see 5.3.2 and 5.3.2) indicating the vanishing of platoons. The introduced methods are basically capable of measuring the lengths of the platoons. This can be done by counting the number of succeeding ants below a certain threshold value of the distance headway. But like for a more detailed analysis of distance headway distributions more data is needed.

The Bidirectional Case

For the bidirectional model the results are less clear. The dominating direction generally shows the characteristic features known from the unidirectional trail (see 5.4.3). In absence of counterflow platoons are formed. This is clearly visible on the videos as well as in the velocity- and distance headway distributions (see 5.3.3 and 5.3.3). Also the fundamental diagram exhibits the same features observed for the strictly bidirectional trails (see 5.3.3).

In case of counterflow these features are slightly changed. As the LR-direction was identified to be the dominating one some kind of "follow the leader behaviour" is observed. This is indicated by a non-linear increase of flow in case of counterflow. In comparison to the unidirectional case the average velocity is only slightly decreased. But still platoons are found.

As already pointed out the RL-direction is affected quite strongly by counterflow. So the uni- and the bidirectional case are hardly distinguishable. This is consequence of the finite length of the observed section. The characteristics of platoon formation are strongly suppressed. This is reflected in the distribution of distance headways (see 5.3.3). The random-headway state is dominating over the whole range of distance headways. Also the velocity distribution has a much higher variance than the one for the opposite direction (see 5.3.3).

The RL-direction also shows a decrease in velocity with increasing density (see 5.3.3). Correspondingly a kink in flow is observed. This resembles the plateau in flow due to latticewise disorder induced by counterflow.

It is quite difficult to discuss the possible advantage of the observed traffic patterns in case of counterflow as in principle two characteristic patterns have been observed. The "follow the leader" behaviour clearly favours the direction of heavier flow. This leads to a self-amplification and prevents congestion in the more frequented direction. Also platoon formation is found. The second feature resembles the one also observed in the bidirectional models. At sufficiently high densities flow reaches a nearly constant plateau value. This might be advantageous in case of roughly symmetric traffic flow in both directions. The same number of ants per time would reach or leave a certain destination like a foodsource or the nest as long as the actual density stays in a certain regime. A constant flow of food or workers could be ensured. This scenario might be appropriate during the exploitation of a food source. On the other hand at the beginning or at the end of a raid, the "follow the leader" pattern would be more reasonable [46].

6.2 Outlook

Based on the presented results new questions and approaches are motivated. The theoretical framework as well as the experimental setup now can be extended in order to capture more general situations. But also some applications might be interesting. Overall the strategies developed for the present study can also be applied to more complex scenarios.

6.2.1 Theoretical Studies

For the unidirectional trail platoons are observed. Although the characteristics of particlewise disorder emerge the mechanisms of formation are still unknown. The unidirectional ant trail model predicts a *non-monotonicity* in the average velocity due to the pheromones. This is not observed in the present field study. Nevertheless depending on the evaporation rate the non-monotonicity can be suppressed to an order of magnitude not detectable with the employed setup. But still the constant average velocity and not the non-monotonicity is the main feature. A maximum of average velocity attained at ρ_c would lead to strong fluctuations as density can not be expected to be constant. Still other mechanisms like some kind of *pushing* by following ants could be incorporated. Tactile stimuli from behind might be the key mechanism leading to platoon formation. Simulations incorporating this effect show the emergence of some kind of platoon which is nevertheless quite unstable.

For bidirectional trails the beginning of a *plateau* in flow has been observed in RL-direction. Unfortunately the number of datapoints in that particular density regime is quite small. Overall a scenario with a *symmetric* traffic flow

in both directions will be of interest. Further investigations might address the question of the existence of plateaus in flow. Nevertheless the mutual hindrance due to *counterflow* is not restricted to ants. Pedestrians moving in opposite directions are also affected by the same mechanism. In that particular example ant trails exhibit more common feature with pedestrians than with cars on a road (see Fig. 6.1). Due to these similarities the next step of extension would be a two-dimensional ant trail model. Here also the formation of trails themselves will be incorporated. Extensive theoretical and empirical investigations have already been carried out with respect to structure formation (e.g. [21, 32]) of trail networks. Nevertheless a connection between these patterns and traffic flow itself seems to be missing. Also the extension to different kinds of multilane traffic could be incorporated more naturally.

But also analogies to artificial systems exist. Recently the unidirectional ant trail model has been implemented as a robotic system [67, 80]. Overall concepts like swarm intelligence are successfully applied to various artificial systems [46, 55].



Fig. 6.1. Both photographs show traffic jams in quite different systems. On the left a multi-lane road is crowded with many different vehicles. Unlike in ant-traffic no coupling between lanes in opposite directions exists. Obviously only the road in one direction is blocked. On the right a traffic jam of monomorphic workers of *Oecophylla smaragdina* is shown. Due to the cooperative transport of large prey a queue has been accumulated.

6.2.2 Experiments

Further studies might address more complex situations in the field. The videos used for data collection within the present field-study showed first *elementary* examples of ant-traffic in a natural ecological context. But also videos with unidirectional *multi-lane* traffic have been recorded. Data extraction could lead to interesting results as a comparison to multi-lane vehicular traffic becomes possible. For the observed cases of heavy multi-lane traffic also different kinds of load were carried by the ants. This might also be interesting for assigning certain traffic patterns to a particular ecological context.

But still laboratory experiments are the next crucial step. Basically they are *complementary* to the field studies. Field studies have the advantage that evolutionary generated patterns will most likely emerge in the natural situations they originate from. On the other hand environmental conditions and natural situations are never exactly the same. Here the laboratory offers a reasonable alternative. Once the basic patterns known from field studies have been reproduced more detailed quantitative investigations become possible. As the environment can be controlled better certain patterns for solving problems can be tested in situations not found in the field. One interesting example would be the crossing of two traffic streams. Overall the flexibility of direct behavioural adaptation could be investigated. Additionally one would be sure that the traffic stream does not react dynamically on a changing ecological context. At least the whole trail is observable.

Nevertheless not all species are suitable for laboratory experiments. Leaf-cutting ants exhibit a huge variety of interesting traffic patterns [11,12]. But the required space would be quite enormous in order to ensure natural conditions. In a natural environment the raiding grounds can extend up to a few square miles. The observed trails are of corresponding length and complexity [11, 12, 36]. Also the species chosen for the field studies of the present work (*Leptogenys processionalis*) can hardly be kept in a laboratory environment¹. As this species is nomadic one would have to ensure that the suppression of migration does not affect the behavioural patterns one seeks to investigate.



Fig. 6.2. The photographs show a controlled experimental setup in a laboratory situation. A colony of the weaver ant species *Polyrhachis dives* is kept in a plastic box. Inside a nearly natural environment has been constructed. For implementing a trail an arena is used. The underground is pure sand which can be manipulated easily.

For first laboratory experiments we chose *Polyrhachis dives* a weaver-ant species. Weaver ants are widely known for building conspicuous nests and exhibiting a wide range of highly evolved cooperativity [36]. Colonies of *Polyrhachis dives* are comparably small and can easily be kept in an artificial environment (see Fig. 6.2). Although natural habitats are found mainly in

¹ R. Gadagkar and T. Varghese, personal communication

south-east Asia environmental conditions and temperature can be reproduced. Our colony is kept inside a plastic box of sufficient size (see Fig. 6.2). The box also provides nesting material like leaves and twigs. Natural nutrition like nectar and water is also made available. A suitable nesting site at one corner of the box together with plants and natural ground are also provided.

Traffic experiments are conducted within an arena of comparably small dimensions ($1m \times 1m$). The whole experimental setup is of the size of a desktop. Collective foraging was triggered by starving the colony for five days. Food was offered within the arena which was made accessible by a small ramp. For accelerating the process the activity level was raised by increasing the temperature inside of the box with a heating lamp (see Fig. 6.2).

Ants entered the arena in search for food and returned back to the nest. Although the colony size is still small by that time first ordered traffic lanes were visible. Nevertheless for investigating a *collective effect* still a collective is necessary. Once the colony size is large enough, more detailed investigations are possible. Also some automatization of counting might be possible as ants are clearly visible on the white sand used for covering the ground of the arena. The ramp connecting the box and the arena has to be passed by any ant in search for food. This will be a suitable place for a video camera. Digital data collection should be possible by employing software available for counting pedestrians. In a laboratory scenario this should be comparably easy. The traffic lane is restricted by the ramp. Even between the ramp and the food source a static traffic lane emerged. Unlike for example in pedestrians the employed species *Polyrhachis dives* is monomorphic which makes the ants comparably easy to detect. Overall an *automatization* of measurements would lead to an enormous increase of available data. Especially for analysing distance headway distributions and cluster sizes this will be advantageous.

Overall future studies will make use of the concepts and strategies demonstrated to be effective in the present study. Optimisation strategies in ants can obviously also be found in the organisation of traffic flow. So a detailed comparison to human traffic systems and possible adaptations offer an interesting perspective. One example might be the formation of platoons of cars on a highway. By coupling several cars to a platoon the required space will be decreased drastically. The results should be comparable to those of the computer simulations of the unidirectional ant trail models or to the empirical observations for the unidirectional trails. In case of bidirectional traffic the exchange of information with cars in counterdirection might be advantageous. Information about the road condition or traffic flow could be exchanged via strictly local interaction. These aspects are not incorporated in the present study. Nevertheless coupling to counterflow for ensuring a constant flow in both directions which is independent from density might also be desirable in artificial systems like communication networks.

A Appendix

A.1 Error Correction

Although the method of cumulative counting used for quantitative measurements is in principle exact some error correction had to be done. Errors are mainly caused for two reasons. At first there are the random mistakes arising from counting by hand which will be discussed in the next section (see App. A.2). A second source of error is systematically involved and arises out of the assumption that ants do not change their order or do not vanish within the observed section.

A.1.1 Detectable Errors

Data points (t_{\pm}, n) are labelled by the number of entering n which should also be the same as for leaving. Two kinds of events can disturb the labelling. An ant n_0 entering the section at point A produces a datapoint (t_+, n_0) . If this ant leaves the section somewhere between A and B no corresponding datapoint for leaving exists. So datapoints for entering are shifted by one place upwards in comparison to the datapoints for leaving. Also ants leaving the section thereby producing a datapoint (t_-, n_0) without having entered the section at point A disturb the order. The datapoints for leaving are shifted one place upwards in comparison to the datapoints for entering:

$$\begin{aligned} (t_+(n), n) &\longrightarrow (t_+(n), n+1) & \forall_{n \geq n_0} \text{cause: leaving} \\ (t_-(n), n) &\longrightarrow (t_-(n), n+1) & \forall_{n \geq n_0} \text{cause: entering} \end{aligned} \quad (\text{A.1})$$

As a result travel-time is calculated based on wrong datapoints. If time headways are small the difference between $t(n)$ and $t(n+1)$ is small and therefore also the travel-time is only affected slightly. But at large time headways, travel times and also velocities are heavily affected. The same is also true for the instantaneous particle number $N(t)$ which can even get negative.

Both kinds of error occur as a result of the method when the underlying assumptions about traffic flow are not valid. Ants leaving the section between

points A and B were mainly observed in case of nearly vanishing traffic when time headways and thus the impact of miscountings was large. Ants entering the section between points A and B have not been observed in case of unidirectional traffic. But in case of bidirectional traffic so called U-turns lead to both kinds of error. An ant leaving the lane say from left to right leads to a missing datapoint for leaving in that direction. But at the same time a datapoint for leaving in the opposite direction is added. Obviously the datasets for both directions are affected. Besides the behaviourally induced errors there is also always the possibility of miscounting by hand.

A.1.2 Correction of Detectable Errors

The impact of the discussed errors is obviously quite strong. But for that reason they are also easy to detect. Basically the curve (t_+, n_+) for entering ants should resemble the curve (t_-, n_-) for the leaving ones. The curve for entering should roughly look like the one for leaving just shifted to the right by the travel-time. Due to the movement of ants in platoons one can make use of the corresponding clustering of datapoints. The number of datapoints should be the same for every platoon. Additionally one can also count the events of disturbing in order to localise the superfluous datapoints. This might also give additional information about the real system.

In order to reestablish the correct pairwise structure of datapoints the superfluous points are deleted from the data set. Once the wrong point n_0 has been identified, this is done by shifting all the following points $n \geq n_0$:

$$\begin{aligned} (t_+(n+1), n+1) &\longrightarrow (t_+(n+1), n) & \forall_{n \geq n_0} \text{correction: leaving} \\ (t_-(n+1), n+1) &\longrightarrow (t_-(n+1), n) & \forall_{n \geq n_0} \text{correction: entering} \end{aligned} \quad (\text{A.2})$$

The solution thus is just to ignore the event causing the error and deleting the corresponding datapoint. Nevertheless this completely neglects the contribution of the leaving or entering ants to flow or density. Investigating the number of those events shows that they are negligible for the trail sections investigated here. Nevertheless with increasing efforts one could use a finer sectioning of the trail with each section contributing to the global density.

A.1.3 Hidden Errors

Errors not causing a superfluous or missing datapoint are harder to detect. One example is the swapping of datapoints. As discussed, some rare events of overtaking have been observed. A disoriented ant (n_0) might temporarily leave the trail and is passed by the succeeding one ($n_0 + 1$). As the labelling of datapoints depends on the order of ants datapoints get swapped:

$$\begin{aligned} (t_-(n+1), n+1) &\longrightarrow (t_-(n), n) & \forall_{n \geq n_0} \text{succeeding ant} \\ (t_-(n), n) &\longrightarrow (t_-(n+1), n+1) & \forall_{n \geq n_0} \text{passed ant} \end{aligned} \quad (\text{A.3})$$

In case of x overtaking ants, the leaving ant will move to index $n + x$. The index of all overtaking ant is decreased by one. The resulting error will be of the order of the corresponding time headway. But unlike in the cases of missing datapoints the effect for velocity measurements is restricted to the swapped points. Also the instantaneous particle number is hardly affected.

A.2 Statistical Errors

Measuring times for counting is affected by statistical (normally distributed) errors. A brief discussion of their order of magnitude is given here.

A.2.1 Average Velocity

Measuring the average velocity for passing the observed section involves measuring times and lengths.

$$v(n) = \frac{L}{dT(n)} = \frac{L}{t_-(n) - t_+(n)} \quad (\text{A.4})$$

Errors of measuring time can be assumed to be normally distributed. The same also holds for measuring the sections length L as multiple measurements were carried out.

$$\begin{aligned} \Delta v(n) &= \sqrt{\left(\frac{L}{dT(n)^2} \Delta t_+\right)^2 + \left(\frac{L}{dT(n)^2} \Delta t_-\right)^2 + \left(\frac{\Delta L}{dT(n)}\right)^2} \\ &= \frac{1}{dT(n)} \sqrt{\Delta L^2 + 2 \left(\frac{L}{dT(n)} \Delta t\right)^2} \end{aligned} \quad (\text{A.5})$$

The length L of the observed section is the same for all single-ant velocities $v(n)$. Therefore ΔL is a systematic error and will be neglected in the following.

$$\Delta v(n) = C(L)v(n)^2 \quad \text{with} \quad C(L) = \sqrt{2} \frac{\Delta t}{L} \quad (\text{A.6})$$

Counting is done by watching the videos at 50 percent of real time. So assuming an error of half a second leads to an error of $\Delta t = 0.25[\text{sec}]$ in real time.

A.2.2 Time- and Distance Headway

The definition of time headway used here is the time it takes two succeeding ants (ant n and ant $n+1$) to pass a certain point. Time headways were measured for ants entering the observed section (t_+) at point A and leaving the observed section (t_-) at point B :

	Video 13	Video 19	Video 6
$L[bl]$	21	17	14
$C(L)[sec \cdot bl^{-1}]$	1.68×10^{-2}	2.08×10^{-2}	2.53×10^{-2}

Table A.1. This tabular gives a brief survey over the order of magnitude of the statistical errors. Although one finds $\Delta v(n) \sim v(n)^2$ the factor $C(L)$ determines the effective numerical value.

$$dt_{\pm} = t_{\pm}(n+1) - t_{\pm}(n). \quad (\text{A.7})$$

Together with $\Delta t = 0.25[sec]$ one finds a comparably small statistical error for measuring time headways:

$$\Delta(dt_{\pm}) = \sqrt{\Delta t_{\pm}(n+1)^2 + \Delta t_{\pm}(n)^2} = \sqrt{2} \cdot \Delta t \approx 0.35[sec]. \quad (\text{A.8})$$

Obviously $\Delta(dt)$ only depends on the error for measuring time which is assumed to be independent of the measuring point (entering or leaving) or the particular time headway $dt_{\pm}(n)$.

For calculating the distance headway measuring time is also involved. Under the same assumptions as for the time headway one finds:

$$d_+(n) = dt_+(n)v(n) = (t_+(n+1) - t_+(n))v(n), \quad (\text{A.9})$$

$$\Delta d_+(n) = \sqrt{2((v(n)\Delta t)^2 + (dt\Delta v(n))^2)}.$$

A.3 Distance Headway Cut-Off

Given the number of ants N and the length L of the observed section in body lengths one finds for the average distance headway:

$$d(N) = \frac{L - N}{N} \quad (\text{A.10})$$

Averaging over particle numbers from N_1 to N_2 leads to:

$$\bar{d}_c(N_1, N_2) = \int_{N_1}^{N_2} dN d(N) = \frac{L}{N_2 - N_1} \log\left(\frac{N_2}{N_1}\right) - 1 \quad (\text{A.11})$$

A.4 Supplementary Data

A.4.1 Video 13

Type:	unidirectional
Path length:	21bl
Observed time interval:	0:00:10 - 0:05:45 (335sec)
Number of datapoints:	85
Carried load:	none
U-turns:	none
Departures:	none

Table A.2. Video 13 shows an unidirectional trail with only light traffic. Although ant densities are comparably low, no ant left the trail within the observed section. As no load was observed the trail is probably in the final state of a migration or a raid.

Techniques of data extraction are exemplified for the cumulative counting of video 13. The basic- and derived quantities are shown in chapter 5 (see Figs. 5.4, 5.5).

A.4.2 Video 19

Type:	unidirectional with minimal counterflow
Path length:	17bl
Observed time interval:	00:01:02 - 00:13:20 (738sec)
Number of datapoints:	723
Carried load:	larvae and pupae (rare)
U-turns:	2
Departures:	approx. 4

Table A.3. Video 19 shows an unidirectional trail with heavy traffic and light counterflow. Based on the few observations of carried load a migration takes place. As traffic ceased after approximately 12 minutes, migration was nearly finished.

Basic Data Video 19:

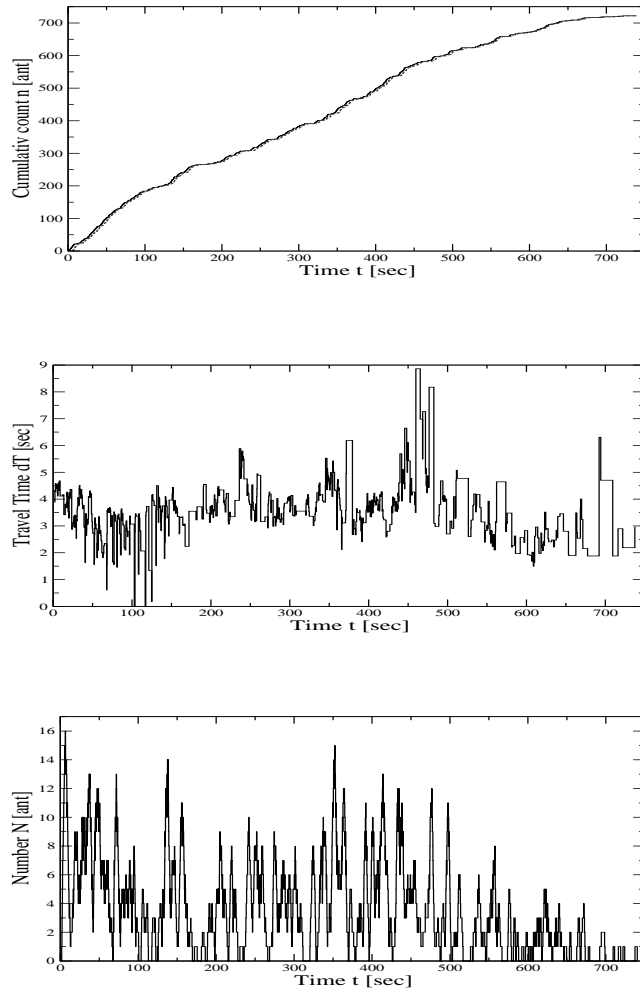


Fig. A.1. The figures show the basic data extracted from video 19 by cumulative counting. Due to the large number of counts the clustering of datapoints can not be seen. Travel time shows oscillation around the mean value. The instantaneous particle number shows some peaks corresponding to the movement of platoons. A closer investigation shows the same features already observed for the more simple case (video 13).

A.4.3 Video 6 (Parts A, B, C)

Type: full bidirectional trail
 Path length: 14bl
 Carried load: none

Observed time interval:	0:00:01 - 0:10:04 (602sec)
Number of datapoints (LR):	517
Number of datapoints (RL):	172
U-turns (LR):	23
U-turns (RL):	11
Departures (LR):	1
Departures (RL):	5

Table A.4. Video 6a shows a bidirectional trail with heavy traffic in LR-direction. No load was observed. But U-turns happen at a relatively high frequency.

Observed time interval:	0:00:11 - 00:09:35 (564sec)
Number of datapoints (LR):	362
Number of datapoints (RL):	131
U-turns (LR):	14
U-turns (RL):	11
Departures (LR):	0
Departures (RL):	1

Table A.5. Video 6b shows a bidirectional trail. Traffic from left to right is still dominant but U-turns happen less frequently.

Observed time interval:	0:00:11 - 0:04:52 (278sec)
Number of datapoints (LR):	122
Number of datapoints (RL):	93
U-turns (LR):	9
U-turns (RL):	7
Departures (LR):	0
Departures (RL):	2

Table A.6. Video 6c shows roughly symmetric bidirectional traffic. Traffic flow is nearly the same for both directions. Also the number of U-turns is nearly the same.

Basic Data Video 6A:

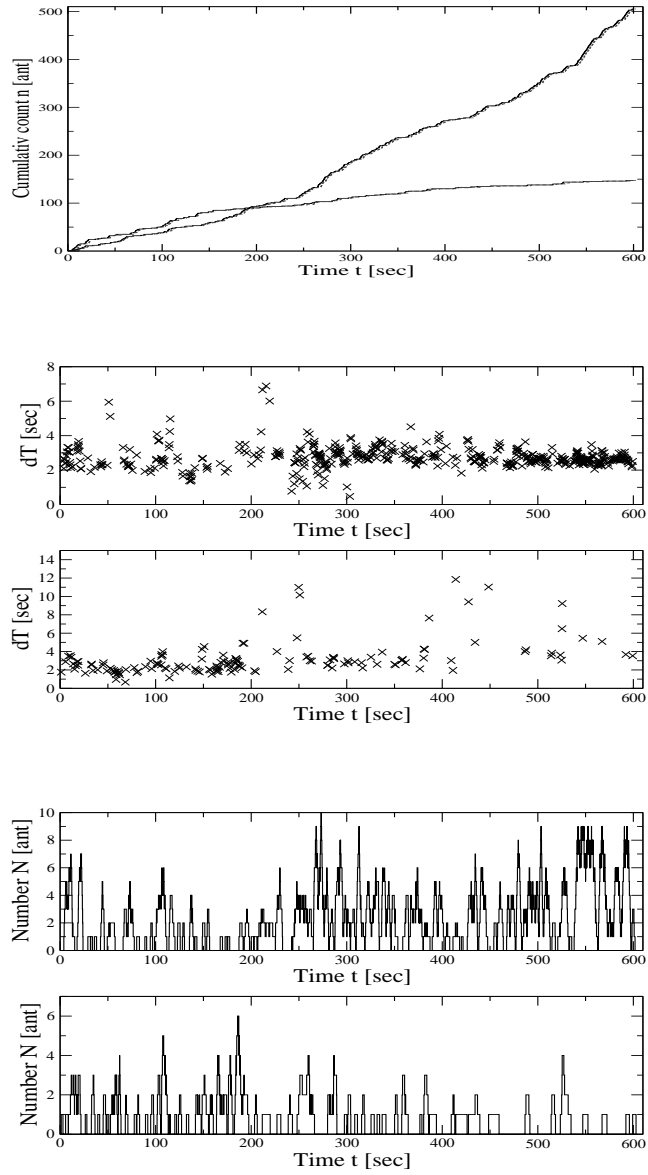


Fig. A.2. The figures show the basic data extracted from video 6a by cumulative counting. After $t = 200\text{sec}$ flow from left to right becomes dominant.

Basic Data Video 6B:

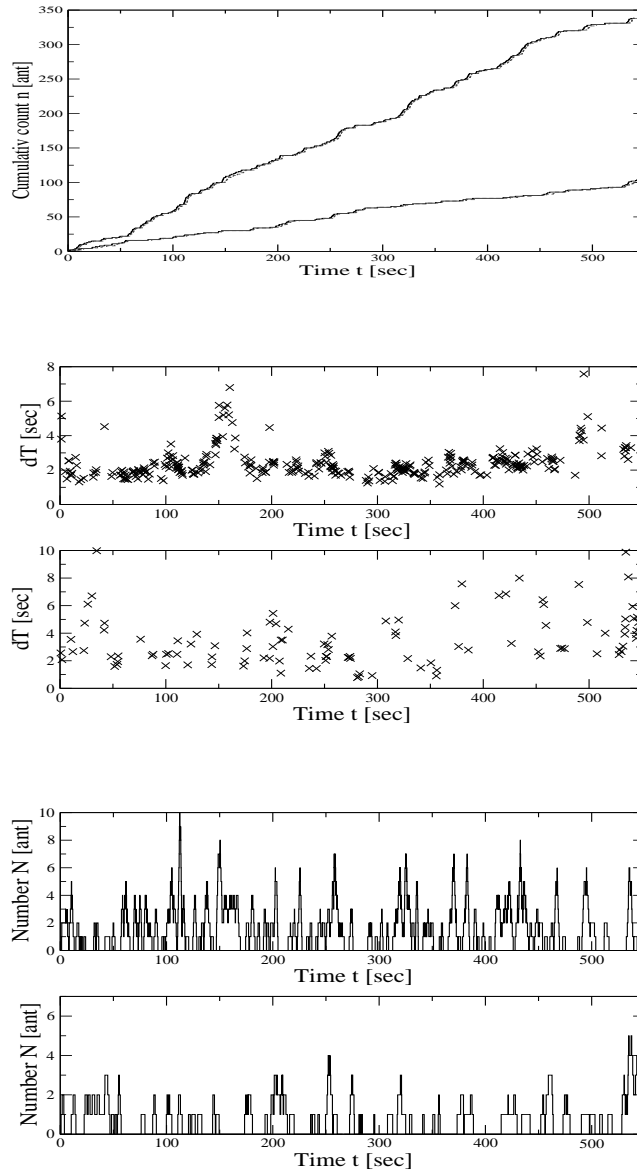


Fig. A.3. The figures show the basic data extracted from video 6b by cumulative counting. Traffic flow from left to right is still dominant but not as much as observed in part A.

Basic Data Video 6C:

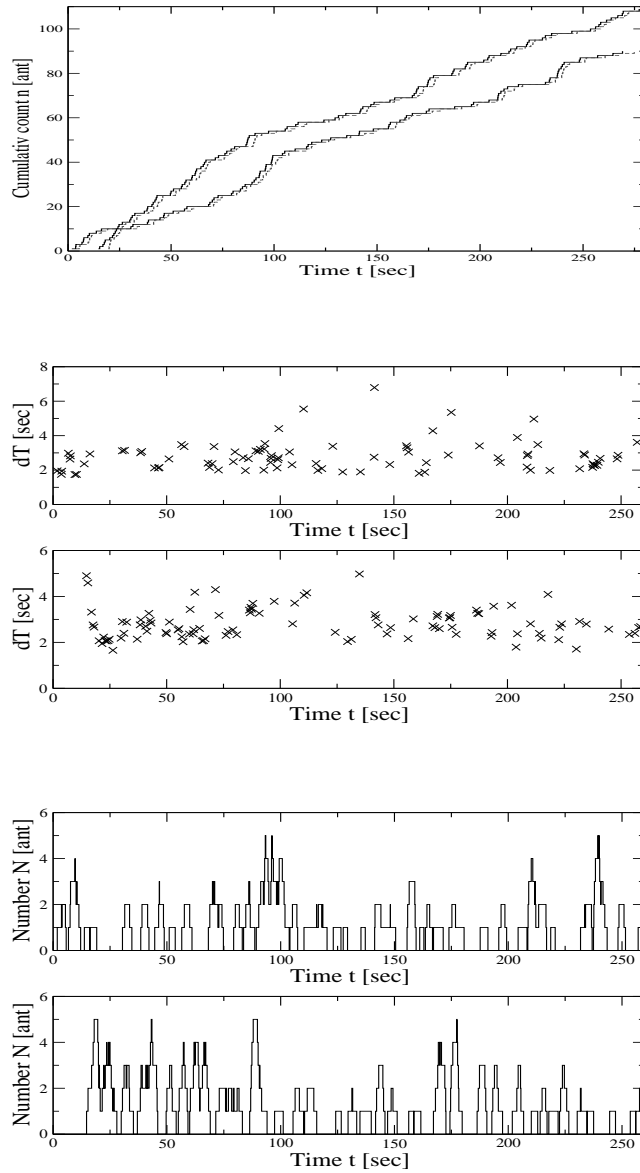


Fig. A.4. The figures show the basic data extracted from video 6c by cumulative counting. Obviously traffic is symmetric for both directions. The slope of the countings which is equivalent to the instantaneous flow is roughly constant.

References

1. P.F. Arndt, T. Heinzel, and V. Rittenberg. Spontaneous breaking of translational invariance and spatial condensation in stationary states on a ring. *J. Stat. Phys.*, 97:1, 1999.
2. A. Basu and D. Chowdhury. unpublished.
3. V. Belitsky, J. Krug, E. Jordão Neves, and G.M. Schütz. A cellular automaton model for two-lane traffic. *J. Stat. Phys.*, 103:516, 2001.
4. M. Bengrine, A. Benyoussef, H. Ez-Zahraouy, J. Krug, M. Loulidi, and F. Mhirech. A simulation study of an asymmetric exclusion model with disorder. *M.J. Condensed Matter*, 2:1, 1999.
5. E. Bonabeau. Agent based modelling: Methods and techniques for simulating human systems. *PNAS*, 99:3, 2002.
6. E. Bonabeau, M. Dorigo, and G. Theraulaz. *Swarm Intelligence: From Natural to Artificial Systems*. Oxford University Press, 1999.
7. E. Bonabeau, M. Dorigo, and G. Theraulaz. Inspiration for optimisation from social insect behaviour. *Nature*, 400:39–42, 2000.
8. E. Bonabeau and C. Meyer. Swarm intelligence. *Harvard Business Review*, May, 2001.
9. I. N. Bronstein, K. A. Semendjajew, G. Musiol, and Mühlig. *Taschenbuch der Mathematik*. Verlag Harri Deutsch, 2005.
10. M. Burd. Ecological consequences of traffic organisation in ant societies. *Physica A*, 372:124–131, 2006.
11. M. Burd and N. Aranwela. Head-on encounter rates and walking speed of foragers in leaf-cutting ant traffic. *Insectes Soc.*, 50:3–8, 2003.
12. M. Burd, D. Archer, N. Aranwela, and D. J. Stradling. Traffic dynamics of the leaf-cutting ant, *atta cephalotes*. *American Natur.*, 159:283–293, 2002.
13. S. Camazine, J. L. Deneubourg, N. R. Franks, J. Sneyd, G. Theraulaz, and E. Bonabeau. *Self-organisation in Biological Systems*. Princeton University Press, 2001.
14. B. Chopard and M. Droz. *Cellular Automata Modelling of Physical Systems*. Cambridge University Press, 1998.
15. D. Chowdhury and R. C. Desai. Steady-states and kinetics of ordering in bus-route models: connection with the nagel-schreckenberg model. *Eur. Phys. J. B*, 15:375–384, 1999.

16. D. Chowdhury, V. Guttal, K. Nishinari, and A. Schadschneider. A cellular-automata model of flow in ant-trails: Non-monotonic variation of speed with density. *J. Phys. A: Math. Gen.*, 35:L573–L577, 2002.
17. D. Chowdhury, K. Nishinari, and A. Schadschneider. Self-organised patterns and traffic flow in colonies of organisms: from bacteria and social insects to vertebrates. *Phase Trans.*, 77:601, 2004.
18. D. Chowdhury, L. Santen, and A. Schadschneider. Vehicular traffic: A system of interacting particles driven far from equilibrium. *Current Science*, 77:411, 1999.
19. D. Chowdhury, L. Santen, and A. Schadschneider. Statistical physics of vehicular traffic and some related systems. *Phys. Rep.*, 329:199–329, 2000.
20. D. Chowdhury, A. Schadschneider, and K. Nishinari. Physics of transport and traffic phenomena in biology: from molecular motors and cells to organisms. *Phys. Life Rev.*, 2:318–352, 2005.
21. I. D. Couzin and N. R. Franks. Self-organised lane formation and optimised traffic flow in army ants. *Proc. Roy. Soc. London B*, 270:139–146, 2003.
22. C. F. Daganzo. Remarks on traffic flow modelling and its applications. In W. Brilon, F. Huber, M. Schreckenberg, and H. Wallentowitz, editors, *Proceedings of Traffic and Mobility*. Springer, 1999.
23. B. Derrida, J. L. Lebowitz, and E. Speer. Shock profiles for the asymmetric simple exclusion process in one dimension. *J. Stat. Phys.*, 89:135–167, 1997.
24. K. Dumpert. *Das Sozialleben der Ameisen*. Pareys Studentexte 18, 2001.
25. A. Dussutour, J. L. Deneubourg, and V. Fourcassié. Temporal organisation of bi-directional traffic in the ant *Lasius niger* (L.). *J. Exp. Biol.*, 2005.
26. A. Dussutour, V. Fourcassié, D. Helbing, and J. L. Deneubourg. Optimal traffic organisation under crowded condition. *Nature*, 428:70, 2004.
27. M. R. Evans and R. A. Blythe. Nonequilibrium dynamics in low-dimensional systems. In H. van Beijeren and J. Indekeu, editors, *Fundamental Problems in Statistical Physics*. North-Holland, 2001.
28. M. R. Evans, D. P. Foster, C. Godrèche, and D. Mukamel. Spontaneous symmetry breaking in a one dimensional driven diffusive system. *Phys. Rev. Lett.*, 74(2):208, 1995.
29. R. P. Feynman. *Surely you're joking Mr. Feynman*. Vintage, 1992.
30. M. Fleischer. *Foundations of swarm intelligence: From principles to practice*. 2005.
31. N.R. Franks. Teaching in tandem-running ants. *Nature*, 439:153, 2006.
32. K. N. Ganeshaiah and T. Veena. Topology of the foraging trails of *Leptogenys processionalis*- why they are branched. *Behav. Ecol. Sociobiol.*, 29:263–270, 1991.
33. J. D. Halley and M. Burd. Nonequilibrium dynamics of social groups: insights from foraging argentine ants. *Insectes Sociaux*, 51, 2004.
34. D. Helbing. Fundamentals of traffic flow. *Phys. Rev. E*, 3:3735–3738, 1997.
35. E. K. O. Hellén and J. Krug. Coarsening of sand ripples in mass transfer, models with extinction. *Phys. Rev. E*, 66:011304, 2002.
36. B. Hölldobler and E. O. Wilson. *The Ants*. Cambridge, Belknap, 1990.
37. J. Howard. Mechanics of motor proteins and the cytoskeleton. *Sinauer Associates*, 2001.
38. S. A. Janowky and J. L. Lebowitz. Finite-size effects and shock fluctuations in the asymmetric simple exclusion process. *Phys. Rev. A*, 45:2, 1992.
39. S. A. Janowky and J. L. Lebowitz. Exact results for the asymmetric simple exclusion process with a blockage. *J. Stat. Phys.*, 77:35–51, 1994.

40. R. Jiang, M. B. Hu, B. Jia, and Q. S. Wua. Realistic bus route model considering the capacity of the bus. *Eur. Phys. J. B*, 34:367372, 2003.
41. A. John. Evolutionäre Flussoptimierung auf Ameisenpfaden. Master's thesis, Universität zu Köln.
42. A. John and et al. in preparation.
43. A. John, A. Kunwar, A. Namazi, D. Chowdhury, K. Nishinari, and A. Schadschneider. Traffic on bi-directional ant-trails. In P. Gattermann, N. Waldau, and M. Schreckenberg, editors, *Proceedings of Pedestrian and Evacuation Dynamics'05*. Springer, 2005.
44. A. John, A. Kunwar, A. Namazi, D. Chowdhury, K. Nishinari, and A. Schadschneider. Traffic on bi-directional ant-trails: Coarsening behaviour and fundamental diagrams. In R. Kühne, T. Pöschel, A. Schadschneider, M. Schreckenberg, and D.E. Wolf, editors, *Proceedings of Traffic and Granular Flow'05*. Springer, 2007.
45. A. John, A. Schadschneider, D. Chowdhury, and K. Nishinari. Collective effects in traffic on bi-directional ant-trails. *J. Theor. Biol.*, 231:279, 2004.
46. A. John, A. Schadschneider, D. Chowdhury, and K. Nishinari. Traffic patterns and flow characteristics in an ant trail model. In M. Dorigo, L.M. Gambardella, M. Birattari, A. Martinoli, R. Poli, and T. Stützle, editors, *Ant Colony Optimisation and Swarm Intelligence, 5th International Workshop, ANTS 2006*, volume 4150 of *LNCS*, Berlin, Germany, 2006. Springer Verlag.
47. K. Johnson and L. F. Rossi. A mathematical and experimental study of ant foraging line dynamics. *J. Theor. Biol.*, 2006.
48. A Kirchner and Schadschneider A. Simulation of evacuation processes using a bionics-inspired cellular automaton model for pedestrian dynamics. *Physica A*, 312:260, 2002.
49. W. Knosppe, L. Santen, A. Schadschneider, and M. Schreckenberg. Disorder effects in ca-models of traffic flow. 1997.
50. W. Knosppe, L. Santen, A. Schadschneider, and M. Schreckenberg. Single-vehicle data of highway traffic: Microscopic description of traffic phases. *Phys. Rev. E*, 65:056133, 2002.
51. A.B. Kolomeisky, G.M. Schütz, E.B. Kolomeisky, and J.P. Straley. Phase diagram of one-dimensional driven lattice gases with open boundaries. *J.Phys. A: Math Gen.*, 31:6911–6919, 1998.
52. J. Krug. Boundary-induced phase transitions in driven diffusive systems. *Phys.Rev.Lett.*, 67:14, 1991.
53. J. Krug. Phase separation in disordered exclusion models. *Braz. J. Phys.*, 30:1, 2000.
54. J. Krug and P.A. Ferrari. Phase transitions in driven diffusive systems with random rates. *J. Phys. A*, 29:L465, 1996.
55. C. R. Kube and E. Bonabeau. Cooperative transport by ants and robots. *Robotics and Autonomous Systems*, 30:85–101, 2000.
56. A. Kunwar, D. Chowdhury, A. Schadschneider, and K. Nishinari. Competition of coarsening and shredding of clusters in a driven diffusive lattice gas. *to appear in J. Stat. Mech.*, 2006.
57. A. Kunwar, A. John, K. Nishinari, A. Schadschneider, and D. Chowdhury. Collective traffic-like movement of ants on a trail: dynamical phases and phase transitions. *J. Phys. Soc. Jpn.*, 73:2979, 2004.
58. E. Limpert, W. A. Stahel, and M. AbbT. Log-normal distributions across the sciences: Keys and clues. *BioScience*, 51:5, 2001.

59. C.T. MacDonald, H. J. Gibbs, and A. C. Pipkin. Kinetics of biopolymerisation on nucleic acid templates. *Biopolymers*, 6:1, 1968.
60. A.D. May. *Traffic Flow Fundamentals*. Prentice Hall, 1990.
61. P. Meakin, P. Ramanlal, L. M. Sander, and R. C. Ball. Ballistic deposition on surfaces. *Phys. Rev. A*, 34:5091, 1986.
62. M. W. Moffet. Ants that go with the flow: A new method of orientation by mass communication. *Naturwissenschaften*, 74:551–553, 1987.
63. J. C. Muñoz and C.F. Daganzo. Structure of the transition zone behind freeway queues. *Transportation Science*, 37 No.3:312–329, 2003.
64. A. Nagar, M. Barma, and S. Majumdar. Clustering of advected passive sliders on a fluctuating surface. *National Conference on Nonlinear Systems and Dynamics*, 2003.
65. K. Nagel and M. Schreckenberg. A cellular automaton model for freeway traffic. *J. Phys. I France*, 2:2221, 1992.
66. K. Nishinari, D. Chowdhury, and A. Schadschneider. Cluster formation and anomalous fundamental diagram in an ant trail model. *Phys. Rev. E*, 67:036120, 2003.
67. K. Nishinari, K. Sugawara, T. Kazama, A. Schadschneider, and D. Chowdhury. Modelling of self-driven particles: foraging ants and pedestrians. *Physica A*, 2006.
68. O. J. O’Loan, M. R. Evans, and M. E. Cates. Jamming transition in a homogeneous one-dimensional system: The bus route model. *Phys. Rev. E*, 58:1404, 1998.
69. O. J. O’Loan, M. R. Evans, and M. E. Cates. Spontaneous jamming in one-dimensional systems. *Europhys. Lett.*, 42(2):137–142, 1998.
70. V. Popkov and M. Salerno. Hydrodynamic limit of multichain driven diffusive models. *Phys. Rev. E*, 69:2221, 2004.
71. V. Popkov, L. Santen, A. Schadschneider, and G. M. Schütz. Boundary-induced phase transitions in traffic flow. *Europhys. Lett.*, 2004.
72. V. Popkov and G. M. Schütz. Steady-state selection in driven diffusive systems with open boundaries. *Europhys. Lett.*, 48(3):257–263, 1999.
73. V. Privman. *Nonequilibrium Statistical Mechanics in One Dimension*. Cambridge University Press, 1997.
74. N. Rajewsky, L. Santen, A. Schadschneider, and M. Schreckenberg. The asymmetric exclusion process: Comparison of update procedures. *J. Stat. Phys.*, 92:151, 1998.
75. A. Schadschneider. Cellular automaton approach to pedestrian dynamics - theory. In M. Schreckenberg and S. D. Sharma, editors, *Proceedings of Pedestrian and Evacuation Dynamics’01*. Springer, 2001.
76. A. Schadschneider, D. Chowdhury, A. John, and K. Nishinari. Anomalous fundamental diagrams in traffic on ant trails. In S.P. Hoogendoorn, S. Luding, P.H.L. Bovy, M. Schreckenberg, and D.E. Wolf, editors, *Proceedings of Traffic and Granular Flow’03*. Springer, 2003.
77. A. Schadschneider, A. Kirchner, and K. Nishinari. From ant trails to pedestrian dynamics. *Applied Bionics and Biomechanics*, 1:11, 2003.
78. G. M. Schütz. Exactly solvable models for many-body systems far from equilibrium. In C. Domb and J.L. Lebowitz, editors, *Phase Transitions and Critical Phenomena, Vol. 19*. Academic Press, 2000.
79. F. Spitzer. Interacting markov processes. *Adv. in Math*, 5:246, 1970.
80. K. Sugawara, T. Kazama, and T. Watanabe. Foraging behaviour of interacting robots with virtual pheromone. In *Proc. of IEEE/RSJ Int. Conf. on Intel. Robots and Sys. (IROS2004)*.

81. G. Tripathy and M. Barma. Steady state and dynamics of driven diffusive systems with quenched disorder. *Phys. Rev. Lett.*, 78:3039, 1997.
82. G. Tripathy and M. Barma. Driven lattice gases with quenched disorder: Exact results and different macroscopic regimes. *Phys. Rev. E*, 58:1063, 1998.
83. P. Wagner. Modelling traffic flow fluctuations. *Journal of insect behaviour*, 2004.
84. E. O. Wilson. *The Insect Societies*. Cambridge University Press, 1971.
85. V. Witte and U. Maschwitz. Raiding and emigration dynamics in ponerine army ant *leptogenys distinguenda* (hymenoptera, formicidea). *Ins. Soc.*, 47:76–83, 2000.
86. V. Witte and U. Maschwitz. Coordination of raiding and emigration in the ponerine army ant *leptogenys distinguenda* (hymenoptera: Formicidae: Ponerinae): A signal analysis. *Journal of insect behaviour*, 15:2, 2002.
87. S. Wolfram. *Theory and Applications of Cellular Automata*. World Scientific, 1986.
88. M. Wölki, A. Schadschneider, and M. Schreckenberg. Asymmetric exclusion process with shuffled dynamics. *J.Phys. A.: Math. Gen.*, 39:33–44, 2006.

List of Figures

1.1	Photography: cooperation and scale	3
2.1	ASEP: definition	6
2.2	TASEP: definition	8
2.3	TASEP: space-time plot and phase diagram	12
2.4	TASEP: model for surface growth	14
2.5	NaSch: model of vehicular traffic	16
2.6	NaSch: space-time plot and fundamental diagram	18
2.7	NaSch: distance headway distribution	19
2.8	TASEP: space-time plots, particlewise disorder	20
2.9	TASEP: $l(\rho)$, particlewise disorder	22
2.10	TASEP: $V(\rho)$ and $F(\rho)$, particlewise disorder	23
2.11	TASEP: space-time plots, sitewise disorder	23
2.12	TASEP: $V(\rho)$ and $F(\rho)$, sitewise disorder	24
2.13	TASEP: $l(\rho)$, sitewise disorder	26
3.1	ATM: definition	28
3.2	BRM: definition	30
3.3	ATM: space-time plots	32
3.4	ATM: density-density correlation function	34
3.5	ATM: zero crossings	35
3.6	ATM: fundamental diagram	37
3.7	ATM: cluster properties	39
4.1	ATMs: survey of bidirectional ATMs	42
4.2	ATM 1: space-time plots 1	44
4.3	ATM 1: space-time plots 2	44
4.4	ATM 1: fundamental diagram	45
4.5	ATM 2: space-time plots 1	46
4.6	ATM 2: space-time plots 2	47
4.7	ATM 2: fundamental diagram	48
4.8	ATM 3: photography of a narrow trail	49

4.9	ATM 3: space-time plots 1	49
4.10	ATM 3: space-time plots 2	50
4.11	ATM 3: fundamental diagram	51
4.12	ATM 2: density-density correlation function	53
4.13	ATM 2: zero crossings	54
4.14	ATM 2: dynamic latticewise disorder	55
4.15	ATM 2: cluster properties	56
4.16	ATM 2: density profile and flow	57
4.17	Extended ATM 2: fundamental diagrams	60
5.1	Mapping: trail to ca-model	66
5.2	Photography: experimental setup	68
5.3	Photography: first observations	69
5.4	Cumulative counting: video 13	72
5.5	Derived quantities: video 13	73
5.6	Single-ant velocities: video 13	76
5.7	Distance headways: video 13	77
5.8	Fundamental diagram: video 13	78
5.9	Single-ant velocities: video 19	79
5.10	Velocity distributions: video 19	81
5.11	Fundamental diagram: video 19	82
5.12	Distance headways: video 19	83
5.13	Distance headway distributions: video 19	83
5.14	Velocity distributions: video 6(LR)	87
5.15	Velocity distributions: video 6(RL)	87
5.16	Fundamental diagram: video 6(LR), uni	88
5.17	Fundamental diagram: video 6(LR), bi	88
5.18	Fundamental diagram: video 6(RL), uni	89
5.19	Fundamental diagram: video 6(RL), bi	89
5.20	Distance headway distributions: video 6(LR)	91
5.21	Distance headway distributions: video 6(RL)	92
5.22	Catching up: mechanisms	94
5.23	Catching up: unidirectional	96
5.24	Catching up: bidirectional	96
6.1	Photography: traffic jam	103
6.2	Photography: laboratory experiments	104
A.1	Basic data: video 19	112
A.2	Basic data: video 6a	114
A.3	Basic data: video 6b	115
A.4	Basic data: video 6c	116

Acknowledgments

The present work consists of many parts from different fields. Therefore it is quite difficult to mention all the people having contributed to it. Nevertheless I would like to thank Prof. Dr. Andreas Schadschneider for being the supervisor and always being willing to discuss new ideas. He encouraged even the excursion to empirical research. Prof. Dr. Dietrich Stauffer thankfully agreed being the coreferee and accepted to read even preliminary versions of the manuscript. I am also thankful to Prof. Dr. Peter Reiter and Priv.-Doz. Dr. Ute Löw for accepting to be a part of the commission.

Most of the underlying research has been conducted within the group of Prof. Dr. Achim Rosch. I thank him for supporting research far from his own field and especially for supporting the laboratory experiments.

I would also like to thank the members of the group, beside many other things, for showing interest in a topic very different from their own research but also for collecting hundreds of ants attempting to take over the office. So I try to give a list roughly ordered by time:

Dr. Marc André Ahrens, Dr. Erik Bartel, Dr. Alireza Namazi, Dr. Theo Costi, Dr. Nayana Shah, Peter Jung, Rolf Helmes, Clemens Müller-Gugenberger, Philip Greulich, Dr. Fabrizio Anfuso and finally Dr. Inga Fischer.

The presented empirical studies were conducted in India. So I thank the German Academic Exchange Service (DAAD) for kindly providing support. Field research itself has been carried out at the Centre for Ecological Sciences of the Indian Institute of Science (IISc). There I enjoyed numerous discussions while learning more about ant-biology and indian food. So I would like to thank Prof. Dr. Raghavendra Gadagkar for offering the opportunity to work within his research group which is too big to mention all members. But I learned a great deal about Indian ants from Dr. Thresiamma Varghese and a lot about India from Swati Samudre and Alok Bang.

Major parts of this work originate from the friendly relationship and collaboration with Prof. Dr. Debashish Chowdhury. He kindly offered me the opportunity to work within his research group at the physics department of the Indian Institute of Technology in Kanpur (IITK). Also here I enjoyed discussions with many people especially Dr. Ambarish Kunwar and Ashok Garai. During my stay there I learned a lot about traffic engineering at the department of civil engineering from Prof. Dr. Partha Chakroborty. I am very thankful for many discussions especially about the techniques employed in the present study for collecting ant-traffic data.

I thank Prof. Dr. Katsuhiko Nishinari from the University of Tokyo for the fruitful collaboration especially during his sabbatical stay at the University of Cologne.

Prof. Dr. Martin Burd from the School of Biological Sciences at Monash University, Australia inspired parts of the present study by sharing his experience with conducting field research on living ants.

Finally I would like to thank my parents and friends for supporting my work in any respect.

Abstract

The main aim of the present work is the investigation of the dynamical properties of traffic on preexisting ant trails. It is mainly divided into two parts which are based on the interplay between theory and experiment. Both parts are developed independently and compared later on in a final discussion. Methods from statistical and non-equilibrium physics were employed for theoretical studies. New models for bidirectional traffic on preexisting ant trails were introduced. Also the understanding of the already existing unidirectional ant trail model was improved. The results of the presented empirical studies are compared to the models predictions. Ant-traffic data are extracted using methods from traffic engineering and behavioural biology. Similar approaches have already been employed successfully for vehicular traffic. Nevertheless the crucial differences between the already investigated systems and ant-traffic are the main motivation of the present study.

Chapters 2,3 and 4 cover the theoretical part. In *chapter 2* a broad introduction to driven non-equilibrium systems in the context of traffic flow is given. Standard models like the *TASEP* and the *Nagel-Schreckenberg* model for vehicular traffic are introduced. As the ant trail models are based on the TASEP with dynamically induced disorder, a review of the TASEP with static particlewise- and latticewise disorder is given.

Chapter 3 introduces a model for unidirectional traffic on ant trails. *Pheromone marks* lead to different hopping rates depending on the distance headway to the preceding ant. As a result *dynamically induced* particlewise disorder emerges. Phase separation namely the formation of *moving particle clusters* is observed. The fundamental diagram exhibits a *non-monotonicity* in the average velocity when particlewise disorder is dissolved at high densities. New techniques like measuring the density profile within the moving system seen from a modified second-class particle are applied and analogies to the static case are drawn. Also the coarsening behaviour is investigated. Obviously the process is describe by a power-law with two *dynamic exponents* depending on the particular temporal regime.

Chapter 4 discusses different extensions of the unidirectional model to the multi-lane case. Bidirectional models incorporating the coupling to counterflow are introduced. A large *localised particle cluster* emerges due to mutual hindrance by *counterflow*. Effectively latticewise disorder is induced *dynamically*. The same tools as for the unidirectional model are applied and a mean-field description based on symmetries of the large localised cluster is developed. Coarsening is investigated and the same dynamic exponents as for the unidirectional model are found. At low densities also the periodic process of *coarsening* and *shredding* is investigated.

The empirical part of the present study is discussed in *chapter 5*. Techniques and strategies for collecting ant-traffic data are introduced. Also an *experimental setup* is described. Uni- as well as bidirectional trails are investigated. Qualitative observations are carried out and compared to quantitative data. *Distance headways* and *single-ant velocities* are extracted. The corresponding distributions as well as the *fundamental diagrams* are discussed. As a main result *platoon formation* and coupling to counterflow is found. Also comparisons between the models' predictions and the empirical data are drawn.

A review of theoretical and empirical results is given in *chapter 6*. Main results from both parts are compared in a final discussion. Also an outlook to future studies is given.

Zusammenfassung

Ziel der vorliegenden Arbeit ist die Untersuchung der dynamischen Eigenschaften des Verkehrs auf Ameisenpfaden. Basierend auf dem Wechselspiel zwischen Theorie und Empirie gliedert sich die Arbeit in zwei Teile. Beide Teile werden unabhängig voneinander entwickelt und in einer abschließenden Diskussion verglichen. Für die theoretischen Untersuchungen werden Methoden aus der Statistischen- und Nichtgleichgewichtsphysik verwandt. Es werden neue Modelle für bidirektionalen Verkehr auf bereits bestehenden Ameisenpfaden eingeführt. Zusätzlich wird das bereits bestehende unidirektionale Modell untersucht und zum besseren Verständnis detailliert diskutiert. Die Ergebnisse der empirischen Untersuchungen werden mit den Vorhersagen der Modelle verglichen. Durch die Anwendung von Methoden aus der Verhaltensbiologie und des Verkehrswesen werden Daten zum Verkehrsfluss gewonnen. Grundsätzlich sind ähnliche Methoden schon erfolgreich auf Fahrzeugverkehr angewendet worden. Dennoch motiviert der grundlegende Unterschied zwischen den bereits untersuchten Systemen und dem Verkehr auf Ameisenstraßen die vorliegende Studie. Die Kapitel 2, 3 und 4 bilden den theoretischen Teil. Kapitel 2 gibt eine breite Übersicht zu getriebenen Nichtgleichgewichtssystemen im Zusammenhang mit dem Fluß in Verkehrssystemen. Standardmodelle zur Beschreibung von Straßenverkehr, wie das Nagel-Schreckenberg Modell, werden diskutiert. Die Modelle zur Beschreibung des Verkehrs auf Ameisenstraßen basieren auf dem TASEP mit dynamisch-induzierter Unordnung. Daher wird der TASEP mit statischer teilchen- und gitterartiger Unordnung besprochen.

In Kapitel 3 wird das Modell für einspurige Ameisenpfade eingeführt. Pheromonmarkierungen induzieren unterschiedliche Hüpfraten, die vom Abstand zur vorauslaufenden Ameise abhängen. Dies führt zu dynamisch-erzeugter teilchenartiger Unordnung. Eine Phasenseparation tritt ein, bei der die Ameisen sich in Kolonnen über den Pfad bewegen. Die Fundamentaldiagramme zeigen eine Nicht-Monotonizität bei der Dichte, bei der die teilchenartige Unordnung aufgelöst wird. Neue Untersuchungsmethoden, wie die Messung des Dichteprofiles, das von einem modifizierten passiven Teilchen gesehen wird, werden angewandt. Dadurch werden Analogien zum statischen Fall ermöglicht. Darüber hinaus wird die zeitliche Entwicklung der Phasenseparation untersucht. Offenbar wird diese durch ein Potenzgesetz beschrieben. Abhängig vom jeweiligen Bereich findet man zwei dynamische Exponenten.

Kapitel 4 diskutiert die Erweiterung des Einspur-Modells zu einem Mehrspur-Modell. Drei Modelle, die eine Koppelung zum Gegenverkehr als zusätzliche Wechselwirkung beinhalten, werden eingeführt. Diese Koppelung führt durch gegenseitige Behinderung zur Bildung einer lokalisierten Kolonne von Ameisen. Grundsätzlich werden die gleichen Untersuchungsmethoden wie für das Einspur-Modell verwendet. Basierend auf den so nachgewiesenen Symmetrien wird eine Molekularfeld-Beschreibung des stationären Zustandes entwickelt. Auch hier wird die Entstehung der Phasenseparation untersucht. Diese folgt wieder einem Potenzgesetz mit den gleichen dynamischen Exponenten wie auch das Einspur-Modell. Für niedrige Dichten wird zusätzlich das periodische Zerstören und Neubilden der sich bewegenden Ameisenkolonne untersucht. In Kapitel 5 werden schließlich die empirischen Ergebnisse dargestellt. Die Methoden und Techniken zur Datengewinnung sowie die Konstruktion der Experimente werden beschrieben. Uni- und bidirektionale Pfade werden untersucht. Zusätzlich werden qualitative Untersuchungen durchgeführt und mit den Ergebnissen der Messungen verglichen. Die Einzelgeschwindigkeiten der Ameisen und der Abstand zur vorauslau-

fenden Ameise werden gemessen. Die dazugehörigen Verteilungen wie auch die Fundamentaldiagramme werden diskutiert. Als ein wesentliches Ergebnis stellt sich die Kolonnenbildung und deren Störung durch Gegenverkehr heraus. Schließlich werden die empirischen Ergebnisse mit den Vorhersagen der Modelle verglichen.

Kapitel 6 gibt eine Übersicht der wichtigsten Ergebnisse - sowohl des theoretischen als auch des empirischen Teils. Abschließend wird ein Ausblick auf zukünftige Untersuchungen diskutiert.

Erklärung

Ich versichere, dass ich die von mir vorgelegte Dissertation selbständig angefertigt, die benutzten Quellen und Hilfsmittel vollständig angegeben und die Stellen der Arbeit einschließlich Tabellen, Karten und Abbildungen, die anderen Werken im Wortlaut oder Sinn nach entnommen sind, in jedem Einzelfall als Entlehnung kenntlich gemacht habe; dass diese Dissertation noch keiner anderen Fakultät oder Universität zur Prüfung vorgelegen hat; dass sie abgesehen von unten angegebenen Teilpublikationen noch nicht veröffentlicht worden ist, dass ich eine solche Veröffentlichung vor Abschluss des Promotionsverfahrens nicht vornehmen werde. Die Bestimmungen dieser Promotionsordnung sind mir bekannt. Die von mir vorgelegte Dissertation ist von Herrn Prof. Dr. Andreas Schadschneider betreut worden.

(Alexander John)

Köln, den 27. September 2006

Teilpublikationen

1. A. Schadschneider, D. Chowdhury, A. John, and K. Nishinari. Anomalous fundamental diagrams in traffic on ant trails. In S.P. Hoogendoorn and S. Luding, P.H.L. Bovy, M. Schreckenberg, and D.E. Wolf, editors, *Proceedings of Traffic and Granular Flow'03*. Springer, 2003.
2. A. Kunwar, A. John, K. Nishinari, A. Schadschneider, D. Chowdhury. Collective traffic-like movement of ants on a trail: dynamical phases and phase transitions. *J.Phys.Soc.Jp.* **73**, 2979 (2004).
3. A. John, A. Schadschneider, D. Chowdhury and K. Nishinari. Collective effects in traffic on bi-directional ant-trails. *Journal of Theoretical Biology*, vol.231, 279 (2004).
4. A. John, A. Kunwar, A. Namazi, D. Chowdhury, K. Nishinari, and A. Schadschneider. Traffic on bi-directional ant-trails. In N. Waldau, P. Gattermann, H. Knoflacher and M. Schreckenberg, editors, *Proceedings of Pedestrian and Evacuation Dynamics'05*. Springer, 2006.
5. A. John, A. Kunwar, A. Namazi, D. Chowdhury, K. Nishinari, and A. Schadschneider. Traffic on bi-directional ant-trails: Coarsening Behaviour and Fundamental Diagrams. In R. Kühne ,T. Pöschel, A. Schadschneider, M. Schreckenberg and D.E. Wolf, editors, *Proceedings of Traffic and Granular Flow'05*. Springer, 2007.
6. A. John, A. Schadschneider, D. Chowdhury, and K. Nishinari. Traffic patterns and flow characteristics in an ant trail model. In M. Dorigo, L.M. Gambardella, M. Birattari, A. Martinoli, R. Poli and T. Stützle, editors, *Ant Colony Optimization and Swarm Intelligence, 5th International Workshop, ANTS 2006*, volume 4150 of *LNCS*, Berlin, Germany, 2006. Springer Verlag.